AN ABSTRACT OF THE THESIS OF

WILLARD ORVIN OLSON (Name of student) for the DOCTOR OF PHILOSOPHY (Degree)

in Nuclear Engineering (Major Department) presented on June 7, 1974 (Date)

Title: ONE AND TWO DIMENSIONAL SPACE-ENERGY FLUX SYNTHESIS WITH SPATIALLY DISCONTINUOUS TRIAL FUNCTIONS

Abstract approved: Alan H. Robinson

The development of nuclear reactors as an energy source requires a substantial invesment in capital and effort. This development depends heavily on accurate calculational methods.

Space-energy flux synthesis, also variously called the spectral synthesis method, modal method, and overlapping group method, is one possible method. In this method the energy dependent flux is approximated by a superposition of energy trial functions (spectra). This thesis examines the use of this expansion in the context of diffusion theory.

One and two dimensional diffusion theory codes have been written to accommodate a very general formulation of the spectral synthesis method. These codes use simultaneous solution methods to eliminate many of the convergence problems previously encountered with overlapping groups, while allowing a wide choice of interface conditions.

Numerical experiments using these codes compare various choices of trial functions and types of weighting. A major portion of the investigation concerns the use of different sets of trial functions in different regions (spatially discontinuous trial functions). Particular attention is accorded to trial function and material interface conditions. Results favor conditions which preserve energy integrals of flux and current at interfaces.

One and Two Dimensional Space-Energy Flux Synthesis with Spatially Discontinuous Trial Functions

by

Willard Orvin Olson

A THESIS

submitted to

Oregon State University

in partial fulfillment of
the requirements for the
degree of

Doctor of Philosophy

Completion June 7, 1974
Commencement June, 1975

APPROVED:

Redacted for privacy

Associate Professor of Nuclear Engineering

Redacted for privacy

Head of Department of Nuclear Engineering

Redacted for privacy

Dean of Graduate School

Date thesis is presented June 7, 1974

Typed by Deanna L. Cramer for Willard Orvin Olson

ACKNOWLEDGEMENTS

I would like to thank my major professor, Dr. Alan H. Robinson. His advice and encouragement, and the excellence of his teaching, are greatly appreciated.

I also wish to express my appreciation to the Nuclear Engineering Department at Oregon State University. It has been a privilege to have been associated with such a positive and energetic group. Special thanks to Dr. John C. Ringle, an instructor for several of my courses, for his teaching and encouragement and for his help in editing this thesis. I extend my appreciation to my fellow students in the Department and especially to the original group in C-124. The help from and interaction with this group added considerably to my education.

The financial support of the Atomic Energy Commission during a portion of my work was appreciated.

Finally, to my wife, Sally, a thank you beyond words, for her help, encouragement and patience.

TABLE OF CONTENTS

Chapter		Page
I	INTRODUCTION AND LITERATURE	
	1.1 Introduction	1
	1.1.1 The Modal Approximation	1
	1.1.2 The Diffusion Equation	2
	1.1.3 The Weighted Residuals Approach	3
	1.1.4 The Multigroup Method	4
	1.2 Early History of Synthesis Methods	7
	1.3 Discussion of the Synthesis Method	10
	1.3.1 The Modal Expansion	10
	1.3.2 Trial Functions	12
	1.3.3 Weighting Functions	16
	1.4 Survey of Fast Reactor Synthesis Methods	19
	1.5 Objectives of this Study	22
II	DEVELOPING THE METHOD	24
	2.1 Development in a Homogeneous Medium	24
	2.1.1 The Multigroup Method as a Special Case	26
	2.1.2 Further Development	28
	2.2 Trial Function and Material Interface Conditions	29
	2.2.1 The Multigroup Method as a Special Case	32
	2.2.2 Method of Lorenzini and Robinson	33
	2.3 Numerical Form; The Difference Equations	34
	2.4 Producing the Input	37
	2.4.1 Input for Interface Conditions	40
III	SOLUTION OF MULTIDIAGONAL MATRIX PROBLEMS	42
	3.1 Introduction	42
	3.2 General Form and Solution Methods	42
	3.2.1 Intuitive Development of Crout Method	47
	3.2.2 Algorithms of the Crout Method	50
	3.3 Comparisons of Calculational Effort	52
	3.4 Form for the Computer Code	57
IV	FAST REACTORS AND FAST REACTOR PARAMETERS	65
	4.1 The Place of Breeder Reactors in the Nation's Energy Picture	65

Chapter		Page
	4.2 Fast Reactors, General	66
	4.3 Reactor Parameters	68
	4.3.1 Temperature Coefficient	68
	4.3.2 Sodium Void	69
	4.3.3 Reaction Rates	70
	4.4 26-Group Calculation	70
	4.5 The General Electric Pancake Design	71
	4.6 The EBR-II Reactor	76
V	ONE DIMENSIONAL CALCULATIONS AND RESULTS	83
	5.1 Introduction	83
	5.2 Galerkin Weighting	84
	5.2.1 Two Bracketing Modes Per Region	84
	5.2.2 Comments on Comparisons	86
	5.2.3 Improving the Fit	87
	5.2.4 Problems	90
	5.2.5 Relation Between Regional and Interface Weighting	91
	5.2.6 Sodium Void and Doppler Coefficients	92
	5.3 Interface Conditions	93
	5.3.1 Discussion	93
	5.3.2 Overlap of Trial Function Sets	96
	5.3.3 Weight Functions at Trial Function Interfaces: Discussion	97
	5.3.4 Forcing the Conservation of Flux and Current Across Interfaces	100
	5.4 Regional Weighting	104
	5.4.1 Introduction	104
	5.4.2 Three Modes per Region	105
	5.4.3 Spatially Continuous Trial Functions	111
	5.4.4 Two Trial Functions	115
VI	TWO DIMENSIONAL METHODS AND RESULTS	119
	6.1 Introduction	119
	6.2 Developing the Method	119
	6.3 The Difference Equation for Two Dimensional Geometry	121
	6.4 The Two Dimensional Code	126
	6.4.1 The Equation Form	126
	6.4.2 Some Restrictions on Mesh Spacing for Computational Simplicity	126

Chapter		Page
	6.4.3 General Interative Scheme	128
	6.4.4 The Interface between Axial Regions/Integrals Over a Half Interval	130
	6.4.5 The Interface between Axial Regions/General Scheme	132
6.5	Results of Two Dimensional Calculations	135
	6.5.1 Analysis of the Two Dimensional Results	139
6.6	Assessment of the Code, Suggestions	145
BIBLIOGRAPHY		148
APPENDIX:	One Dimensional Diffusion Code WDIF1	153

LIST OF TABLES

Table		Page
3-1	Calculations for a Multidiagonal Matrix	53
3-2	Comparison of Multidiagonal and Group by Group Solution	56
4-1	26-Group Structure	72
4-2	Composition of G.E. Reactor	74
4-3	Composition of EBR-II Model	77
5-1	Galerkin Weighting with Bracketing Functions	85
5-2	Regional Absorption Errors for EBR Axial Calculations	89
5-3	Two Bracketing Modes with Various Weighting at Interfaces	91
5-4	Sodium Void and Doppler Changes in k_{eff}	93
5-5	Various Degrees of Trial Function Set Overlap with Galerkin Weights	97
5-6	Use of Unity as the Third Weight Function at Interfaces	103
5-7	Results with Three Modes per Region	106
5-8	Modal Sets for Table 5-7	106
5-9	Results with Continuous Trial Functions	113
5-10	G.E. Radial Geometry - Two Modes with Various Weighting	116
6-1	Two Dimensional Results	136
6-2	Fit of Synthesized Flux at Core Center	140
6-3	Fit of Synthesized Flux at Core-Blanket Interface	141
6-4	Fit of Synthesized Flux in the Blanket	142
6-5	Regional Reaction Rate Errors for Two Dimensional Calculations	145

LIST OF FIGURES

Figure		Page
1-1	Untitled Sketch	7
3-1	Reactor Model for Discussion of the Code	58
3-2	Multidiagonal Matrix for the Model of Figure 3-1 using Two Modes	63
4-1	G.E. Pancake Model	73
4-2	Flux Shapes for G.E. Radial Positions	75
4-3	EBR-II Model	78
4-4	EBR Fluxes for Various Radial Positions	80
4-5	Fluxes for EBR Axial Positions	81
5-1	Absorption Error for EBR Axial Case	88
5-2	Absorption Error with Trial Function Set A	108
5-3	Reaction Rates and Adjoint Weighting, Trial Function Sets A and B	109
5-4	Absorption Error with Trial Function Sets C and D	110
5-5	Absorption Errors with Continuous Trial Functions	114
5-6	Absorption Error with Two Bracketing Modes	117
6-1	Mesh Notation	123a
6-2	Regional Notation	127
6-3	Finite Difference Mesh	130
6-4	Absorption Error as a Function of Radial Position	144

ONE AND TWO DIMENSIONAL SPACE-ENERGY FLUX SYNTHESIS WITH SPATIALLY DISCONTINUOUS TRIAL FUNCTIONS

I. INTRODUCTION AND LITERATURE

1.1 Introduction

In a time of increasing technology and a decreasing reservoir of fossil fuel, the development of nuclear power seems destined to play an important part in supplying the world's energy needs. In the development of this resource, safety aspects and the magnitude of the investment to be made require accurate predictive methods. The complexity of the problems involved requires that approximations be made and that large computers be used.

The investment in nuclear power and in the calculations necessary for its development is substantial. Thus, there has been and is a continuing interest in optimizing the approximations and calculational methods employed. This thesis is a portion of that investigation and optimization.

1.1.1 The Modal Approximation

Specifically, this thesis concerns itself with the approximation known variously as the spectral synthesis method, space-energy synthesis method, modal method and overlapping group method. The basic approximation is the assumption that the energy dependence of the neutron flux can be expressed as a superposition of a few energy shapes

(spectra), called modes or trial functions. This approximation to the flux is represented by

$$\phi(r,E) = \sum_{i=1}^{N} a_i(r) f_i(E) \qquad (1\text{-}1)$$

The $f_i(E)$ are the trial functions and the $a_i(r)$ are often called combining coefficients or mixing functions.

1.1.2 The Diffusion Equation

This thesis is restricted to the use of this approximation within the context of diffusion theory. The energy dependent diffusion equation for a homogeneous medium is

$$-D(E)\nabla^2\phi(\vec{r},E) + \Sigma_t(E)\phi(\vec{r},E) = \frac{1}{\lambda}\chi(E)\int_o^\infty \nu\Sigma_f(E')\phi(r,E')dE' + \int_o^\infty \Sigma_s(E'\to E)\phi(r,E')dE' \qquad (1\text{-}2)$$

$\phi(\vec{r},E)$ is the flux or number of neutrons per unit volume at $\vec{r}$ and unit energy at E times the velocity corresponding to E. D(E) is the diffusion coefficient and $\Sigma_t(E)$ the macroscopic total cross section. $\chi(E)$ is the fission spectrum, that is, the fraction of fission neutrons per unit energy at E. $\nu\Sigma_f(E)$ is the macroscopic cross section for the production of neutrons, a product of the cross section for fission, Σ_f, times ν, the neutrons per fission. Both are functions of incident neutron energy. $\Sigma_s(E'\to E)$ is the cross section for scattering from E' to E. λ is the eigenvalue of the equation. The largest eigenvalue is the effective multiplication factor.

The terms in the above equation from left to right represent neutron leakage, neutron interaction with nuclei, neutrons supplied by fission and neutrons supplied by scattering, all at energy E and position $\vec{r}$. Each of the terms are per unit energy, volume, and time. This is perhaps more easily understood if we note that a macroscopic cross section is a probability per unit path length, and flux, being the product of number density (per unit energy and volume) and velocity, is the total path length per unit time, volume, and energy.

1.1.3 The Weighted Residuals Approach

The energy dependent diffusion equation is generally not soluble due to its complexity, requiring some approximations. The spectral synthesis approach is to substitute an expansion of the form (1-1) into equation (1-2), giving

$$\sum_{i=1}^{N} [-D(E) f_i(E) \nabla^2 a_i(\vec{r}) + \Sigma_t(E) f_i(E) a_i(\vec{r})] \approx$$
$$\frac{1}{\lambda} \chi(E) \sum_{i=1}^{N} \int_0^{\infty} \nu\Sigma_f(E') f_i(E') dE' \; a_i(\vec{r}) + \qquad (1\text{-}3)$$
$$\sum_{i=1}^{N} \int_0^{\infty} \Sigma_s(E' \rightarrow E) f_i(E') dE' \; a_i(\vec{r})$$

This relation is some approximation to (1-2) and is again not generally soluble. For the present study the $f_i(E)$ are known functions of E and the $a_i(\vec{r})$ are the desired information.

To produce a set of soluble equations this development uses the method of weighted residuals (23). Applying this to (1-3), one multiplies through by a weight function $g_j(E)$ and integrates over all energies and requires equality. This yields an equation in position alone.

$$\sum_{i=1}^{N} [-D_{ji}\nabla^2 a_i(\vec{r}) + (\Sigma_t)_{ji} a_i(\vec{r})] = \sum_{i=1}^{N} [\frac{\chi_j}{\lambda} (\nu\Sigma_f)_i a_i(\vec{r}) + (\Sigma_s)_{ji} a_i(\vec{r})] \tag{1-4}$$

where

$$D_{ji} = \int_0^\infty g_j(E)\ D(E)\ f_i(E)\ dE \tag{1-5}$$

$$(\Sigma_t)_{ji} = \int_0^\infty g_j(E)\Sigma_t(E) f_i(E) dE \tag{1-6}$$

$$\chi_j = \int_0^\infty g_j(E)\ \chi(E)\ dE \tag{1-7}$$

$$(\nu\Sigma_f)_i = \int_0^\infty \nu\Sigma_f(E') f_i(E') dE' \tag{1-8}$$

$$(\Sigma_s)_{ji} = \int_0^\infty dE\ g_j(E) \int_0^\infty dE' \Sigma_s(E' \to E) f_i(E') \tag{1-9}$$

Using N, such weight functions provide the N equations corresponding to the N unknowns $a_i(\vec{r})$.

This has been a brief introduction to provide some background for discussion of the literature and philosophy involved in the method. A more thorough treatment follows in Chapter II.

1.1.4 The Multigroup Method

It is helpful to compare the development of the modal method with that for the multigroup method, the multigroup

method being the primary approximation in present usage. In the multigroup formulation, the energy dependent diffusion equation is integrated over an energy increment or group. Using N such increments to cover the total energy range, the energy dependent diffusion equation is reduced to N coupled equations which are a function of position only.

Of course, if the functional dependence was known so that the integrations could be performed, there would be no reason for solving the equations, hence an approximation. Consider the integral of one of the terms of the diffusion equation as an example:

$$\int_{\Delta E_g} \Sigma_t(E)\phi(r,E)\,dE \tag{1-10}$$

To obtain a tractable form, a group average cross section (flux averaged) is defined by use of an appropriate averaging spectrum, $\Phi(E)$. This spectrum is often obtained from a zero dimensional calculation. The group average cross section for the sample term is defined as

$$\Sigma_{t_g} \equiv \frac{\int_{\Delta E_g} \Sigma_t(E)\Phi(E)\,dE}{\int_{\Delta E_g} \Phi(E)\,dE} \tag{1-11}$$

Replacing the energy dependent cross section in (1-10) with this average cross section yields

$$\int_{\Delta E_g} \Sigma_t(E)\phi(r,E)\,dE = \Sigma_{t_g} \int_{\Delta E_g} \phi(r,E)\,dE = \Sigma_{t_g}\phi_g(r) \tag{1-12}$$

where $\phi_g(r)$, the group flux, is defined by the right hand equation of (1-12)

If the process of (1-10) is repeated to provide average cross sections for each of the terms of the diffusion equation and the integration over each term is carried out, one obtains the multigroup diffusion equation.

$$-D_g\nabla^2\phi_g(r) + \Sigma_{t_g}\phi_g(r) = \frac{\chi_g}{\lambda}\sum_{h=1}^{N}(\nu\Sigma_f)_h\phi_h(r) + \sum_{h=1}^{N}\Sigma_s(h\to g)\,\phi_h(r) \qquad (1\text{-}13)$$

The above description is obviously incomplete; reference is made to standard texts (5, 10, 37) and to an article on collapsing schemes (28) for further description. However, this introduction is sufficient to provide an insight into some of the difficulties inherent in the multigroup method. The approximation in the method is in replacing the energy dependent cross section by an averaged value. The choice of the averaging flux, $\Phi(E)$, is obviously a critical factor in the accuracy of the method. Also, since a single $\Phi(E)$ is typically used over a given material region while the actual spectral shape will vary across the region, the degree of fit will be a function of position.

In Chapter II the formalism of the modal method is extended. We will see that the multigroup method is a special case within that formalism. With that insight we can examine the multigroup formulation further.

1.2 Early History of Synthesis Methods

The use of an expansion of the form of equation (1-1) rests upon the assumed separability of a function of several variables into a product of functions of single variables and also upon a notion of superposition. Both of these are a time honored part of mathematical physics.

However, while separability is a part of reactor theory (25), it is strictly applicable only to certain very simple geometries, boundary conditions and material homogeneities.

The use of functions of form (1-14) to synthesize three

$$\phi^{g}_{(x,y,z)} = Z^{g}(z)H^{g}_{i}(x,y) \qquad (1\text{-}14)$$

dimensional spatial dependence from a splicing of two dimensional solutions appears to have originated at Bettis Laboratory in 1957 (14, 38, 49). This form was applied whether the flux was theoretically separable or not. For example, consider a system composed of two axial regions as shown in Figure 1.1. The idea is to make an x,y calculation for each axial zone (for example, zone 1 might have control rods out and zone 2 have control rods in). These are used for the $H^{g}_{i}(x,y)$ in equation (1-20), where i denotes axial zone and g denotes group. Thus, the x,y dependence is fixed in each axial zone. This method

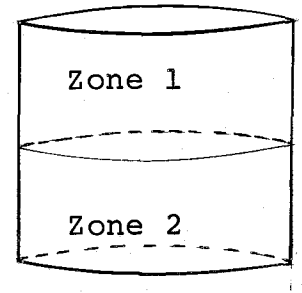

Figure 1-1

has the advantage of not requiring a three dimensional calculation, but suffers discontinuities at interfaces between axial zones. For example, one may require that the integral of flux over the x,y plane be conserved across an interface, but the flux at a typical x,y point will not be conserved at the interface.

Of these three papers, the one by J. E. Meyer (38) is the most explicit and useful.

In 1958, three more papers from Bettis using and expanding on the above method were written. These expanded the method to more complex control rod patterns (32), extended it to R-Z geometry (19), and combined the method with use of a depletion code (1).

Also in 1958, a paper by Selengut (48) established new insight and a sounder theoretical basis to the method by a development from a variational principle. This established the use of weighting functions and the use of adjoints as a theoretically preferred weighting method. This will be discussed further in section 1.3.3.

In 1961, Calame and Federighi (9) made the first use of overlapping groups of the form of equation (1-1). Their development was from a variational principle and was applied to synthesis of the thermal flux. They also point out the applicability of the expansion to higher order transport theory.

A paper by S. Kaplan (22) in 1962 contained the first superposition in space-space synthesis, i.e.,

$$\phi^g(x,y,z) = \sum_{i=1}^{N} Z_i^g(z) H_i^g(x,y) \qquad (1\text{-}15)$$

This allows the spectrum near an interface to be a combination of the spectra of adjacent media, eliminating the interface discontinuity of equation (1-14).

Both of these superposition papers, which Kaplan labels the "new synthesis" exhibit a marked improvement, especially in their treatment near material interfaces.

Kaplan's paper (22) is also noteworthy for other innovations. His development is from a variational principle, but having done this he notes that the results are identical in form to those which are obtained from the weighted residuals approach. He then explores the use of other weighting functions, namely Galerkin (20), region balance and multispot balance, in addition to adjoint weighting. These weightings will be discussed further in the section 1.3.3. Briefly, Galerkin weighting uses the trial function [in this case $H_i^g(x,y)$] as weight functions and region balance weighting uses unity over a certain region of x,y space and zero outside. These are used to define "digested" cross sections such as

$$(\Sigma_t^g)_{ji} = \int_{\text{area}} W_j^g(x,y)\ \Sigma_t^g(x,y)\ H_i^g(x,y)\ dx\ dy \qquad (1\text{-}16)$$

where W_j is the weight function.

These are equivalent to equations (1-5) through (1-9) for space-energy synthesis and are used in a one-dimensional (z) calculation. For spot balancing one has

$$(\Sigma_t)_{ji} = \Sigma_t^g(x_j,y_j)\, H_i^g(x_j,y_j) \qquad (1\text{-}17)$$

This is equivalent to using $W_j(x,y) = \delta(x-x_j,y-y_j)$, that is, a Dirac delta function, in equation (1-16). $H_i^g(x_j,y_j)$ is the ith trial function at the jth space point. For an N mode expansion one uses N such points.

An article by Kaplan in 1966 (23) is an excellent review of methods and developments to that time.

At that point, the use of space-energy synthesis for fast reactors was just beginning. To properly discuss the work done in that area, we will first expand upon the philosophy and theoretical basis for the various choices of trial and weight functions.

1.3 Discussion of the Synthesis Method

1.3.1 The Modal Expansion

The modal expansion and trial and weight functions have been formally introduced in sections 1.1.1 and 1.1.3. The purpose of this section is to give some meaning to the framework developed there. Thus, it includes a number of physical arguments for particular choices of trial and weight functions as well as a survey of the usage and relative success these methods have enjoyed.

One simple way of viewing the expansion of flux in modes, and one which suggests many applications, is to consider it as an interpolation procedure. Thus, if the energy dependent flux at point A has one spectral shape and that at a nearby point B has a different shape, it seems reasonable that the flux at points between A and B should be expressable as a linear combination of these two shapes. This idea is not restricted to a space-energy expansion. For example, for a system using two axial regions such as is illustrated in Figure 1.1, an expansion of the form of equation (1-15) can be used, where there is an $H_i^g(x,y)$ to represent each axial region.

Another method which suggests interpolation is the superposition of spectra which are characteristic of material compositions which bracket the actual composition (44). Two core spectra, with and without sodium present, have been used in sodium voiding calculations (24).

From a mathematical point of view, the expansion of equation (1-1) can be considered as a statement that the vector $\phi(r,E)$ is the linear sum of vectors $f_i(E)$, with combining coefficients $a_i(r)$. The symmetry of the expansion obviously allows one to exchange the positions of the f_i and a_i, but the form expressed will be useful here. In principle, the $\phi(r,E)$ are vectors in an infinite dimensional vector space. In practice, since 26-group cross sections and fluxes are used in this study, this has been reduced to

a 26-dimensional energy space. In equation (1-1), if N = 26 and the $f_i(E)$ are any 26 linearly independent vectors, the equation can be satisfied exactly. The statement of equality with N=2, as in the paragraph above, is a statement that $\phi(r,E)$ is coplaner with the two $f_i(E)$ in the 26 dimensional space. In general, any expansion in N independent vectors in a J-dimensional space, where $N < J$, restricts the $\phi(r,E)$ to an N-dimensional subspace. This mathematical approach is useful in suggesting techniques and other areas of application, but the choice of the number of modes to use and what to use as modes is made chiefly on the basis of experience and on physical grounds. As the number of independent modes increases, the accuracy of the expansion increases but the calculational costs also increase. Some compromise must be reached on the basis of acceptable accuracy and cost.

1.3.2 Trial Functions

In general, the most important choice is that of trial functions or modes. If the expansion is exact, the choice of weight functions is irrelevant, as long as they are linearly independent. A number of methods have been proposed to supply trial functions.

One choice is to use fundamental mode or infinite medium fluxes for the material regions (43, 54). Here a zero-dimensional multigroup calculations gives the infinite medium flux characteristic of the material. Then the expansion (1-1) will be in terms of the infinite medium fluxes

of the region and of neighboring regions and perhaps other spectra. Infinite medium fluxes are obviously best where regions are large. An improvement on this which helps for small systems is to add to the absorption term to account for leakage from the system. Specifically, one adds $D_i B^2$ to the ith group absorption where D_i is the diffusion coefficient and B^2 is the buckling or curvature of the flux (43, 28).

In the above, zero dimensional calculations provided trial functions for one dimensional calculations. An obvious extension of this is to use one dimensional calculations to provide fluxes which can be used as modes for a two dimensional calculation. This study uses that technique.

A physically meaningful method is to use the neutron current from a fueled to a non-fueled region as a source term in the non-fueled region (42, 43). Then a solution of the multigroup equations with this source produces a spectrum to represent the non-fueled region.

For thermal calculations, a Maxwellian plus an infinite medium spectrum for the fueled region has proved useful (7, 40).

The fission spectrum has been used as one of the trial functions in fast reactor synthesis (33). Other functions that have been used are scattering spectra, namely, the inelastic scattering spectrum (39) and spectra produced by inelastic plus elastic scattering (33).

A calculation for a mixture of two adjacent material regions has been used (11) to produce a spectrum characteristic of their interface.

Finally, a number of schemes have been presented for producing improved modes by iterative processes (54, 27). This iteration is to alternatively solve for $a_i(r)$ and then for new $f_i(E)$, etc. Suppose one makes a modal calculation for the $a_i(r)$ for a system, using an initial set of $f_i(E)$. Then one assumes a new (unknown) energy dependence, $f_i'(E)$, and substitutes the expansion $\phi(r,E) = \sum_{i=1}^{N} a_i(r) f_i'(E)$ into the diffusion equation. Multiplying this by a spatial weighting function $w_j(r)$ and integrating over space and requiring equality, one has an equation. Again, one needs N such equations and thus N weighting functions. Solving these equations produces the improved set of trial functions $[f_i'(E)]$.

Lancefield (27) uses this type of scheme in transport theory. The paper by Cockayne and Ott (11) uses a similar procedure for producing a trial function to represent the interface between two regions. A modal calculation produces the $a_i(r)$ using two trial functions which represent the two regions. Reconstructing the group fluxes, $\phi_g^{(r)}$, one calculates $f_g(r,r_i) = \frac{\phi_g(r)}{\phi_g(r_i)}$ where r_i is the interface position. Substituting $\Phi_g(r) = \psi_g(r_i) f(r,r_i)$ into the diffusion equation and integrating over space, using the group diffusion kernel as a weighting function, gives an equation in $\psi_g(r_i)$,

an element in the desired trial function for the interface. This calculation appears to be quite successful.

In this paper, the modes will be fluxes from one dimensional multigroup calculations. These should be good since they fit the problem. Thus, this paper examines the question of what accuracy can be achieved with a variety of methods, given good modes.

There are a number of reasons for making this choice. First, there have been a number of successes in producing trial functions for material regions and the last paper above (11) appears to be successful in producing interface trial functions. Thus the emphasis on other areas of investigation.

Second, the competing method is the few group calculation. The development of the multigroup method as a special case of the weighted residuals approach in Chapter II [equations (2-11) to (2-16)] points out that the use of fluxes from a many group calculation to average (collapse) cross sections for a few group calculation is exactly parallel to using these fluxes as trial functions in a modal calculation. Another comparison might use zero dimensional calculations to produce fluxes for both uses.

Finally, this paper will present two dimensional calculations. The use of a one dimensional multigroup calculation to produce trial functions for the two dimensional calculations is a reasonable extension of the method.

1.3.3 Weighting Functions

The choice of weighting functions appears to be something of an art, the choice resting upon experience, areas of emphasis in the problem being studied, and availability.

Developments from variational principles have used adjoint weighting. The adjoint flux is also called the adjoint function or importance function (25). If the multigroup diffusion equations are written in the form $\bar{\bar{M}}\bar{\phi} = 0$, the adjoint equations are written $\bar{\bar{M}}^{+}\bar{\phi}^{+} = 0$, where $\bar{\phi}^{+}$ is the adjoint flux, $\bar{\bar{M}}^{+}$ is the adjoint operator defined by

$$\int \bar{u}\bar{\bar{M}}\bar{v}\, dV = \int \bar{v}\bar{\bar{M}}^{+}\bar{u}\, dV$$

where u and v are vectors which have the same boundary conditions as ϕ and ϕ^{+}. Further development establishes that M^{+} is just the transpose of the M matrix. Thus, one can obtain ϕ^{+} from a standard multigroup diffusion code by interchanging cross sections. For example, $\Sigma_s(1\rightarrow 2)$ becomes $\Sigma_s(2\rightarrow 1)$ and $\chi_3(\nu\Sigma_f)_4$ becomes $\chi_4(\nu\Sigma_f)_3$, etc., where the numbers signify groups. The adjoint flux is called the importance function because the group adjoint flux at a point is proportional to the reactivity change per neutron per second introduced at that point, that is, it is the importance of these neutrons to reactivity.

The developments using variational principles have the strongest theoretical basis. Briefly, this basis is as

follows. If R and S are continuous functions which have the same boundary conditions as the flux and its adjoint, a functional, F(R,S), is written which is stationary only if R and S are the flux and its adjoint. That is, a functional is written which has the diffusion equation and its adjoint equation, or alternatively the P-1 equations and their adjoints, as its Euler-Lagrange equations.

Then, this functional is applied to the class of functions of the modal expansion form and stationary conditions for this class are obtained. The resulting equations are of the same form as obtained by the weighted residuals approach used in this paper, with the weight functions being the functions in which the adjoint was expanded. This is by no means a total endorsement of adjoint weighting for at least a couple of reasons. First, in going to the approximate expansion, one obtains a best method of using this set of expansion functions but no insight on how to choose the energy functions in which to expand fluxes and adjoints. Second, the notion of an adjoint or importance function for a particular flux has meaning only if the whole system is specified. Thus, an adjoint from one system may not fit another system. For these reasons, and also because of the extra calculation involved, other choices of weighting functions have been made.

Another choice which is often made is to use the modes or trial functions as weighting functions. This is called

Galerkin weighting (20). This is convenient since no extra calculations are required. For many purposes Galerkin weighting has been found to give accuracy comparable to that from adjoint weighting so that the extra calculational effort was not worthwhile. Whether the choice is reasonable depends upon the accuracy obtained.

A recent addition to weighting methods is reaction rate weighting (43). Here the trial function times some appropriate cross section is used as the weight function. The notion behind this use is that reaction rates such as absorption, or fission, or power are usually the meaningful quantities one wishes to obtain from a calculation. Thus, weighting heavily where these reaction rates are large should optimize the accuracy in these quantities.

Some other methods have been suggested and used. One is to use weight functions which are not continuous in energy (13, 55, 42). For example, for an N trial function problem, one might break the energy range into N intervals and let the weight function W_i be one over the ith interval and zero outside it. For that matter, the W_i could have a shape within the interval, perhaps that for the region average flux, and be zero without. These are the so-called group or group balance and weighted group (balance) weightings, respectively.

One could also require equality at a single energy point (a fine energy group, in practice) which is called spot balancing.

Suggested references for weighting methods are Kaplan (22, 23) and Neuhold (42, 43), the latter in space-energy synthesis. The paper by Neuhold and Ott (43) also contains comparative studies in space-energy synthesis.

1.4 Survey of Fast Reactor Synthesis Method

The first application of space-energy synthesis to fast reactors appears to be that of Storrer and Chaumont (52) in 1966. Another early usage was by Stacy (51) in 1967. Ombrellero and Federighi had earlier treated the fast neutron spectrum in a thermal reactor (12, 45).

The choice of weight functions has followed previous development, with adjoint and Galerkin weighting having the greatest usage. Neuhold and Ott (43) introduced the use of reaction rate weighting. This has been further investigated by Neuhold (42) and used by Cockayne and Ott (11). Group (balance) weighting, which corresponds to region balance weighting in space-space synthesis, has seen limited usage (13, 55).

The paper by Neuhold (42) examines the choice of interface weighting functions using two continuous trial functions and a variety of weight functions. This includes using different weighting at the interface than in the regions. His results are rather inconclusive. One suspects this is at least partially due to the lack of spectral variation in his system.

The application of the synthesis expansion to transport theory was suggested much earlier (9), but first applied by Lancefield (27) in 1969. A recent paper (40) also examines this usage for thermal calculations. Lancefield also iterates between solving for space and energy functions, following Toivanen (54).

The use of spatially discontinuous trial functions is limited (24, 44, 27). Lancefield (27) has made a limited introduction to transport theory. A paper by Kiguchi et al. (24) achieves reasonable results. They expand the current at interfaces in terms of trial functions and equate the currents on each side to this expansion, following Buslik (8). Their results appear good but their reactor model has a small spectral variation and is probably not a sufficient test. There is some question regarding the interface treatment. It is difficult to see how introducing an intermediary, for which one must provide trial functions, can increase accuracy.

Ombrellaro (44) makes use of discontinuous trial functions, including use in his method which divides the energy range into a few intervals and then uses two overlapping groups in each interval. His usage is restricted to spatially continuous weight functions.

There is a rather extensive body of literature concerning synthesis methods with discontinuous trial functions. A major portion of it concerns the development of variational

methods which can handle the discontinuities. This is summarized in a review article by Stacy (50). The original paper by Wachspress and Becker (58) includes the interface conditions as part of the functional. Their choice of treatment led them to believe that a functional which produces second order diffusion equations as its Euler-Lagrange equations could not be used and that the functional must be written to produce the first order P-1 equations. This has since been shown to be unnecessary (26). Buslik (8) has included the interface conditions by use of Lagrange multipliers. Kiguchi, et al. (24) use this general method and present some numerical results, their improvement in Buslik's method is their admitting of different sets of current expansion functions at different interfaces.

There is also a group of theoretical papers discussing the proper treatment at trial function interfaces (2, 34, 57, 50). These address themselves to the question, given different weight functions on opposite sides of an interface, what are the proper weight functions to be used at the interface? A number of investigators (44, 55) have avoided the issue by using spatially continuous weight functions. Staggering of discontinuities has been suggested (16). This will be discussed further in section 5.3.3. Becker (3, 4) has discussed the choice of weight functions at the interface in terms of information flow. His contention is that the transmitted information should be weighted

by its importance in the region in which the information is to be used. This appears to be verified in section 5.2.5.

Multi-dimensional space-energy synthesis has been introduced by Lorenzini and Robinson (34) and their method has been further evaluated by Greenspan (13).

1.5 Objectives of This Study

The basic motivation of the present study is to develop and evaluate space-energy synthesis for multi-dimensional calculations. As noted in the previous section, multi-dimensional calculations have seen examination in two papers (34, 13). Both of these are based on the development by Lorenzini and Robinson, which adapts the synthesis equations (1.4) to solution by standard multigroup codes. The examination has been limited to spatially continuous trial functions using Galerkin and group weighting. Interface conditions have been limited to a single functional form.

The above method has given very encouraging results. However, further work was considered necessary for a number of reasons. First, the solution of synthesis equations by standard multigroup codes has proven less than satisfactory, primarily due to convergence problems arising from the large upscatter terms inherent to overlapping groups. Second, the class of problems that has been treated is very limited. In particular, only two weighting methods have been used, only a single functional form of interface condition has been

investigated, and the above method is limited to spatially continuous trial functions.

It should also be noted that there is a scarcity of papers which compare various weighting methods (42, 43). A second observation is that the typical reactor model chosen is very simple, very often a two region slab, and exhibits little spectral variation.

Thus, the present paper has as its objectives:

1. The development of very general one and two dimensional codes which are highly convergent.
2. To make a comparative study of various weighting methods and to develop and evaluate various interface conditions using these codes, including spatially discontinuous modes.

II. DEVELOPING THE METHOD

2.1 Development in a Homogeneous Medium

A brief development of the modal method from a weighted residuals approach has been made in Chapter I. This was done there to allow a meaningful discussion of the literature. For the sake of ease in using this chapter, the equations will be repeated here.

This development is restricted to diffusion theory. Since the material interfaces are to be treated separately, this section will concern itself with the diffusion theory for a homogeneous medium (5),

$$-D(E)\nabla^2\phi(r,E) + \Sigma_t(E)\phi(r,E) = \frac{1}{\lambda}\chi(E)\int_0^\infty \nu\Sigma_f(E')\phi(r,E')dE' + \int_0^\infty \Sigma_s(E'\to E)\phi(r,E')dE \tag{2-1}$$

This is an approximation to the Boltzmann Transport Equation (5, 10) when the directional flux is isotropic.

In this equation and in the rest of the chapter the vector notation $\vec{r}$ has been dropped. The symbol r will represent any linear dimension in rectangular, cylindrical or spherical coordinates. The position vector notation will be applied later in the chapter on two-dimensional results.

The basic premise of space-energy synthesis is that one can represent the energy dependent flux by superposition of a few energy functions

$$\phi(r,E) \approx \sum_{i=1}^{N} a_i(r) f_i(E) \tag{2-2}$$

where these functions, $f_i(E)$, are obtained from physical considerations and are not members of the usual orthogonal sets used in expansions.

Substituting (2-2) into (2-1) gives an approximation which is generally not soluble in that form.

$$\sum_{i=1}^{N} [-D(E) f_i(E) \nabla^2 a_i(r) + \Sigma_t(E) f_i(E) a_i(r)] = \sum_{i=1}^{N} [\frac{\chi(E)}{\lambda} \int_0^\infty \nu\Sigma_f(E') f_i(E') dE' a_i(r) + \int_0^\infty \Sigma_s(E' \to E) f_i(E') dE' a_i(r)] \tag{2-3}$$

The development of this paper follows the method of weighted residuals (23). Using this method, one multiplies equation (2-3) by a weight function, $g_j(E)$, integrates over E, and requires equality. One notes that, in common with the multigroup development, this removes the energy dependence from the equation. This process results in the equation:

$$\sum_{i=1}^{N} [-D_{ji} \nabla^2 a_i(r) + \Sigma_{t_{ji}} a_i(r)] = \sum_{i=1}^{N} [\frac{\chi_j}{\lambda} (\nu\Sigma_f)_i a_i(r) + \Sigma_{s_{ji}} a_i(r)] \tag{2-4}$$

where

$$D_{ji} = \int_0^\infty g_j(E) D(E) f_i(E) dE \tag{2-5}$$

$$\Sigma_{t_{ji}} = \int_0^\infty g_j(E)\,\Sigma_t(E)\,f_i(E)\,dE \qquad (2\text{-}6)$$

$$\chi_j = \int_0^\infty g_j(E)\,\chi(E)\,dE \qquad (2\text{-}7)$$

$$(\nu\Sigma_f)_i = \int_0^\infty \nu\Sigma_f(E')\,f_i(E')\,dE' \qquad (2\text{-}8)$$

$$\Sigma_{s_{ji}} = \int_0^\infty dE\; g(E) \int^\infty dE'\,\Sigma_s(E'\rightarrow E)\,f_i(E') \qquad (2\text{-}9)$$

Using N weight functions leads to N coupled equations which can be expressed in matrix form

$$-\bar{\bar{D}}\nabla^2\overline{a(r)} + \bar{\bar{\Sigma}}_t\,\overline{a(r)} = \frac{1}{\lambda}\,\bar{\bar{S}}\,\overline{a(r)} + \bar{\bar{\Sigma}}_s\,\overline{a(r)} \qquad (2\text{-}10)$$

where $S_{ji} = \chi_j\,\nu\Sigma_{fi}$ and otherwise the symbols are as defined above. $\overline{a(r)}$ is a column vector of the $a_i(r)$.

2.1.1 The Multigroup Method as a Special Case

Digressing at this point, the complete generality of the method is noted. The $f_i(E)$ and $g_j(E)$ are completely arbitrary at this point in the discussion. For example, the multigroup formulation results if one makes a proper choice of $f_i(E)$ and $g_i(E)$. In this case the $f_i(E)$ are an appropriate normalized spectrum over which to average cross sections within the energy interval and zero outside the interval. Defining these,

$$f_i(E) = \Gamma_i F_i(E) = \frac{\Gamma_i \Phi(E)}{\int_{\Delta E_i} \Phi(E)\,dE} \qquad (2\text{-}11)$$

where Γ_i is one over the ith interval and zero outside and $\Phi(E)$ is the non-normalized averaging spectrum. The weight

function is $g_j(E) \equiv \Gamma_j$. Thus,

$$\Sigma_{t_{ji}} = \int_0^\infty \Gamma_j \Gamma_i \Sigma_t(E) F_i(E)\,dE = \delta_{ji} \int_{\Delta E_i} F_i(E) \Sigma_t(E)\,dE \tag{2-12}$$

where δ_{ji} is the Kronecker delta function. Similarly,

$$D_{ji} = \delta_{ji} \int_{\Delta E_i} D(E) F_i(E)\,dE, \tag{2-13}$$

$$\chi_j = \int_{\Delta E_j} \chi(E)\,dE, \tag{2-14}$$

$$(\nu\Sigma_f)_i = \int_{\Delta E_i} \nu\Sigma_f(E') F_i(E')\,dE', \tag{2-15}$$

$$\Sigma_{s_{ji}} = \int_{\Delta E_j} dE \int_{\Delta E_i} dE' \Sigma_s(E' \to E) F_i(E') \tag{2-16}$$

and equation (2-4) becomes

$$-D_{jj}\nabla^2 a_j(r) + \Sigma_{t_{jj}} a_j(r) = \frac{\chi_j}{\lambda} \sum_{i=1}^{N} (\nu\Sigma_f)_i a_i(r) + \sum_{i=1}^{N} \Sigma_{s_{ji}} a_i(r) \tag{2-17}$$

which, with the above definitions, is precisly the multigroup formulation. Furthermore, multiplying through equation (2-2) with the multigroup $g_j(E)$ and integrating over E yields

$$a_j(r) = \int_{\Delta E_j} \phi(r,E)\,dE \tag{2-18}$$

or just the usual definition for the multigroup flux.

2.1.2 Further Development

Returning to the main development in equations (2-4) to (2-10), one notes that the D and $\sum_t$ matrices are full, rather than being diagonal as in the multigroup formulation [equation (1-17)]. Equations of this form have been developed using this general method (43, 51), and by variational principles (9, 24). Beyond this point treatments vary. Equation (2-10) has been solved analytically for simple cases (43), solved numerically in the above form (24), and manipulated into a form suitable for standard diffusion theory codes (34).

Multiplying through (2-10) by the inverse of the D matrix, yields a form in which the identity matrix replaces the D matrix.

$$-\bar{\bar{I}}\nabla^2 \overline{a(r)} + \overline{\overline{\sum_t'}}\ \overline{a(r)} = \frac{1}{\lambda}\overline{\overline{S'}}\ \overline{a(r)} + \overline{\overline{\sum_s'}}\ \overline{a(r)} \qquad (2\text{-}19)$$

Combining the scattering and total cross-section matrices, one obtains a form which is used extensively in this paper, namely

$$-\bar{\bar{I}}\nabla^2\overline{a(r)} + \overline{\overline{\sum_{st}}}\ \overline{a(r)} = \frac{1}{\lambda}\overline{\overline{S'}}\ \overline{a(r)} \qquad (2\text{-}20)$$

The primary motivation in going to this formulation is to reduce storage space and increase calculational efficiency. This will be expanded in the sections on numerical methods

(Chapter III). Obviously, the same information is contained in (2-20) as in (2-10).

Another formulation which has been used is to multiply (2-19) or (2-20) by a diagonal matrix $\overline{\overline{DI}}$ with elements

$$(DI)_{i,i} = \int_0^\infty D(E) f_i(E) dE \qquad (2\text{-}21)$$

This form was first used by Lorenzini and Robinson (34) in the context of spatially continuous modes. They adapted the form (2-19) for solution by standard multigroup codes by transfering the off diagonal terms of the $\sum_t$ matrix to the scatter matrix, leaving the necessary diagonal form. The multiplication by (2-21) was necessary to satisfy the multigroup interface conditions. This will be discussed in section 2.2.2.

The form obtained by multiplying (2-19) by $\overline{\overline{DI}}$ is

$$\overline{\overline{DI}}\nabla^2\overline{a(r)} + \overline{\overline{\sum_t''}}\ \overline{a(r)} = \frac{1}{\lambda}\overline{\overline{S''}}\ \overline{a(r)} + \overline{\overline{\sum_s''}}\ \overline{a(r)}, \qquad (2\text{-}22)$$

where $\overline{\overline{DI}}$ and $\overline{\overline{\sum_t''}}$ are diagonal matrices and $\overline{\overline{S''}}$ and $\overline{\overline{\sum_s''}}$ have the digested form explained above. This form has essentially the same storage and calculational requirements as (2-20) since it has a diagonal D matrix.

2.2 Trial Function and Material Interface Conditions

Most of the papers in space-energy synthesis have used spatially continuous trial and weight functions, that is, a single set of energy trial functions is used throughout the

problem. This is quite satisfactory for the simple two or three region problems typically used for sample calculations. However, as the complexity of the problem and the number of material regions increases, the number of trial functions which are necessary to accurately represent the flux must necessarily increase.

One dimensional multigroup codes use relatively little computer time. For two and three dimensional codes this certainly is not true. Thus, it would appear that synthesis methods will most likely find their greatest use there, where the savings can be appreciable. Spatially discontinuous modes should be especially useful in treating the additional complexity of multidimensional systems.

In either case, one wishes to keep the number of modes small to minimize calculational time and storage space. Thus, if one can expand the flux in terms of modes relevant to a particular region without having to carry those which apply to other regions, the savings in time and space will be appreciable.

The interface conditions are continuity of flux and current:

$$\phi(r^-,E) = \phi(r^+,E) \tag{2-23}$$

$$D^-(E)\nabla\phi(r^-,E) = D^+(E)\nabla\phi(r^+, E) \tag{2-24}$$

Expanding these in terms of the modes one obtains

$$\sum_{i=1}^{N} a_i(r^-) f_i^-(E) \approx \sum_{i=1}^{N} a_i(r^+) f_i^+(E) \tag{2-25}$$

$$\sum_{i=1}^{N} D^-(E) f_i^-(E) \nabla a_i(r^-) \approx \sum_{i=1}^{N} D^+(E) f_i^+(E) \nabla a_i(r^+) \tag{2-26}$$

Consistent with the treatment within a region, the method of weighted residuals is applied here. Thus, one multiplies through each of the equations by a weight function $g_j(E)$ and integrates over E and requires equality. If N different weight functions are used, these N equations of each type can be summaried in matrix form as

$$\bar{\bar{G}}\ \overline{a(r^-)} = \bar{\bar{H}}\ \overline{a(r^+)} \tag{2-27}$$

and

$$\bar{\bar{K}}\ \overline{\nabla a(r^-)} = \bar{\bar{L}}\ \overline{\nabla a(r^+)}, \tag{2-28}$$

where

$$G_{ji} = \int_0^\infty g_j(E) f_i^-(E)\, dE, \tag{2-29}$$

$$H_{ji} = \int_0^\infty g_j(E) f_i^+(E)\, dE, \tag{2-30}$$

$$K_{ji} = \int_0^\infty g_j(E) D^-(E) f_i^-(E)\, dE, \tag{2-31}$$

and

$$L_{ji} = \int_0 g_j(E) D^+(E) f_i^+(E)\, dE. \tag{2-32}$$

The generality of the method is noted. For example, one can use a different set of functions to weight the current equations from that used to weight the flux equations. In principle, the choice of weight functions is completely open.

Forms (2-27) and (2-28) are the forms used in the present paper except that one generally multiplies through by the inverse of one of the matrices so that single matrices can express the interface conditions. Thus,

$$\overline{a(r^+)} = \bar{\bar{M}}\ \overline{a(r^-)} = \overline{\overline{H^{-1}}}\ \overline{\overline{G}}\ \overline{a(r^-)} \tag{2-33}$$

and

$$\overline{\nabla a(r^+)} = \bar{\bar{N}}\ \overline{\nabla a(r^-)} = \overline{\overline{L^{-1}}}\ \bar{\bar{K}}\ \overline{\nabla a(r^-)} \tag{2-34}$$

Each $a_i(r^+)$ or $\nabla a_i(r^+)$ is thus expressed as a weighted sum of all of the $a_i(r^-)$ or $\nabla a_i(r^-)$.

2.2.1 The Multigroup Method as a Special Case

Again, the multigroup relations will be developed as a special case. The f(E) and g(E) will be the same as defined above (Section 2.1.1), with the group structure the same in all regions but the averaging spectrum, and thus the $f_i(E)$, region dependent.

Then,

$$G_{ji} = \delta_{ji} \int_{\Delta E_i} F_i^-(E)\,dE = \delta_{ji} \tag{2-35}$$

following (2-11), and similarly $H_{ji} = \delta_{ji}$. Also,

$$K_{ji} = \delta_{ji} \int_{\Delta E_i} D^-(E) F_i^-(E)\,dE = \delta_{ji} D_i^- \tag{2-36}$$

where D_i^- is just the averaged group diffusion coefficient of (2-13) and (2-17). The treatment of L_{ji} is identical. Thus one has the relations for the multigroup method

$$a_i(r^-) = a_i(r^+) \text{ and } D_i^- \nabla a_i(r^-) = D_i^+ \nabla a_i(r^+) \quad (2\text{-}37)$$

2.2.2 Method of Lorenzini and Robinson

The development by Lorenzini and Robinson multiplies through the full matrix formulation (2-10) by the inverse of the D matrix to obtain a form where the identity matrix occupies the position of the D matrix. To fit a standard multigroup code, the Σ_t matrix must also be diagonal, so the off diagonal elements of this matrix are transferred to the Σ_s matrix.

The material interface conditions are continuity of flux and current. Expanding these in terms of the modal expansions one has

$$\sum_{i=1}^{N} a_i(r^-) f_i(E) = \sum_{i=1}^{N} a_i(r^+) f_i(E) \quad (2\text{-}25)$$

and

$$\sum_{i=1}^{N} D(E,r^-) f_i(E) \nabla a_i(r^-) = \sum_{i=1}^{N} D(E,r^+) f_i(E) \nabla a_i(r^+) \quad (2\text{-}26)$$

The first is met with spatially continuous modes by $a_i(r^-) = a_i(r^+)$ for all i, which is the multigroup relation. Integrating (2-26) over energy, one has

$$\sum_{i=1}^{N} DI_{ii}^- \nabla a_i(r^-) = \sum_{i=1}^{N} DI_{ii}^+ \nabla a_i(r^+) \quad (2\text{-}38)$$

where

$$DI_{ii}^{\pm} = \int_0^{\infty} D(E,r^{\pm}) f_i(E)\, dE \quad (2\text{-}39)$$

Requiring that (2-38) be satisfied term by term provides a diagonal D matrix to fit multigroup codes. Thus, to complete this form [equation (2-22)], one multiplies the matrix form discussed in the first paragraph by $\overline{\overline{DI}}$ appropriate to the material region.

In this paper, the modes were orthogonalized. Then the term by term equality requirement proved to be a satisfactory boundary condition.

2.3 Numerical Form; The Difference Equations

For a given point in space, equations (2-20) and (2-22) can be written in the form

$$-\bar{\bar{D}}\,\nabla^2\,\overline{a(r)} + \overline{\overline{\Sigma_{st}}}\,\overline{a(r)} = \frac{1}{\lambda}\,\overline{\overline{\chi\nu\Sigma_f}}\,\overline{a(r)} \qquad (2\text{-}40)$$

with the matrices defined in that section. Thus $\bar{\bar{D}}$ may be the identity matrix or have diagonal elements $DI_{i,i} = \int D(E) f_i(E)\,dE$, depending upon the formulation. The $\overline{a(r)}$ vector is made up of the N combining coefficients at that space point.

Considering a one dimensional problem with geometry factor p (p=0 for slab, p=1 for cylindrical, p=2 for spherical geometry), the Laplacian term can be written as

$$\nabla^2 a_i(r) = \frac{1}{r^p}\,\frac{d}{dr}\left(r^p\,\frac{da_i(r)}{dr}\right) \qquad (2\text{-}41)$$

Further, consider a one dimensional space divided into a finite number of intervals. In this discussion, the space

points will be on the mesh lines between intervals. The kth space point will have intervals of length Δr_k to its right and Δr_{k-1} to its left. Substituting (2-41) into (2-40), multiplying by r^p and integrating from $r_k - \frac{\Delta r_{k-1}}{2}$ to $r_k + \frac{\Delta r_k}{2}$, one has the following for a single algebraic equation of the matrix equation.

$$-D_{ii} \int_{r_k-\frac{\Delta r_{k-1}}{2}}^{r_k+\frac{\Delta r_k}{2}} \frac{d}{dr}\left(r^p \frac{d\, a_i(r)}{dr}\right) dr + \sum_{j=1}^{N} (\Sigma_{st})_{ij} \int_{r_k-\frac{\Delta r_{k-1}}{2}}^{r_k+\frac{\Delta r_k}{2}} r^p a_j(r)\, dr = \frac{1}{\lambda} \sum_{j=1}^{N} (\chi\nu\Sigma_f)_{ij} \int_{r_k-\frac{\Delta r_{k-1}}{2}}^{r_k+\frac{\Delta r_k}{2}} a_j(r)\, r^p dr \qquad (2\text{-}42)$$

In the above, it has been assumed that the medium is homogeneous.

For the integrals in the last two terms, $a_j(r)$ is treated as a constant over the interval and denoted as a_{kj} in the numerical approximation giving

$$\int_{r_k-\frac{\Delta r_{k-1}}{2}}^{r_k+\frac{\Delta r_k}{2}} a_j(r)\, r^p dr = a_{kj} \left[\frac{\left(r_k+\frac{\Delta r_k}{2}\right)^{P+1}}{P+1} - \frac{\left(r_k-\frac{\Delta r_{k-1}}{2}\right)^{P+1}}{P+1}\right] = a_{kj}\, V_k \qquad (2\text{-}43)$$

V_k is the volume associated with the kth space point. The first term in (2-42) becomes

$$-D_{ii}r^p \frac{d\, a_i(r)}{dr}\Bigg|_{r_k-\frac{\Delta r_{k-1}}{2}}^{r_k+\frac{\Delta r_k}{2}} = -D_{ii}\left[(r_k+\frac{\Delta r_k}{2})^p\right.$$

$$\left.(\frac{a_{k+1,i}-a_{k,i}}{\Delta r_k}) - (r_k - \frac{\Delta r_{k-1}}{2})^p\right. \tag{2-44}$$

$$\left.(\frac{a_{k,i}-a_{k-1,i}}{\Delta r_{k-1}})\right]$$

This is the usual three point difference approximation for the Laplacian. It should be noted that D_{ii} is the diagonal element. If one had used a full D matrix formulation, one would have had a summation here.

Substituting (2-43) and (2-44) into (2-42) one obtains

$$\frac{-D_{ii}(r_k+\frac{\Delta r_k}{2})^p}{\Delta r_k} a_{k+1,i} - \frac{D_{ii}(r_k-\frac{\Delta r_{k-1}}{2})}{\Delta r_{k-1}} a_{k-1,i} +$$

$$\left[\frac{D_{ii}(r_k+\frac{\Delta r_k}{2})}{\Delta r_k} + \frac{D_{ii}(r_k-\frac{\Delta r_{k-1}}{2})^p}{\Delta r_{k-1}} + \right. \tag{2-45}$$

$$\left.(\Sigma_{st})_{i,i}V_k\right]a_{k,i} + \sum_{j\neq i}(\Sigma_{st})_{i,j}V_k a_{k,j} =$$

$$\frac{1}{\lambda}\sum_{j=1}^{N}(\chi\nu\Sigma_f)_{ij}V_k a_{k,j}$$

Defining

$$g_{k,i} = -D_{ii}(r_k + \Delta r_k/2)^p/\Delta r_k \tag{2-46}$$

and

$$h_{k,i} = -D_{ii}(r_k - \Delta r_{k-1}/2)^p/\Delta r_{k-1} = g_{k-1,i} \tag{2-47}$$

one can rewrite (2-45) as

$$g_{k,i}\, a_{k+1,i} + h_{k,i} a_{k-1,i} - [g_{k,i} + h_{k,i} -$$

$$(\Sigma_{st})_{i,i} V_k] a_{k,i} + \sum_{j \neq i} (\Sigma_{st})_{i,j} V_k a_{k,j} = \qquad (2\text{-}48)$$

$$\frac{1}{\lambda} \sum_{j=1}^{N} (\chi\nu\Sigma_f)_{ij}\, V_k a_{k,j}$$

Finally, if one wishes, the N equations (i=1,.....N) for the kth space point can be combined into a single matrix equation.

$$\bar{\bar{G}}_k\, \bar{a}_{k+1} + \bar{\bar{H}}_k\, \bar{a}_{k-1} + \bar{\bar{E}}_k\, \bar{a}_k = \frac{1}{\lambda}\, \bar{\bar{S}}_k\, \bar{a}_k \qquad (2\text{-}49)$$

where G_k and H_k are diagonal matrices with elements defined above in equations (2-46) and (2-47), except that as diagonal matrix elements they should be written as $(g_k)_{ii}$ and $(h_k)_{ii}$.

$$(S_k)_{i,j} = V_k (\chi\nu\Sigma_f)_{ij} \qquad (2\text{-}50)$$

and

$$(e_k)_{i,j} = (\Sigma_{st})_{ij} V_k - \delta_{ji} (g_{k,i} + h_{k,i}) \qquad (2\text{-}51)$$

This is the same form as standard multigroup codes with up-scatter except for the full Σ_t matrix and the combining of the total and scatter cross section matrices.

2.4 Producing the Input

Earlier in this chapter the various cross section matrices ($\bar{\bar{\Sigma}}_{st}$, $\overline{\overline{\chi\nu\Sigma_f}}$, $\bar{\bar{D}}$) were defined in terms of integrals over energy. In practice, one doesn't have analytical

expressions and thus uses multigroup cross sectional data. Since the cross section matrices are produced outside the diffusion program, it is possible to use very fine group structure in generating the input. This is a major strength of the method.

The input to the diffusion code is prepared by modified versions of GENERATE, which was written by Paul Lorenzini (33). The development of this section follows his development closely.

The calculations are performed in units of lethargy rather than energy, where lethargy (u) is defined as:

$$u = \ln \frac{E_o}{E} \tag{2-52}$$

where E_o is some arbitrary reference energy.

For a given material region, equations (2-5) to (2-9) and (2-37) become

$$D_{ji} = \sum_{m=1}^{M} g_j(u_m) D_m f_i(u_m) \Delta u_m \tag{2-53}$$

$$(\Sigma_{st})_{ji} = (\Sigma_t)_{ji} - (\Sigma_s)_{ji} \tag{2-54}$$

where

$$(\Sigma_t)_{ji} = \sum_{m=1}^{M} g_j(u_m) \Sigma_{t_m} f_i(u_m) \Delta u_m \tag{2-55}$$

and

$$(\Sigma_s)_{ji} = \sum_{n=1}^{M} [g_j(u_n) \Delta u_n \sum_{m=1}^{M} \Sigma_s(m \rightarrow u_n) f_i(u_m) \Delta u_m]. \tag{2-56}$$

Similarly,

$$(\chi \nu \Sigma_f)_{ji} = \chi_j (\nu \Sigma_f)_i \tag{2-57}$$

where

$$\chi_j = \sum_{m=1}^{M} g_j(u_m)\chi(u_m)\Delta u_m \tag{2-58}$$

and

$$(\nu\Sigma_f)_i = \sum_{n=1}^{M} \nu\Sigma_{f_n} f_i(u_n)\Delta u_n \tag{2-59}$$

$$(DI)_{i,i} = \sum_{m=1}^{M} D_m f_i(u_m)\Delta u_m \tag{2-60}$$

M is the number of fine groups.

There is a distinction to make at this point between point functions, such as most cross sections, defined to have a particular value for each energy or lethargy, in contrast to distribution functions, such as fluxes, which are defined as per unit energy or lethargy. Related to this, multigroup codes have a number of distribution functions integrated over lethargy or energy.

As an example of this, consider the usage of multigroup fluxes as modes. If one examines the expansion

$$\phi(r,u) \approx \sum_{i=1}^{N} a_i(r) f_i(u) \tag{2-61}$$

or its equivalent in energy units, $\phi(r,u)$ and thus $f_i(u)$ are per unit lethargy or energy. However, multigroup fluxes are defined as integrals over the group, i.e.,

$$\phi_j = \int_{\Delta u_j} \phi(u)\, du \tag{2-62}$$

Thus, if multigroup fluxes are to be used as trial functions, they must be divided by the appropriate lethargy interval.

Proper usage of ϕ_j as an element of the ith trial functions is

$$f_i(u_j) = \phi_j/\Delta u_j \tag{2-63}$$

Except for the scattering cross section and the fission fraction, the cross sections are point functions, and the multigroup values can be used in the equations above. For scattering, the multigroup cross section, $\sum_s(m\to n)$, deals with the probability of a neutron in group m being scattered into group n. Thus, it implies an integral over Δu_n. In the above equations, a distribution function, namely a probability per unit lethargy at u_n, is required. This is calculated as

$$\sum_s(m\to u_n) = \sum_s(m\to n)/\Delta u_n. \tag{2-64}$$

Similarly, the multigroup χ_i is the fraction of the fission neutrons that go into interval Δu_i. What is desired here is the fraction per unit lethargy, or

$$\chi(u_i) = \chi_i/\Delta u_i \tag{2-65}$$

2.4.1 Input for Interface Conditions

A program, MATXER, has been written to calculate the matrices M and N of equations (2-33) and (2-34). First the matrix elements of $\bar{\bar{G}}$, $\bar{\bar{H}}$, $\bar{\bar{K}}$ and $\bar{\bar{L}}$ of equations (2-27) to (2-32) are calculated with fine group input replacing the integrals.

$$G_{ji} = \sum_{m=1}^{M} g_j(u_m) f_i^-(u_m) \Delta u_m \tag{2-66}$$

$$H_{ji} = \sum_{m=1}^{M} g_j(u_m) f_i^+(u_m) \Delta u_m \tag{2-67}$$

$$K_{ji} = \sum_{m=1}^{M} g_j(u_m) D^-(u_m) f_i^-(u_m) \Delta u_m \tag{2-68}$$

$$L_{ji} = \sum_{m=1}^{M} g_j(u_m) D^+(u_m) f_i^+(u_m) \Delta u_m \tag{2-69}$$

Matrix inversion of H and L followed by matrix multiplication produces the matrices $\bar{\bar{M}}$ and $\bar{\bar{N}}$ of equations (2-33) and (2-34).

III. SOLUTION OF MULTI-DIAGONAL MATRIX PROBLEMS

3.1 Introduction

In the earlier work by Lorenzini and Robinson (33, 34), numerical instabilities arose due to the large upscattering terms inherent in the modal method, when a group by group solution method was used. The addition of discontinuous trial functions in this work has added the further complication of a complete coupling between modes at trial function interfaces. For these reasons, the simultaneous solution for all modal combining coefficients is highly desirable.

In this chapter an investigation of an equation of the form $\bar{\bar{B}}\bar{x} = \bar{s}$ is made, where $\bar{\bar{B}}$ is a multidiagonal matrix and $\bar{x}$ an unknown and $\bar{s}$ a known vector. An attempt is also made to systemize and optimize this for the case where a constant B matrix acts on a succession of s vectors to produce x vectors.

3.2 General Form and Solution Methods

Equation (2-49) is a proper starting point for the development.

$$\bar{\bar{G}}_k \bar{a}_{k+1} + \bar{\bar{E}}_k \bar{a}_k + \bar{\bar{H}}_k \bar{a}_{k-1} = \frac{1}{\lambda}\bar{\bar{S}}_k \bar{a}_k \qquad (2\text{-}49)$$

It is in numerical form, with the matrix elements a combination of cross sectional and geometrical information and the a_k vector a column vector with elements $a_{k,j}$ the combining

coefficient for mode j at the kth space point. For an iterative solution of a set of equations of this type, the terms to the left of the equal sign will be assigned to the nth iteration and those to the right to the (n-1)th iteration. This will be implied but not denoted in the following discussion. Multiplying out the right hand side of (2-49) and denoting the resultant vector by F_k (for fission source), one has

$$\bar{\bar{G}}_k \bar{a}_{k+1} + \bar{\bar{E}}_k \bar{a}_k + \bar{\bar{H}}_k \bar{a}_{k-1} = \bar{F}_k \qquad (3\text{-}1)$$

If equations of this type are stacked in a larger matrix in order of increasing k, one obtains a new matrix equation, tridiagonal in form, in which the matrix elements are themselves N by N matrices. The elements of the column vectors are column vectors with N elements each.

$$\begin{vmatrix} \bar{\bar{E}}_1 & \bar{\bar{G}}_1 & & & \\ \bar{\bar{H}}_2 & \bar{\bar{E}}_2 & \bar{\bar{G}}_2 & & \\ 0 & \bar{\bar{H}}_3 & \bar{\bar{E}}_3 & \bar{\bar{G}}_3 & \\ 0 & 0 & \bar{\bar{H}}_4 & \bar{\bar{E}}_4 & \bar{\bar{G}}_4 \end{vmatrix} \begin{vmatrix} \bar{a}_1 \\ \bar{a}_2 \\ \bar{a}_3 \\ \bar{a}_4 \end{vmatrix} = \begin{vmatrix} \bar{F}_1 \\ \bar{F}_2 \\ \bar{F}_3 \\ \bar{F}_4 \end{vmatrix} \qquad (3\text{-}2)$$

In the iteration process, one has a fission source on the right, calculated from the combining coefficients (a_i) of the previous iteration, and wishes to calculate an improved set of combining coefficients, namely the column vector of a_i at the left of the equal sign.

Block tridiagonal matrix problems such as (3-2) can be solved by Gaussian reduction - backward substitution using matrix algebra. Multiplying through the first row with E^{-1}, one has

$$\begin{vmatrix} \bar{\bar{I}} & \bar{\bar{E}}_1^{-1}\bar{\bar{G}}_1 & 0 \\ \bar{\bar{H}}_2 & \bar{\bar{E}}_2 & \bar{\bar{G}}_2 \quad 0 \end{vmatrix} \begin{vmatrix} \bar{a}_1 \\ a_2 \end{vmatrix} = \begin{vmatrix} \bar{\bar{E}}_1^{-1}\bar{F}_1 \\ \bar{F}_2 \end{vmatrix} \tag{3-3}$$

Subtracting H_2 times the first line equation from the second line equation, one puts a zero to the left of the diagonal in the second line. This process can be repeated until there are only zero elements below the diagonal and identity elements on the diagonal. Backward solution follows.

This process will not be followed here since the off-diagonal matrices in (3-2) are diagonal and it is desirable to take advantage of this. Expanding (3-2) in terms of the component matrix elements for the case of two modes yields

$$\begin{vmatrix} e_1^{11} & e_1^{12} & g_1^{11} & & & & & \\ e_1^{21} & e_1^{22} & 0 & g_1^{22} & & & & \\ h_2^{11} & 0 & e_2^{11} & e_2^{12} & g_2^{11} & & & \\ & h_2^{22} & e_2^{21} & e_2^{22} & 0 & g_2^{22} & & \\ & & h_3^{11} & 0 & e_3^{11} & e_3^{12} & g_3^{11} & \\ & & & h_3^{22} & e_3^{21} & e_3^{22} & 0 & g_3^{22} \end{vmatrix} \begin{vmatrix} a_1^1 \\ a_1^2 \\ a_2^1 \\ a_2^2 \\ a_3^1 \\ a_3^2 \end{vmatrix} = \begin{vmatrix} F_1^1 \\ F_1^2 \\ F_2^1 \\ F_2^2 \\ F_3^1 \\ F_3^2 \end{vmatrix} \tag{3-4}$$

where the matrix elements are defined in equations (2-46) (2-47) and (2-51) except that the matrix indices have been

moved to the superscript position for clarity. The two mode formulation above gives a 5-diagonal matrix. In general, an M-modal problem gives a 2M+1 diagonal matrix.

Denoting the matrix above as B, one has

$$\begin{vmatrix} b_{11} & b_{12} & b_{13} & & & & \\ b_{21} & b_{22} & b_{23} & b_{24} & & & \\ b_{31} & b_{32} & b_{33} & b_{34} & b_{35} & & \\ 0 & b_{42} & b_{43} & b_{44} & b_{45} & b_{46} & \\ & & & & & & \\ & b_{k,k-2} & b_{k,k-1} & b_{k,k} & b_{k,k+1} & b_{k,k+2} & \end{vmatrix} \begin{vmatrix} a_1 \\ a_2 \\ a_3 \\ a_4 \\ \\ a_k \end{vmatrix} = \begin{vmatrix} F_1 \\ F_2 \\ F_3 \\ F_4 \\ \\ F_k \end{vmatrix} \qquad (3\text{-}5)$$

where the vector and matrix elements have been relabeled but the symbols and function are retained, for example, a_3 is the combining coefficient of the first mode at the second space point.

It is tempting to call the $\bar{a}$ vector the flux vector. It occupies the same position as the flux vector in a multigroup calculation. In neither case it is properly a flux, the energy dependence having been integrated out. However, this is standard usage. With this terminology, the solution of a problem proceeds as follows. First a flux (a-vector) guess is made and a fission source vector (F) calculated. Then equation (3-5) is solved for a new set of fluxes (a-vector). This is used to calculate a new fission source vector. The

ratio of the new total fission source (sum of elements in the F-vector) to the old is λ. The new source is normalized to the same magnitude as the old by dividing by λ. Then the new source is used to calculate the next generation of fluxes. This source-flux iteration is continued until the fluxes are stationary and the effective multiplication factor λ attains a constant value. (More precisely, until the values of each change less than predetermined fractional amounts per iteration.)

Finding the inverse of the matrix in (3-5) by the usual direct methods is a lengthy and expensive procedure. A more expeditious procedure, in view of the large number of zero elements and the large size of the typical matrix involved, is to use a Gaussian elimination-backward substitution method or some similar method.

It is noted that the B matrix does not change for successive iterations. Thus, in following the Gaussian elimination procedure, many of the same calculations would be repeated for each iteration. A procedure has been devised, the Crout method, which saves the proper numbers such that only calculations involving the right hand side are performed after the first iteration. The method has been developed for a full matrix (17) and has also been developed for a tridiagonal matrix by a matrix factorization scheme (10). In the following section a method will be developed for multidiagonal matrices using an intuitive approach.

Readers not interested in this somewhat detailed development can proceed directly to section 3.2.2. That section includes the developed equations as well as the general algorithms for the Crout method, which can be specialized to the multidiagonal case.

3.2.1 Intuitive Development of Crout Method

Consider the matrix equation (3-5). Using Gaussian elimination and dividing the first algebraic equation by b_{11} yields

$$a_1 + b_{12}/b_{11}\, a_2 + b_{13}/b_{11}\, a_3 = F_1/b_{11} \qquad (3\text{-}6)$$

However, b_{11} will be needed in later iterations to divide a new F_1, and 1, $b'_{12} = b_{12}/b_{11}$, and $b'_{13} = b_{13}/b_{11}$ are the elements which will be used in the backward elimination. Thus we store b_{11} rather than the implied 1 in the b_{11} position and b'_{12} and b'_{13} in the b_{12} and b_{13} positions.

Proceeding to the second line, subtracting b_{21} times the first line from it yields

$$0\, a_1 + (b_{22}-b_{21}b'_{12})a_2 + (b_{23}-b_{21}b'_{13})a_3 + b_{24}a_4 = (F_2-b_{21}F'_1) \qquad (3\text{-}7)$$

where $F'_1 = F_1/b_{11}$. Similarly, removing the first element from the third line gives

$$0\, a_1 + (b_{32}-b_{31}b_{12})a_2 + (b_{33}-b_{31}b_{13})a_3 + b_{34}a_4 + b_{35}a_5 = (F_3-b_{31}F'_1) \qquad (3\text{-}8)$$

Going back to the equation for line two (3-7), one notes that b_{21} is needed to treat a new right hand side. It is stored in place of the zero in the b_{21} position. Also, one divides (3-7) by

$$b'_{22} = (b_{22}-b_{21}b'_{12}) \tag{3-9}$$

to give an equation with 1 in the b_{22} position. This equation is then used to eliminate non-zero elements below it in the second column. This equation is

$$a_2 + b'_{23}a_3 + b'_{24}a_4 = F'_2, \tag{3-10}$$

where

$$b'_{23} = (b_{23}-b_{32}b_{13})/b'_{22} \tag{3-11}$$

$$b'_{24} = b_{24}/b'_{22} \tag{3-12}$$

$$F'_2 = (F_2-b_{21}F'_1)/b'_{22} \tag{3-13}$$

Again, the stored elements are b'_{22}, b'_{23}, b'_{24} in positions b_{22}, b_{23}, and b_{24}, since they are needed in treating a new right hand side [equation (3-13)] and in the equation for the back solution (3-10).

Proceeding to the equation for line three (3-8), b_{13} is stored in its original position, since it is used in treating the right hand side. Rewriting (3-8) as

$$b'_{32}a_2 + b'_{33}a_3 + b'_{34}a_4 + b_{35}a_5 = F'_3 \tag{3-14}$$

the definition of the symbols is apparent by comparison.

Subtracting b'_{32} times equation (3-10) from this, one has

$$0\ a_2 + (b'_{33}-b'_{32}b'_{23})a_3 + (b_{34}-b'_{32}b'_{24})a_4 + b_{35}a_5 = (F'_3-b'_{32}F'_2) \tag{3-15}$$

Dividing (3-15) by

$$b''_{33} = b'_{33}-b'_{32}b'_{23} = b_{33}-b_{31}b'_{13} - b'_{32}b'_{23} \tag{3-16}$$

yields

$$a_3 + b'_{34}a_4 + b'_{35}a_5 = F''_3 \tag{3-17}$$

where

$$b'_{34} = (b_{34}-b'_{32}b'_{24})/b''_{33}, \tag{3-18}$$

$$b'_{35} = b_{35}/b''_{33}, \tag{3-19}$$

and

$$F''_3 = (F'_3-b'_{32}F'_2)/b''_{33} = (F_3-b_{31}F'_1-b'_{32}F'_2)/b''_{33} \tag{3-20}$$

Equation (3-17) is used in the back substitution and (3-20) gives the prescription for treating a right hand side. Proceeding from position b_{31} to b_{35}, the elements stored in successive positions are b_{31}, b'_{32}, b''_{33}, b'_{34} and b'_{35}.

It is now noted that the treatment of the third line is general, that is, with a five diagonal matrix, just the coefficients of the two previous lines are used in treating a given line.

Also, on examination of the prescriptions for the stored forms and treatment of the right hand side of line

three, one notes that by proceeding a line at a time and from the left in a line, the necessary elements are in stored positions. Thus, b_{31} is stored and $b'_{32} = b_{32} - b_{31}b'_{12}$ where b'_{12} is also a stored form. Similarly, $b''_{33} = b_{33} - b_{31}b'_{13} - b'_{32}b'_{23}$ involves only b_{33} and stored forms. Proceeding through (3-18), (3-19), and (3-20), this is also true.

Since the stored form and the element itself are all that are used in treating an element or right hand side, the primes will be dropped from further discussion and the term "Crouted matrix" or "Crouted element" will be used when reference is made to this stored form.

3.2.2 Algorithms of the Crout Method

The prescriptions to produce the stored (Crout) forms of a general (kth) line of a 5-diagonal matrix are summarized in the equations below. All elements on lines above the element being modified and to its left on the same line are of stored form. Thus, all elements in the equations below except the one being modified are of the stored form. A superscript "0" denotes that this has its original value.

$$b_{k,k-2} = b^0_{k,k-2} \tag{3-21}$$

$$b_{k,k-1} = b^0_{k,k-1} - b_{k,k-2}b_{k-2,k-1} \tag{3-22}$$

$$b_{k,k} = b^0_{k,k} - b_{k,k-2}b_{k-2,k} - b_{k,k-1}b_{k-1,k} \tag{3-23}$$

$$b_{k,k+1} = (b^0_{k,k+1} - b_{k,k-1}b_{k-1,k+1})b_{k,k} \tag{3-24}$$

$$b_{k,k+2} = b^0_{k,k+2}/b_{k,k} \tag{3-25}$$

The Gaussian elimination of a new right hand side with this stored form of matrix proceeds as follows, with all elements except the one being modified (denoted by the superscript O) being the stored (Crout) form.

$$F_1 = F_1^O/b_{11}$$

$$F_2 = (F_2^O - b_{21}F_1)/b_{22}$$

$$F_3 = (F_3^O - b_{31}F_1 - b_{32}F_2)/b_{33}$$

$$F_k = (F^O - b_{k,k-2}F_{k-2} - b_{k,k-1}F_{k-1})/b_{kk} \qquad (3\text{-}26)$$

Following this the backward substitution proceeds from the bottom line (index L) upward, using the implied one on the diagonal and the stored elements to the right of the diagonal.

$$a_L = F_L$$

$$a_{L-1} + b_{L-1,L}a_L = F_{L-1}$$

$$a_{L-2} + b_{L-2,L-1}a_{L-1} + b_{L-2,L}a_L = F_{L-2}$$

$$a_k + b_{k,k+1}a_{k+1} + b_{k,k+2}a_{k+2} = F_k \qquad (3\text{-}27)$$

The prescriptions for producing this Crouted matrix are just the standard Crout procedure truncated to the special multidiagonal case. The standard Crout algorithms are

$$b_{ij} = b^{O}_{ij} - \sum_{k=1}^{j-1} b_{ik}b_{kj} \quad \text{for } j \leq i, \tag{3-28}$$

and

$$b_{ij} = (b^{O}_{ij} - \sum_{k=1}^{i-1} b_{ik}b_{kj})/b_{ii} \quad \text{for } j > i. \tag{3-29}$$

This same equation applies to the flux elements, as if they occupy a column in the b matrix. Thus,

$$F_i = (F^{O}_i - \sum_{k=1}^{i-1} b_{ik}F_k)/b_{ii} \tag{3-30}$$

If equations (3-28) to (3-30) are applied to the special multidiagonal case, the equations developed there follow.

3.3 Comparisons of Calculational Effort

It is useful to consider the calculational efforts made in using the Crout method for the case of repeated calculations. Looking at the calculations of equations (3-21) to (3-25) for Crouting a general line of a 5-diagonal matrix, one has 6 multiplications plus divisions and 4 additions plus subtractions, or 10 non-repeated calculations per line. Examining the Gaussian elimination of a right hand element (3-26) and a typical back solution [equation (3-27)], one finds 5 multiplications plus divisions and 4 additions plus subtractions or 9 repeated calculations per line. A similar analysis for other multidiagonal matrices is summarized in Table 3-1.

Table 3-1. Calculations for a Multidiagonal Matrix.

M (Modes)	J-Diagonal J=2M+1	Calculations for Each Line of Matrix: Non-Repeated (Crouting Matrix) + −	x ÷	Total	Repeated − (Treat Right Hand Side and Back Soln.) + −	x ÷	Total	Total − (or Total Calculations in Standard Gauss-Elim. Back Soln.) + −	x ÷	Total
1	3	1	2	3	2	3	5	3	5	8
2	5	4	6	10	4	5	9	8	11	19
3	7	9	12	21	6	7	13	15	19	34
4	9	16	20	36	8	9	17	24	29	53
5	11	25	30	55	10	11	21	35	41	76
M	J=2M+1	M^2	M^2+M	$2M^2+M$	2M	2M+1	4M+1	M^2+2M	M^2+3M+1	$2M^2+5M+1$

Thus, a complete (including R.H.S.) first solution of a J-diagonal matrix (J=2M+1) by Crouting or Gaussian elimination plus back substitution requires $2M^2+5M+1$ calculations per line. Each further solution using the Crouted matrix requires only 4M+1 calculations. This becomes increasingly important as the number of modes increases.

Although the present problem heavily favors a multidiagonal solution of this type, a comparison of this method with the usual group by group solution is in order to determine the relative efficiency of the two methods. For a system with down scatter only, which is not the case here, the two methods will give the same result after each iteration. Upscatter will make the group by group method converge less rapidly than the simultaneous solution method.

In the comparison, both methods will be assumed to have Crouted matrices. Only the repeated calculations will be considered, since, in the usual iterative context, the original Crouting is a minor portion of the calculation.

Consider a one space dimensional problem with N space points. In a group by group (or mode by mode) solution, one has a tri-diagonal matrix problem of N lines to solve for each group. Thus, one has 5NM repeated calculations each iteration (calculations per line)x(no. of lines per matrix)x(no. of matrices). To this one must add the calculations for scatter terms, since these are outside the matrix calculations here but not for the simultaneous solution method.

For a full scattering matrix, the source term for each group (i) at each space point (k) is

$$(\text{Source})_{k,i} = (\text{Fission Source})_{k,i} + \sum_{j=1}^{M} a_{kj}(\Sigma_s)_{ji} V_k \qquad (3\text{-}31)$$

Neglecting the multiplication by V_k, since this can be factored out and performed only once, this gives 2M calculations for each line of each matrix, divided equally between addition and multiplication. The added calculations from scattering are thus (2M calculations per group-spacepoint)x (M groups)x(N spacepoints).

Thus, the total repeated calculations per iteration are $5NM+2M^2N$ or $(2M^2+5M)N$ for a group by group solution.

The number of repeated calculations per line for a multidiagonal solution is given in Table 3-1. This must be multiplied by NM, to compare to the above, since there is one line in the matrix for each mode at each space point and so NM lines in the matrix.

Table 3-2 is a comparison of the two methods. Again, both methods assume Crouted matrices. Examination of this table shows that for more than two modes the multidiagonal method requires more calculations than the group by group treatment. However, for the present type of problem, with full scattering matrices, numerical instability in group by group solution will substantially increase the number of

Table 3-2. Comparison of Multidiagonal and Group by Group Solution.

(Modes)	Diagonal	Repeated Calculations in Treating a Problem of N Space Points					
		Multidiagonal Solution			Group by Group Solution		
		+ -	x ÷	Total	+ -	x ÷	Total
1	3	2N	3N	5N	2N*	3N*	5N*
2	5	8N	10N	18N	8N	10N	18N
3	7	18N	21N	39N	15N	18N	33N
4	9	32N	36N	68N	24N	28N	52N
5	11	50N	55N	105N	35N	40N	75N
M	2M+1	$2M^2N$	$(2M^2+M)N$	$(4M^2+M)N$	$(M^2+2M)N$	$(M^2+3M)N$	$(2M^2+5M)N$

* No self scatter in 1-group calculation.

iterations for convergence and in many cases the problem will fail to converge. Here the multidiagonal solution is a judicious choice.

A discussion of the alternate group by group solution method is in order. Lorenzini and Robinson (33, 34) have had considerable problems due to upscatter. Greenspan (13) has also noted difficulties with group by group solution and suggests and uses what is basically an iteration on groups (cycling inner iterations so that each group flux is calculated successively rather than cycling to improve the spatial flux shape in group one before proceeding to group two, etc.). Another suggestion for the upscatter problem is to adopt a neutron balance scheme (33, 47, 53). Lorenzini (33) examines this for the overlapping group method.

In all these approaches there are extra calculations and convergence problems which tend to override the small calculational advantage per iteration of Table 3-2.

Computer space requirements are not a major concern for a few mode (group) problem in one dimension. Storing only the non-zero elements of the matrices, the M tridiagonal matrices require 3NM storage spaces while the multidiagonal matrix requires (2M+1)MN spaces.

3.4 Form for the Computer Code

To provide a framework on which to base the discussion of the computer code, we will use the simple system of

Figure 3-1. This has two regions, the first having two space intervals and a reflected left boundary. The second region is assumed to have a different material and a different trial function set, but the treatment is general so that either may change independently.

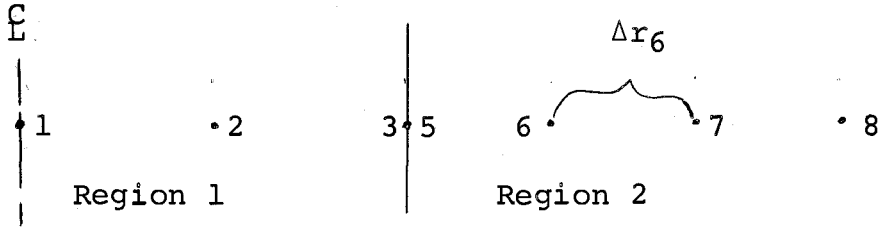

Figure 3-1. Reactor Model for Discussion of the Code.

For the general interior space point, such as 2, or 6, or 7, we use the equation obtained by integrating from one-half interval to the left of the point to a half interval to the right, namely equation (2-49) or in slightly different form (3-1).

$$\bar{\bar{G}}_k \bar{a}_{k+1} + \bar{\bar{E}}_k \bar{a}_k + \bar{\bar{H}}_k a_{k-1} = \bar{\bar{F}}_k \tag{3-31}$$

where

$$g_k^{ii} = -D_{ii}(r_k + \frac{\Delta r_k}{2})^p/\Delta r_k \tag{3-32}$$

$$h_k^{ii} = -D_{ii}(r_k - \frac{\Delta r_{k-1}}{2})^p/\Delta r_{k-1} \tag{3-33}$$

$$e_k^{ij} = (\Sigma_{st})_{ij} V_k - \delta_{ij}(g_k^{ii}+h_k^{ii}) \tag{3-34}$$

$$F_k^i = \chi_i \sum_{j=1}^{N} (\nu\Sigma_f)_j a_k^j V_k/\lambda \tag{3-35}$$

These are the matrix elements defined in (2-46), (2-47), and (2-51) and the notation is that used in equation (3-4), where the matrix indices have been moved to superscript position for clarity.

Note that points 3 and 5 in the figure are the same interface point. The index 3 will be used to refer to expansion in trial functions applicable to the region to the left of the interface and the index 5 applies to the set on the right. Index number 4 is reserved for other use in the code.

The treatment of points 1, 3, and 5 are essentially the same as that in the development of (2-49), except that the integration is over half a space interval.

Considering points 1 and 5 together,

$$
\begin{aligned}
&- \int_{r_k}^{r_k+\frac{\Delta r_k}{2}} D_{ii} \frac{d}{dr} \left[r^p \frac{d}{dr} a_i(r)\right] dr + \\
&\sum_{j=1}^{N} \int_{r_k}^{r_k+\frac{\Delta r_k}{2}} (\Sigma_{st})_{ij} a_j(r) r^p dr = \\
&\sum_{j=1}^{N} \int_{r_k}^{r_k+\frac{\Delta r_k}{2}} \chi_i (\nu\Sigma_f)_j a_j(r) r^p dr
\end{aligned}
\qquad (3\text{-}36)
$$

For the last two terms the cross sections are constant and the common integral is treated as in the development of (2-49) except that now V_k is only a half interval.

$$\int_{r_k}^{r_k+\frac{\Delta r_k}{2}} a_j(r)\, r^p dr = a_k^j \left[\frac{(r_k+\frac{\Delta r_k}{2})^{p+1} - r_k^{p+1}}{p+1}\right] = \tag{3-37}$$

$$a_k^j V_k$$

Moving D_{ii} from inside the integral sign in the first term of (3-36),

$$-D_{ii} \int_{r_k}^{r_k+\frac{\Delta r_k}{2}} \frac{d}{dr}\left(r^p \frac{da_i(r)}{dr}\right) dr = -D_{ii} r^p$$

$$\left.\frac{da_i(r)}{dr}\right|_{r_k+\frac{\Delta r_k}{2}} + D_{ii} r^p \left.\frac{da_i(r)}{dr}\right|_{r_k} = \tag{3-38}$$

$$-D_{ii}\left(r_k + \frac{\Delta r_k}{2}\right)^p \left[\frac{a_{k+1}^i - a_k^i}{\Delta r_k}\right] + D_{ii} r^p \left.\frac{da_i(r)}{dr}\right|_{r_k} =$$

$$g_k^{ii} a_{k+1}^i - g_k^{ii} a_k^i + D_{ii} r^p \left.\frac{da_i(r)}{dr}\right|_{r_k}$$

For point 1, at a reflected boundary, the derivative and the last term in (3-38) are zero. Thus, the matrix H does not appear and the h term in the E matrix is absent.

For point 5, V_5 involves a half interval and again there is no h term in the E matrix. Writing $\left.\frac{da_i(r)}{dr}\right|_{r_5} = \nabla a^i(r^+)$, we write the equation for the integral over the half interval as

$$\bar{\bar{G}}_5\, \bar{a}_6 + \bar{\bar{E}}_5\, \bar{a}_5 + \overline{\overline{D^+}}\, r_5^p\, \overline{\nabla a(r^+)} = \bar{F}_5 \tag{3-39}$$

The corresponding equation for point 3, where the integration is over a half interval to the left of the point, is

$$-\bar{\bar{D}}^{-}\, r_3^p\, \overline{\nabla a(r^-)} + \bar{\bar{E}}_3\, \bar{a}_3 + \bar{\bar{H}}_3 \bar{a}_2 = \bar{\bar{F}}_3 \tag{3-40}$$

The interface conditions in matrix form [equations (2-33) and (2-34)] are

$$\bar{a}_5 = \bar{\bar{M}}\, \bar{a}_3 \tag{3-41}$$

$$\overline{\nabla a(r^+)} = \bar{\bar{N}}\, \overline{\nabla a(r^-)} \tag{3-42}$$

Equation (3-41) will be used directly in the multidiagonal matrix solution. Equation (3-42) could also appear explicitly and did in the original code. However, for numerical efficiency equation (3-42) is substituted into (3-39) to eliminate $\overline{\nabla a(r^+)}$.

$$\bar{\bar{G}}_5\, \bar{a}_6 + \bar{\bar{E}}_5 \bar{a}_5 + \bar{\bar{D}}^{+}\, r_5^p\, \bar{\bar{N}}\, \overline{\nabla a(r^-)} = \bar{\bar{F}}_5 \tag{3-43}$$

Since $\overline{\nabla a(r^-)}$ appears explicitly in the code, it is indexed as point 4, namely

$$\overline{\nabla a(r^-)} = \overline{\nabla a_4} \tag{3-44}$$

The multidiagonal matrix for a two mode expression is shown in Figure 3-2. For simplicty of representation the following substitutions are made:

$$\bar{\bar{X}}_3 = -\bar{\bar{\bar{D}}}^{-}\, r_3^p, \tag{3-45}$$

with elements $X_3^{ii} = D_{ii}^{-} \; r_3^p$ (diagonal matrix), and

$$\bar{\bar{Y}}_5 = r_5^p \; \bar{\bar{D}}^{+} \; \bar{\bar{N}} \tag{3-46}$$

with elements $Y_5^{ij} = r_5^p \; D_{ii}^{+} \; N_{ij}$.

In the figure, all superscripts are indices relative to mode number or matrix position and subscripts refer to space points.

The large matrix on the left is 5-diagonal for the two mode expansion and 2M+1 diagonal for the M mode expansion. However, in the interface conditions, the elements M^{21} and Y_5^{21} lie outside this band. To save space, the large matrix is stored as a 5 by NM (where M = number of modes and N = number of space points) array. The two elements which lie outside this band are stored separately. The Gaussian forward elimination has a "DO LOOP" on regions so that the bulge at the interfaces can be treated correctly (outside the standard 5-diagonal treatment). Since there are only two elements to the right of the diagonal, standard 5-diagonal backward substitution is followed throughout. It was to obtain this form that $\overline{\nabla a(r^{+})}$ was eliminated.

In the M mode problem, one has full $\bar{\bar{M}}$ and $\bar{\bar{Y}}$ matrices in the 2M+1 diagonal matrix. The elements of these to the left of the diagonals in $\bar{\bar{M}}$ and $\bar{\bar{Y}}$ will lie outside the 2M+1 band. Thus, for a three mode formulation, there will be three elements from each or a total of six outside the band. Similarly, for a four mode problem, twelve elements lie outside and are stored separately.

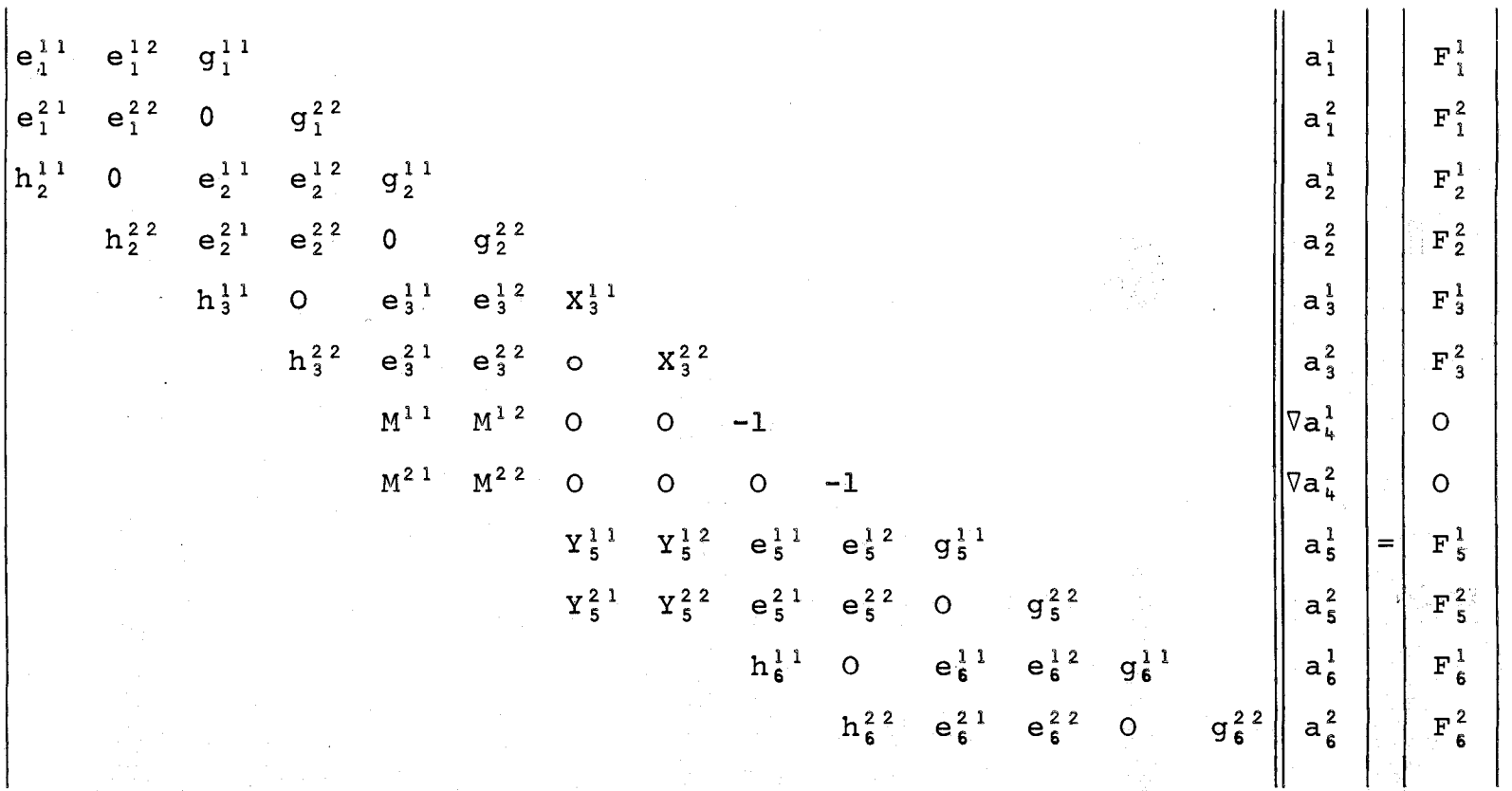

Figure 3-2. Multidiagonal Matrix for the Model of Figure 3-1 using Two Modes.

Thus, the matrix of the figure is stored in the 5 by NM array plus the extra storage for elements that don't fit. This is then "Crouted" and the resulting form stored in the same positions. Then this "Crouted" matrix is used to treat successive sources and produce fluxes (a_k^i) in the usual source-flux iteration scheme.

IV. FAST REACTORS AND FAST REACTOR PARAMETERS

4.1 The Place of Breeder Reactors in the Nation's Energy Picture

At this time, it appears that breeder reactors are destined to play an important part in this nation's energy supply starting in about 1985. This follows from the presently evolving technology of reactor systems and the available sources of energy. A recent report (41) lists the reasonably available supplies of gas and oil in the United States as sufficient for a few tens of years. Coal supplies are larger, sufficient for perhaps two hundred years, but the use of coal is under considerable pressure due to airborne pollutants and to the destructiveness of strip mining.

Uranium deposits, using the present light water reactor systems and cost criteria comparable to those used for fossil fuels above, are also sufficient for only a few tens of years.

Natural uranium has two important natural isotopes, U^{235}, with 0.711% abundance and U^{238} essentially the remainder. Only the former has cross sections which permit a chain reaction. Isotopes having this property are called fissile materials. U^{238} will also undergo fission, but only at energies above 1 MeV, and, more importantly, not with sufficient probability and efficiency at any energy to sustain a chain reaction. However, U^{238} does capture neutrons

and through radioactive decay the product of this reaction produces Pu^{239}, a fissile material. One calls U^{238} a fertile material. The production of fissile material from fertile material is called conversion, or in cases where the production of fissile material is larger than the amount of fissile material burned, breeding.

Thorium is also a fertile material, with a $Th^{232}(n,\gamma)$ reaction followed by decays producing the fissile isotope U^{233}.

The breeder reactor makes it possible to utilize a major portion of the U^{238} isotope as fuel. Since U^{238} is 140 times as abundant as U^{235}, breeding not only multiples the energy available from the uranium recoverable at a given price, but also makes the recovery of much more dilute sources of uranium economically feasible.

4.2 Fast Reactors, General

In a fast reactor most fissions are caused by fast neutrons, with typical spectra having maxima at 100 to 500 keV. This is in contrast to thermal reactors, in which most fissions are caused by neutrons which are in thermal equilibrium with the system.

Fast reactors are important because, with the exception of the U^{233} thorium system, thermal reactors will not breed. This is because, although all of the cross sections decrease to a large extent with increasing energy, capture cross

sections decrease more rapidly than fission cross sections. Thus, the capture to fission ratio decreases with increasing energy. Also, the neutron yield per fission (ν) increases slightly with energy. Thus η, the number of neutrons emitted per neutron capture in fuel, increases with energy. In general, η must be substantially greater than two for breeding, one neutron to continue the fission chain and one or more for capture in fertile material above those lost by leakage and capture in structural material, fission product poisons, coolant, etc. For Pu^{239} this increase in η is from 2.10 for thermal neutrons to 2.4 at 100 KeV and 2.7 at 500 KeV (25).

Neglecting resonances, the cross sections for a typical fuel decrease with increasing neutron energy. For example, Pu^{239} has a fission cross section of 746 barns at 0.0253 eV (thermal), while the same cross section is 1.5 barns at 500 keV. There is typically a region of sharp discrete resonances in the energy range from a few eV to a few keV. Above this is a region of broad peaks (unresolved resonances).

Neutrons produced by nuclear fission are born with a spectrum of energies, with roughly half of them born above 1.5 MeV. In a typical fast reactor there is a moderating influence due to cladding and structural materials (often stainless steel), oxygen or carbon if the fuel is in oxide or carbide form, coolant (probably sodium), as well as inelastic scatter in the fuel itself. The position and shape of

the spectrum will be a strong function of the amounts of these "moderators". This will be illustrated by the reactor models used in this study.

The typical cross section discussed above and the consequent complex shape of the flux in a system of this plus several other materials requires a considerable effort to specify in numerical form. This motivates the method under consideration. The contention is that these complex spectral shapes can be better represented by overlapping modes than by an equal number of nonoverlapping groups.

4.3 Reactor Parameters

4.3.1 Temperature Coefficient

One of the major concerns of a reactor designer is safety. Two parameters which will concern us here are the effects of a sodium void and the temperature coefficient of reactivity, primarily a Doppler broadening effect.

The temperature coefficient of reactivity is the fractional change in K_{eff} per degree temperature change. It is desirable that this number be negative, such that a power excursion is self-limiting. A major portion of this coefficient is due to Doppler broadening. Basically, as temperature increases, the motion of the nuclei increases. Since the relative velocity between the nucleus and the neutron determines the energy available for the reaction, this increased motion of the nucleus effectively broadens the

energy range of neutrons which can interact with the resonance. The area under this Doppler broadened curve (cross section vs. energy) does not change, but the probability of interaction increases because the neutron population is affected over a broader range rather than being severely depleted over a narrow range (essentially self-shielding in an energy sense).

The Doppler coefficient may be positive or negative depending upon whether the resonance affected is a fission or a radiative capture resonance. Resonances of primary interest here are the fission resonances of Pu^{239} and the capture resonances of U^{238} and sodium. Reactors are constructed to have a negative coefficient.

4.3.2 Sodium Void

A sodium void may be created by leakage or by local boiling. It affects the reactivity of the system through a number of mechanisms. These are loss of moderation, increased neutron leakage and reduced neutron absorption by the sodium. The increased leakage has a negative effect on reactivity while the reduced absorption has a positive effect. The geometry of the pancake design used as a model in this paper was proposed to provide a high leakage and high negative coefficient thereby.

The loss of moderation will result in a harder spectrum which decreases the ratio of capture to fission and causes a

positive coefficient. Also, since the typical resonances are in the range of a few eV to a few keV, loss of moderation will deplete the neutron population in the resonances. Thus the usual net Doppler coefficient, which is negative, will be partially lost with sodium voiding.

In general, Na void coefficients will be positive, i.e., loss of sodium will increase k_{eff}. There is no fully satisfactory alternative to living with this. Increased moderation to lower the effect of sodium loss and high leakage cores both lower neutron economy and give poorer breeding. Use of a coolant other than sodium is not attractive since sodium is otherwise an excellent coolant.

4.3.3 Reaction Rates

Reaction rates such as fission, absorption, capture, etc., as a function of position are of interest since they are related to quantities such as power, potential radiation damage, breeding, etc., as functions of position. All of these quantities depend upon an accurate representation of flux as a function of energy and position. This is the basic output which is desired. If the fluxes can be accurately predicted, the other quantities follow.

4.4 26-Group Calculation

A 26-group calculation is used as the exact solution to which all calculations are compared. A paper by Little *et*

al. (31) establishes the validity of this structure by comparison with calculations using much finer group structures (MC^2 and GAFGAR). The 26-group comparison calculations, for the two reactor models considered, are part of the thesis work by Paul Lorenzini (33, 34).

The group structure for these calculations is shown in Table 4-1. The cross sections data is from a Russian data set (6). The 26-group cross section set for the G.E. reactor was generated using FCC-IV (29). For the EBR-II model this set was generated by 1DX (15). For both reactor models the 26-group one dimensional calculations were made using 1DX while the two dimensional calculations were made using 2DB (30).

4.5 The General Electric Pancake Design

The fast power reactor proposed by General Electric (36) is a cylinder with a core diameter of 250 centimeters and a core height of 80 centimeters. It is designed to operate at 1000 MWe. The "pancake" design has been chosen to increase neutron leakage. Thus, when sodium is lost from the core, the increased neutron leakage will decrease the reactivity of the core. This compensates for the increase in reactivity caused by the hardened spectrum.

Figure 4-1 is a quarter geometry sketch of the reactor and Table 4-2 lists the compositions of the different

Table 4-1. 26-group Structure

Group	Energy Range	Lethargy Width
1	6.5 - 10 MeV	.48
2	4.0 - 6.5 MeV	.48
3	2.5 - 4.0 MeV	.48
4	1.4 - 2.5 MeV	.57
5	800 keV - 1.4 MeV	.57
6	400 - 800 keV	.69
7	200 - 400 keV	.69
8	100 - 200 keV	.69
9	46.5 - 100 keV	.77
10	21.5 - 46.5 keV	.77
11	10 - 21.5 keV	.77
12	4.65 - 10 keV	.77
13	2.15 - 4.65 keV	.77
14	1.0 - 2.15 keV	.77
15	.465 - 1.0 keV	.77
16	215 - 465 eV	.77
17	100 - 215 eV	.77
18	46.5 - 100 eV	.77
19	21.5 - 46.5 eV	.77
20	10.0 - 21.5 eV	.77
21	4.65 - 10 eV	.77
22	2.15 - 4.65 eV	.77
23	1.0 - 2.15 eV	.77
24	.465 - 1.0 eV	.77
25	.215 - .465 eV	.77
26	.0252 - .215 eV	1.00

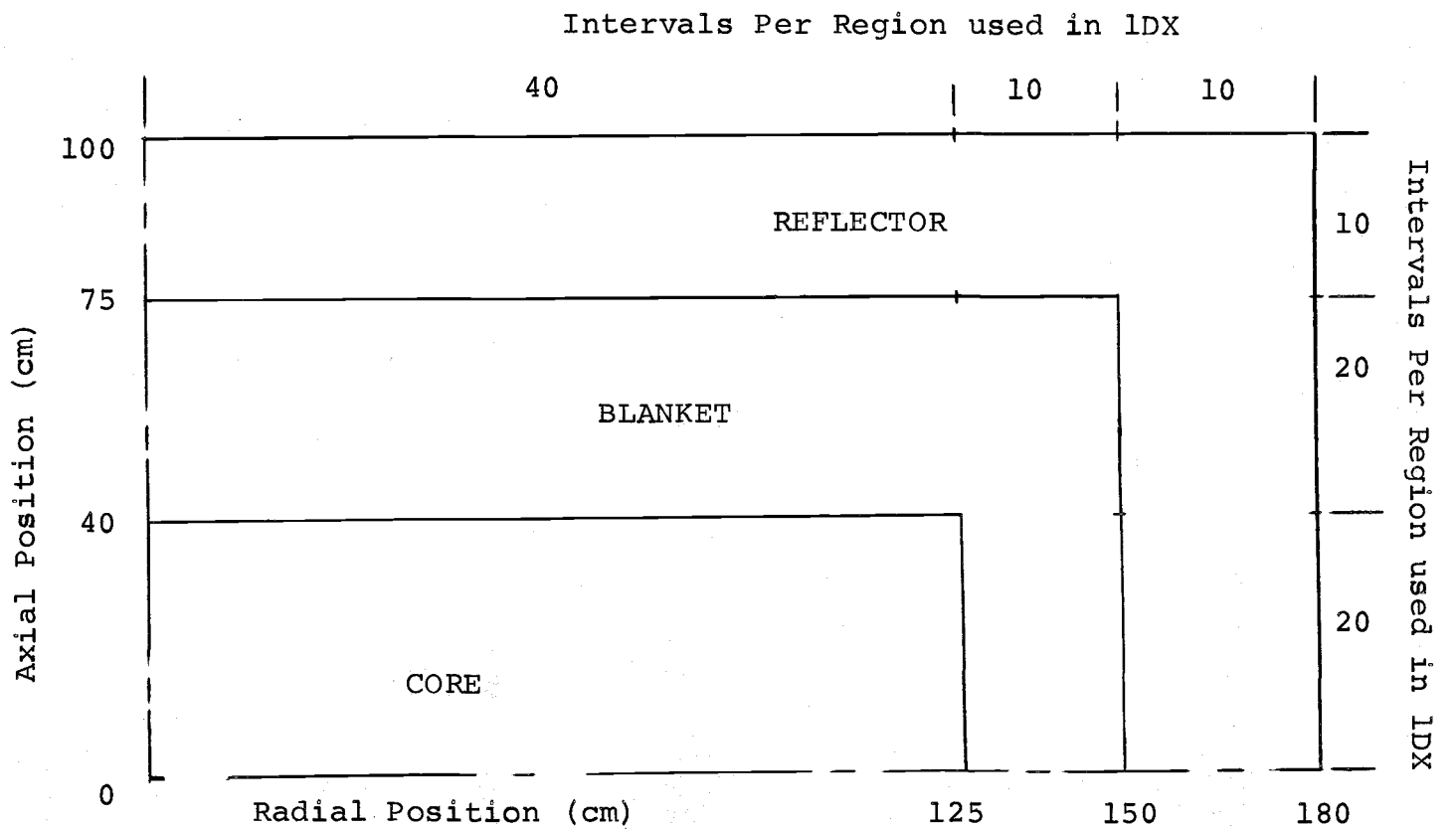

Figure 4.1. G.E. Pancake Model

material regions. Also included are the number of intervals used in each region for the one dimensional calculations.

Table 4-2. Composition of G.E. Reactor (atoms/barn-cm)

Isotope	Core	Blanket	Reflector
U^{238}	7.1303×10^{-3}	1.10×10^{-2}	
Pu^{239}	1.12×10^{-3}	2.315×10^{-4}	
Pu^{240}	5.00×10^{-4}	7.00×10^{-6}	
Oxygen	1.85×10^{-2}	2.2×10^{-2}	
Chromium	2.26×10^{-3}	3.00×10^{-3}	1.05×10^{-2}
Iron	8.90×10^{-3}	1.00×10^{-2}	4.25×10^{-2}
Nickel	1.38×10^{-3}	1.6×10^{-3}	6.6×10^{-3}
Sodium	8.01×10^{-3}	7.00×10^{-3}	6.00×10^{-3}
Tantalum	1.87×10^{-4}	3.50×10^{-5}	

The spectral variation as a function of position is of interest when one wishes to approximate the energy dependent flux by a modal expansion. Where the variation is large, one will need more modes to properly represent the flux. A plot of the energy dependent flux for several radial positions is displayed in Figure 4-2. The radial points are listed in Figure 4-1. 1DX has the flux points at the center of the space interval. For example, space point 40 is at the center of the last interval in the core. Since the interval length is 125 cm/40 or 3.125 cm, point 40 is half of this or 1.5625 cm from the core-blanket interface.

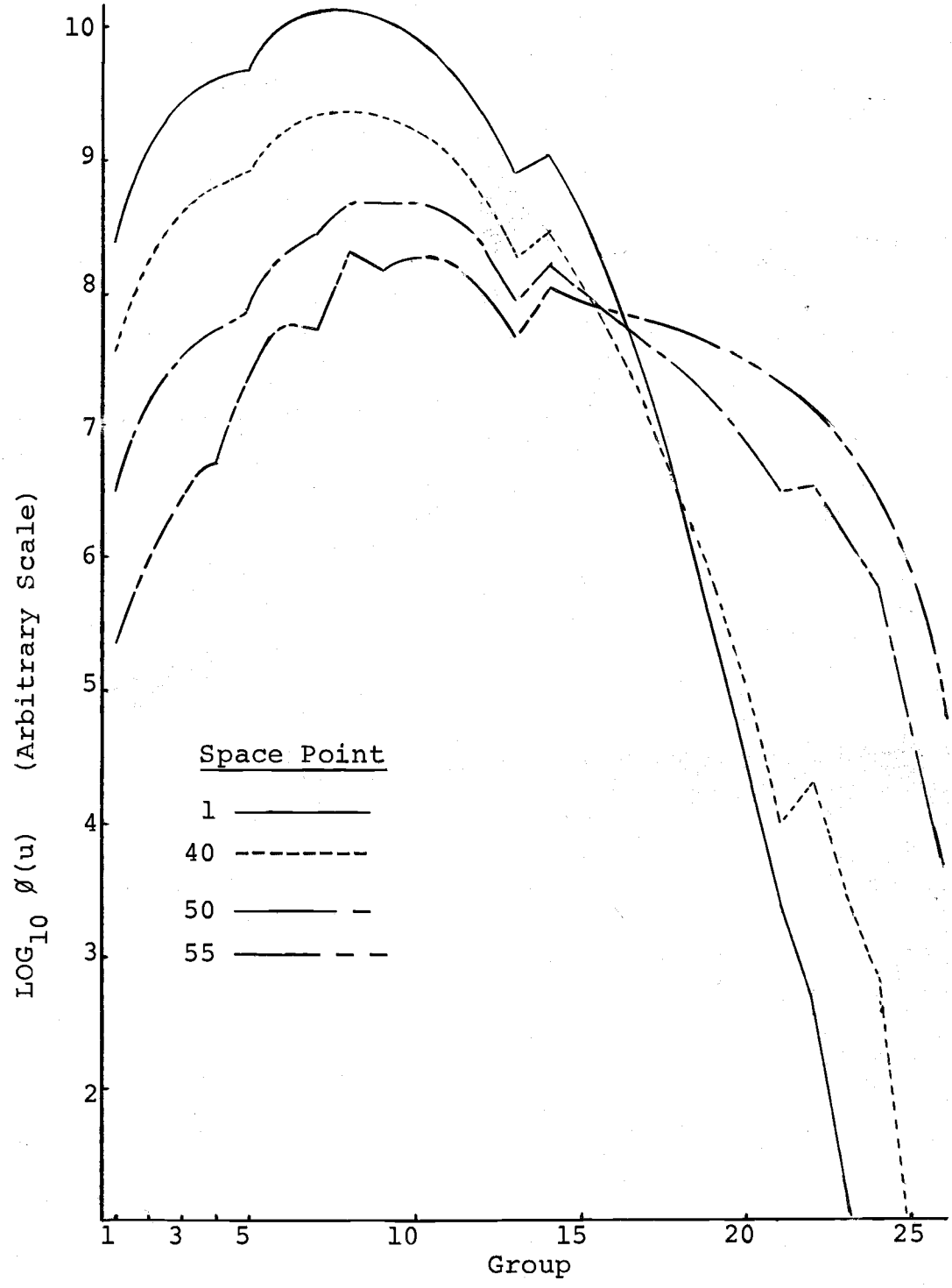

Figure 4-2. Flux Shapes for G.E. Radial Positions.

Examination of the spectral shapes in Figure 4-2 shows that there is little variation over the core. Points 1 and 40, from the center and outer edge of the core, are essentially identical over the first fifteen energy groups and not too different beyond. Approaching and entering the reflector there are appreciable changes due to its moderating influence. A plot of the variation of the spectral shape with axial position is not included since the regional compositions are identical and thus the pattern is very similar to that for the radial case. As will be demonstrated, this will allow the use of radial fluxes for axial trial functions and vice versa.

The fluxes plotted in Figure 4-2 are true fluxes, namely flux per unit lethargy interval. Reference to the energy scale of Table 4-1 helps explain the spectral structure. The flux dip in group 13 corresponds to the 3 keV absorption resonance of sodium. The flux peak in the core is rather flat over groups seven through nine or from 46.5 to 400 keV.

4-6. The EBR-II Reactor

The EBR-II (Experimental Breeder Reactor-II) is a small, fast sodium cooled research reactor (33). It has played a major role in material testing and technology development for fast reactors. It has a core diameter of 60 cm and height of 36 cm. The simplified model considered has

a radial nickel reflector next to the core and a stainless steel axial reflector, with a radial blanket of depleted uranium beyond the reflector.

Figure 4-3 is a quarter geometry sketch of the reactor and Table 4-3 lists its compositions.

Table 4-3. Composition of EBR-II Model (atoms/barn-cm)

Isotope	Core	Blanket	Nickel Reflector	Axial Reflector
U^{235}	.006727	.000089		
U^{238}	.007576	.040026		
U^{234}	.000069			
Aluminum	.019019	.001359		
Iron	.007712	.004539	.004305	.031800
Chromium	.001918	.001129	.001134	.009116
Nickel	.000839	.000494	.073557	.004030
Sodium			.003302	.010400

This reactor model presents a much more stringent test of a calculational method than the G.E. reactor. First, the sodium has been voided from the core and blanket so that one doesn't have this common moderating influence in all regions. A second influence is the reflectors next to the core which moderate and cause a large soft component in the core near these interfaces when compared with the Na voided core. Finally, the spatial dimensions are smaller. This results in a greater fractional error from the edge effects. In

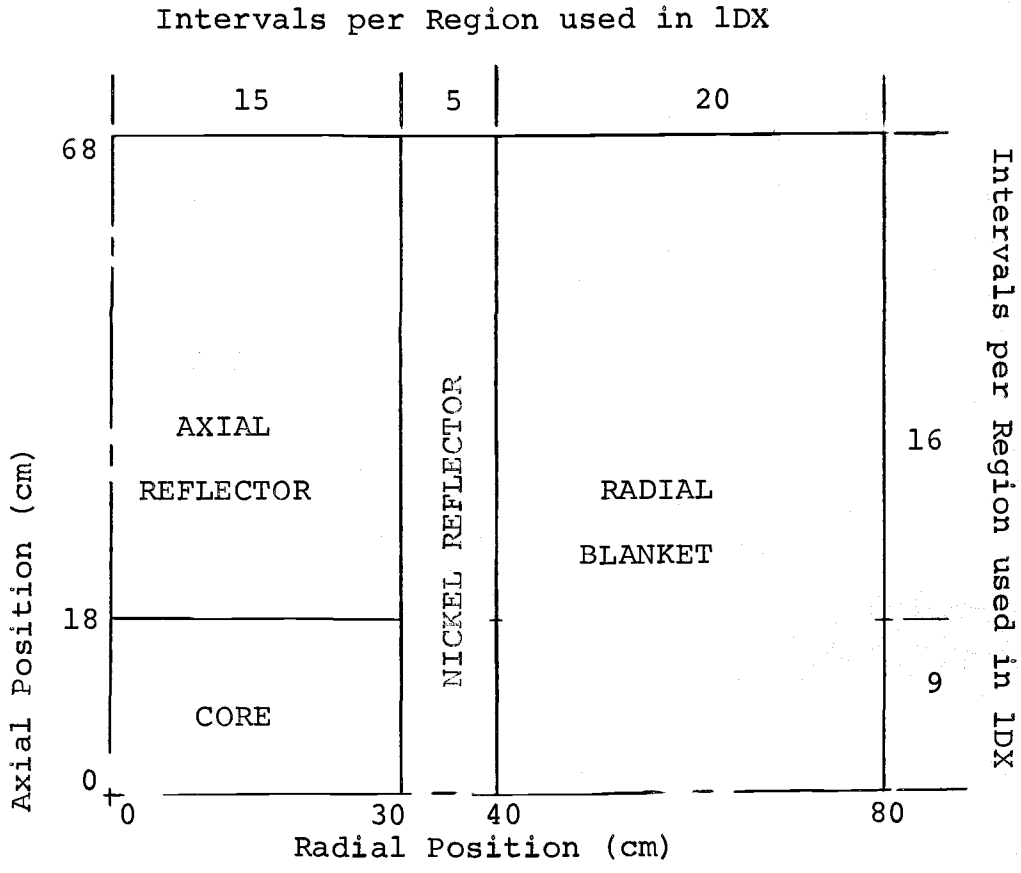

Figure 4-3. EBR-II Model

contrast, for the G.E. radial case the dimension of the core is so large that over a major fraction of the core there is little spectral variation. It is much easier to fit this pseudo infinite core region than the regions of spectral change near material interfaces. It follows that k_{eff}, which represents an integral over the core (more exactly, over the fueled region), will show a smaller fractional error since the interface contribution is a smaller fraction of the total for this case.

Figure 4-4 displays the flux shapes for several radial points. There is considerable variation over the core due to the reflector influence. The flux shows very little change in shape over the nickel reflector, with the fast flux being slightly reduced in magnitude, and the flux having essentially a constant shape. The region acts as something of a flux trap for lower energies due to the absence of uranium. In the blanket the low energies are again depleted with the U^{238} resonances becoming more prominent.

Fluxes for the EBR axial case are presented in Figure 4-5. Again, one has appreciable changes over the core due to the reflector, and large changes near the interface due to the major change in materials. For example, note group 13, which is the sodium absorption resonance at 3 keV. This is present in the reflector, but not in the core. Over the outer portions of the reflector, the changes are fairly gradual.

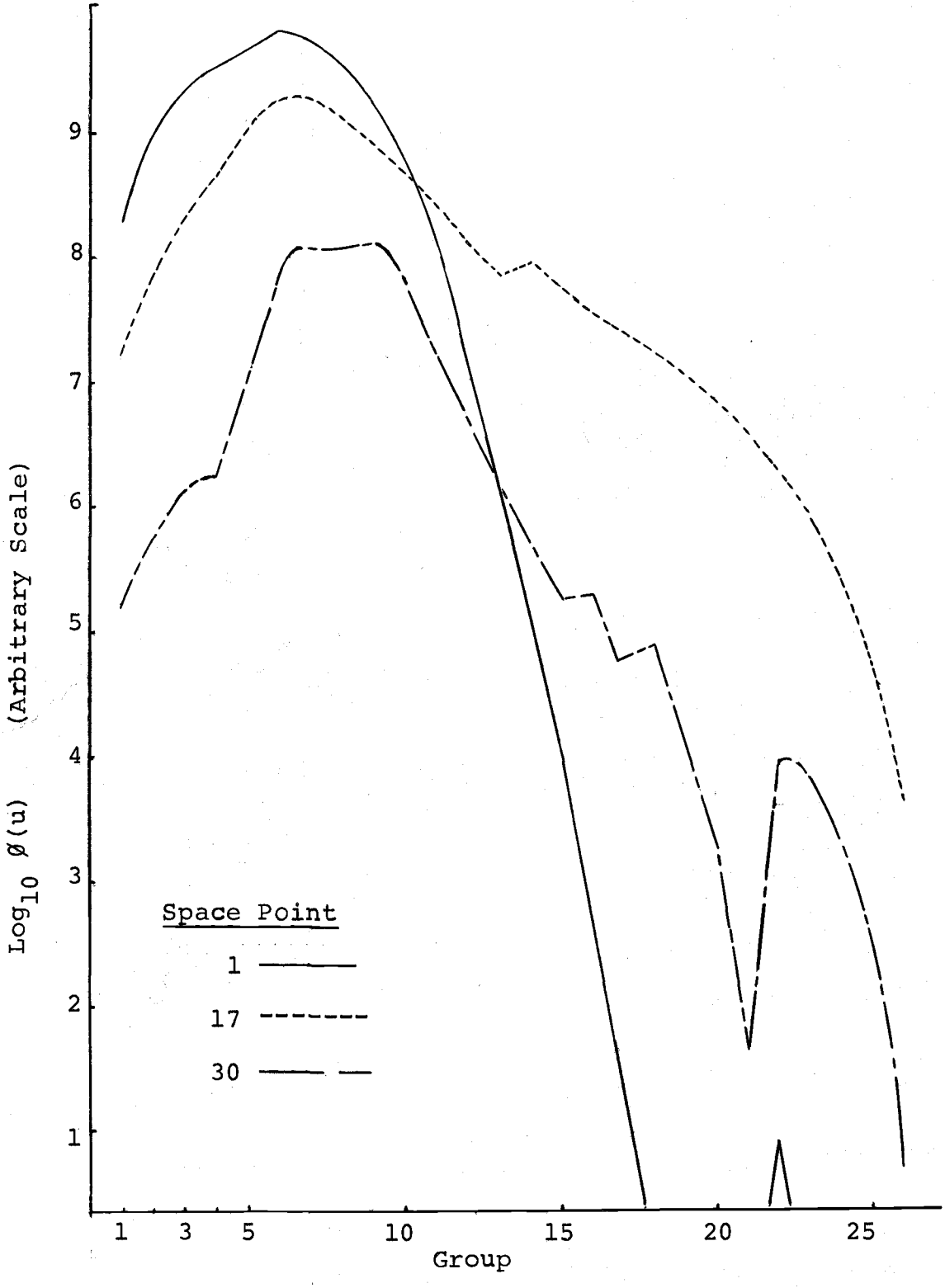

Figure 4-4. EBR Fluxes for Various Radial Positions.

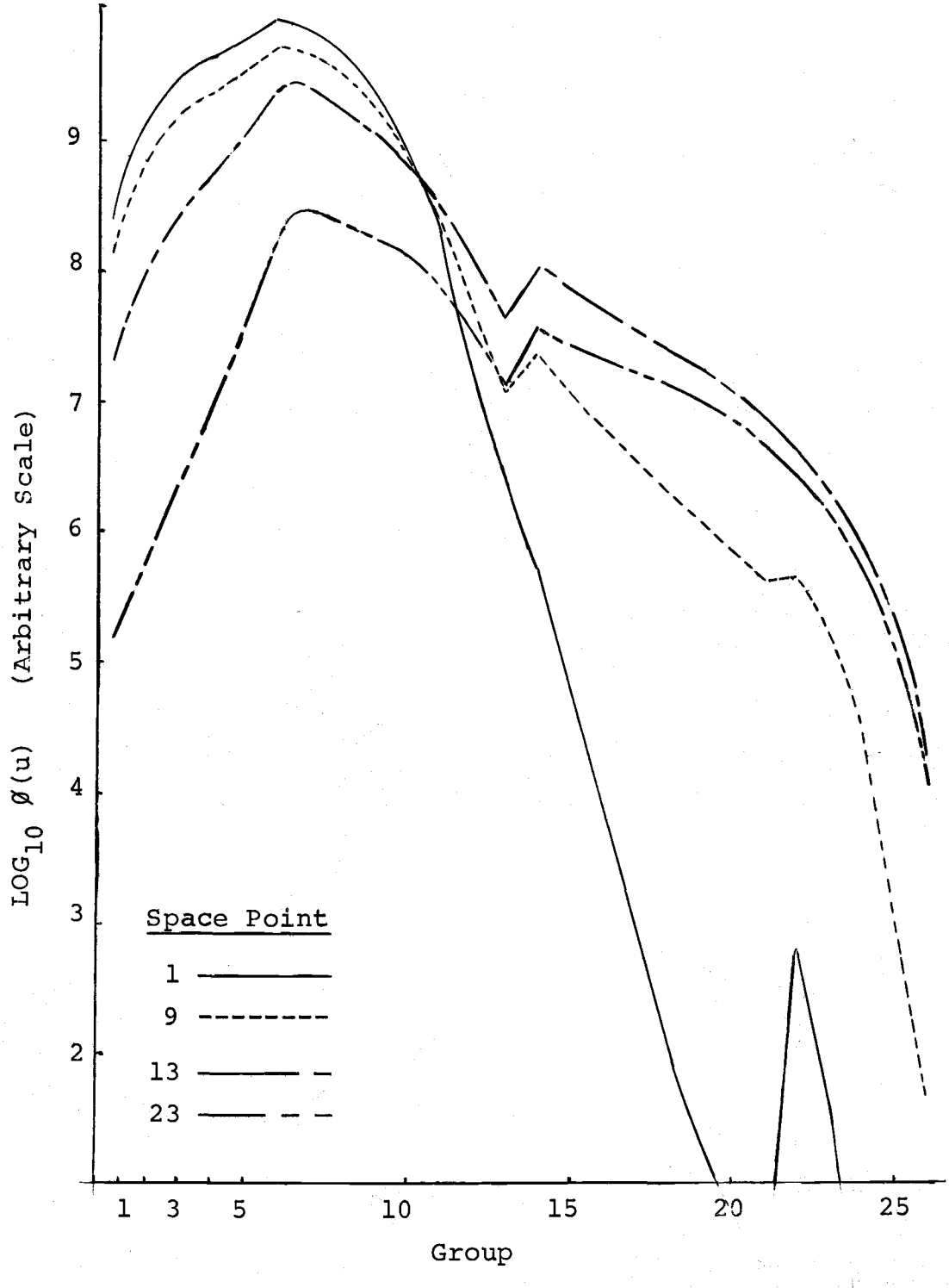

Figure 4-5. Fluxes for EBR Axial Positions.

One should finally compare the EBR-II fluxes with those for the G.E. pancake and note that the variations are much larger for the EBR-II. This is a consequence of the greater variance in moderating properties for different regions in the EBR-II.

V. ONE DIMENSIONAL CALCULATIONS AND RESULTS

5.1 Introduction

There are many parameters and functional dependencies which are of interest to the designer of a fast reactor. Among the former, the effective multiplication constant, Doppler coefficient and sodium void coefficient will be calculated here. Included in the latter are the energy dependent flux and various reaction rates as functions of position.

In this chapter, the accuracy of the modal method in calculating these quantities is investigated. Also, within the framework of the method, comparisons of the accuracies of several choices of trial and weighting functions are made. Since the principle competitive method is the few group approximation, comparisons with few group calculations are also included.

The accuracy of all methods will be assessed by comparison with a multigroup (26 group) diffusion theory calculation which will be treated as exact.

There is some question as to how to best organize the various results to produce a cohesive picture. That is, a large number of output quantities are desired and calculated. These are a function of the many choices made in producing input, namely, number of modes, choice of modes, type

of weighting function in homogeneous regions, weighting functions at interfaces, etc.

The choice has been made to divide the chapter into a series of demonstrations, with considerable cross-referencing. This is an attempt at showing cause and effect which parallels the actual investigation in many ways.

What emerges from the study is a collection of "do's" and "don'ts" to guide further use of the method. Also, it is felt that the physical understanding behind many of the mathematical concepts has been advanced. Application of the "do's" and "don'ts" is very dependent upon the physical world, namely the material changes and the consequent spectral changes for the reactor models.

5.2 Galerkin Weighting

5.2.1 Two Bracketing Modes Per Region

This investigation begins with Galerkin weighting (using the modes as weight functions). The two trial functions used in each region are fluxes from each edge of the region. The weight functions at an interface are the weight functions used in the region to the right of that interface (where the core is at the left). This original choice has proved to be an excellent one. Section 5.3.4 will examine this choice in detail.

Table 5-1 is a summary of some results obtained with these restrictions. Also included are the results from few

Table 5-1. Galerkin Weighting with Bracketing Functions.

Case	Geometry and Reactor	Modes	% Error in K_{eff} Modal	3-Group	4-Group
1	GE-R	1,40;41,50;51,60	-.035	.034	.011
2	GE-A	1,20;21,40;41,50	.65	.439	.168
3	EBR-R	1,15;16,20;21,40	-.026	-	.23
4	EBR-A	1,9;10,25	.48	.31	.07(5grp)
5	EBR-A	1,9;10,B;B,25*	-.018	.31	"
6	EBR-A	1,9;10,B;B,23*	-.024	.31	"
7	EBR-A	1,6,9;10,14,23	-.096	.31	"
8	GE-A	1,15,20;21,27,40; 41,44,50	.27	.439	.168
9	EBR-R	1,11,15;15,18,21; 20,25,35	1.05	-	.23
10	GE-R	1,33,40;41,44,50; 51,55,60	.54	.034	.011

*B is the interpolated flux at the boundary, between points 13 and 14.

group calculations for comparison, mostly from Lorenzini's thesis. These few group calculations were made using 26 group zone average fluxes for cross section collapsing.

The notation in the modes column of Figure 5-1 follows. The modes are fluxes chosen from the 26-group calculation. The numbers listed refer to the flux intervals for the 1DX calculations. These are shown in Figures 4-1 and 4-2. Semi-colons separate the trial function sets for the different regions, with the set for the core on the left, next the set for the region adjacent to the core, etc.

The first four cases are the results obtained for the different reactor geometries when two modes are used in each

material region. These modes are chosen to just bracket each region, that is, they are fluxes chosen from the outside space points in each region from the 26 group calculation. The results are generally encouraging, with the G.E. radial and EBR radial cases showing errors in k_{eff} which are about equal to the three group error in the first case and considerably below the four group error in the second case.

The G.E. axial case presents a more difficult problem, having a much smaller core dimension. Here the error for two modes per region is about 1.5 times the error obtained with a three group calculation. The EBR axial problem is similar, presenting an error in k_{eff} of .48% vs. .31% for the three group calculation.

5.2.2 Comments on Comparisons

The logical question at this point is, "Why aren't the modal answers exact?" Is it a question of poor weighting or of insufficient modes to properly express the fluxes? One way to answer this question is to reconstruct the fluxes from the ubiquitous expansion equation,

$$\phi(r,E) = \sum_{i=1}^{N} a_i(r) f_i(E) \qquad (5\text{-}1)$$

and compare these fluxes to those from the 26 group calculation. This can be done, but viewing a two dimensional (space and energy) comparison such as this is a bit overpowering. One still has the question of how good is a "good fit". A

method which has been found to be extremely useful is to plot reaction rates as functions of position. This is done by multiplying the reconstructed 26 group fluxes by the appropriate cross sections and summing over energy. This reduces the output to one dimension (space), which is considerably more tractable. A number of reaction rates have been calculated, but the absorption rate as a function of position will be shown since it is applicable to all regions.

One might be tempted to go a step further and integrate over space as well, giving the total reaction rate for the system or reaction rates for each material region. These latter numbers are useful and will be used, but they can be good, even with a rather poor fit in the region, if positive and negative errors cancel. The one-dimensional reaction rates add the extra information of where the fit is poor.

5.2.3 Improving the Fit

Consider the EBR axial case. The error in absorption reaction rate for case 4 as a function of position is plotted in figure 5-1. There obviously is some difficulty in properly representing the flux in the rather thick reflector with two modes (case 4). As evidence, this reflector has been split into two trial function regions with two bracketing functions in each of these regions (case 5). This reduces the error in k_{eff} from .48% to -.018% or under the 5 group error. A marked improvement in the error curve as a

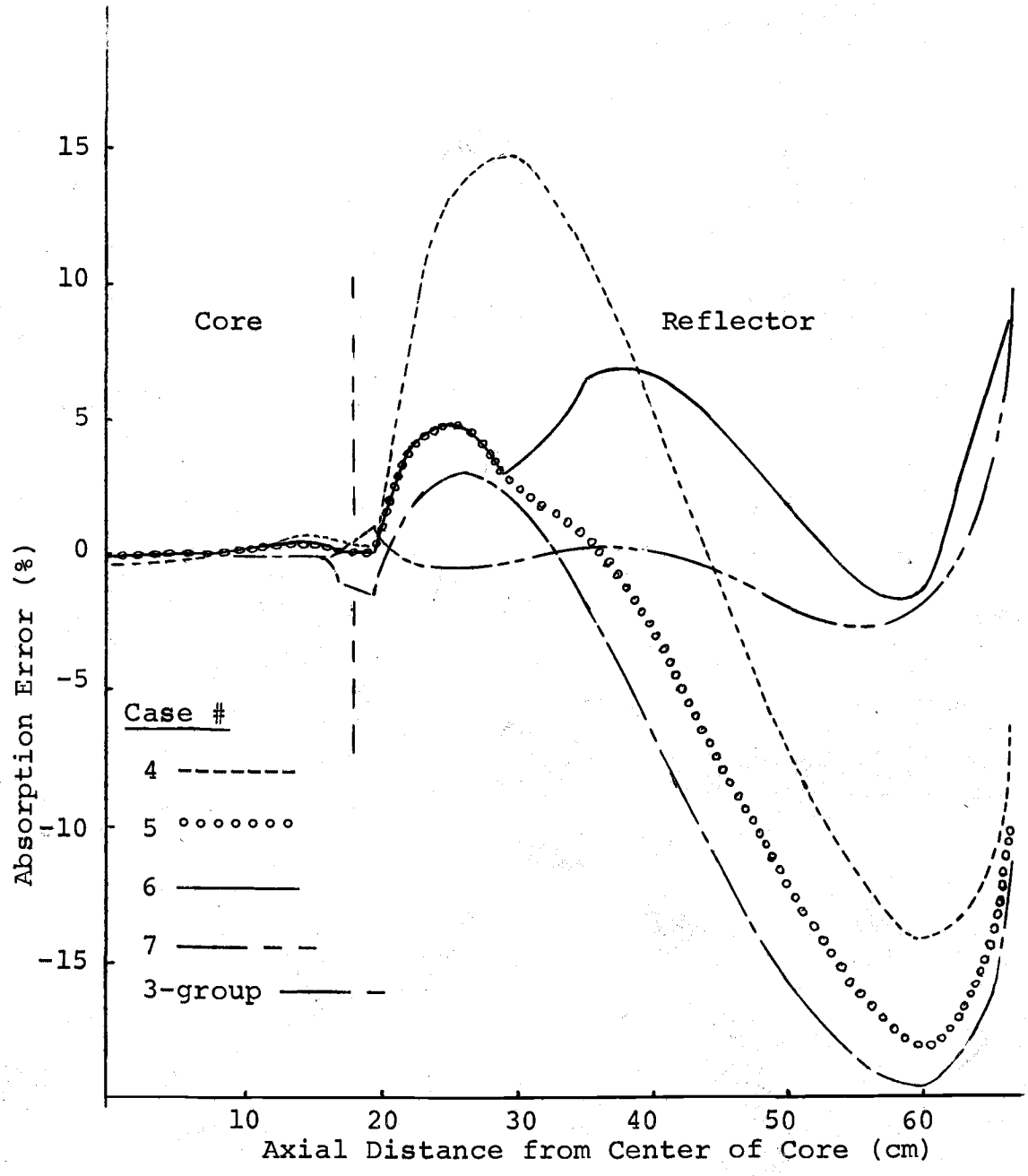

Figure 5-1. Absorption Error for EBR Axial Case.

function of position also results, with the error in the reflector adjacent to the core reduced by almost a factor of three. The percent error near the outer boundary is still large, but this isn't usually of as much consequence, since the flux is small in that region. This can be reduced by choosing the outmost mode away from the edge slightly (case 6).

As an alternative to splitting the reflector, one can add a third mode in each of the two regions (case 7), reducing the error in k_{eff} to the 5 group value and the reaction rate errors by about an order of magnitude.

Also included in Figure 5-1 is the absorption error for a three group calculation. This also gives a poor fit over the outer reflector.

Table 5-2 lists errors in k_{eff} and regional absorption errors for the EBR axial cases. One notes the k_{eff} error for

Table 5-2. Regional Absorption Errors for EBR Axial Calculations

Case	Modes	Error in K_{eff} (%)	Absorption Error (%)	
			Core	Refl.
4	1,1;10,25	.48	.11	5.1
5	1,9;10,B;B,25*	-.018	.11	1.8
6	1,9;10,B;B,23*	-.024	.11	3.5
7	1,6,9;10,14,23	-.096	.071	-.23
3 group	3-group	.31	.081	-4.0

* B is the interpolated flux at the boundry, between points 13 and 14.

two bracketing modes is 50% higher than the three group error, while the two mode split reflector (cases) and the three mode cases are much more accurate than the three group result. The absorption errors are similar in the core, being somewhat better for 3 group and 3 mode calculations. In the reflector, the three mode calculation has about an order of magnitude less error than the other calculations.

5.2.4 Problems

For the EBR axial case, the addition of a third trial function in each region increased the accuracy of the calculation considerably. Addition of a third mode for the G.E. axial problem (case 8 of Table 5-1) also reduces the error in k_{eff}, by about a factor of two, to between the three and four group results.

At this point it would be nice to conclude that one can proceed blithely along, adding another mode from each region and automatically achieve a marked increase in accuracy. This is not the case. Calculations for the EBR radial and G.E. radial cases which include a third mode chosen from each region give results which are inferior to those which were obtained using two modes per region (cases 9 and 10 of Table 5-1). This problem will be examined and alleviated in section 5-3.

5.2.5 Relation Between Regional and Interface Weighting

In this preliminary section on Galerkin weighting, we have used the same weight functions at the interface as are used in the region to the right of the interface, where the reactor core is at the left. In this section we present some evidence that this is the proper choice when using two bracketing modes per region. Section 5-3 is an extensive investigation of the interface conditions and weighting.

Table 5-3 presents the results of a number of calculations using two bracketing modes per region. The first results are for the EBR axial model using two bracketing modes

Table 5-3. Two Bracketing Modes with Various Weighting at Interfaces.

	W.F. In Region	W.F. At Interface	K_{eff} Error (%)
EBR Axial-Galerkin Weighting	1,9;10,25	10,25	0.48
	1,9;10,25	1, 9	1.05
	1,9;10,25	6,15	0.92
GE Radial 1,40;41,40;51,60 Interface W.F.=W.F. from Region to Right			
	Gal.	Gal.	-.035
	Gal.	Gal.+1	6.
	Gal.	Adj.	.151
	Gal.	Group	.181
	Adj.	Adj.	.050
	Adj.	Gal.	-.165

per region. The use of the weight functions in the reflector region to weight the interface is clearly indicated.

The remaining cases use the G.E. radial model and bracketing modes. Weight functions at the interfaces are all chosen from the region to the right of the interface unless otherwise noted. The first four of these calculations use Galerkin weighting in the regions. Galerkin weighting at the interface, or using the weighting as used in the region to the right, is clearly superior. In this table, Gal.+ 1 weighting replaces the weight function furthest from the interface by unity to force conservation of total flux and current across the interface. This will be further discussed in later sections.

The last two cases are adjoint weighting in the regions. Again, using the same weighting at the interface as in the region to the right is superior.

5.2.6 Sodium Void and Doppler Coefficients

Table 5-4 summarizes a series of calculations to evaluate the suitability of the synthesis method for calculating sodium void and Doppler coefficients. The modal calculations were made for the G.E. radial model using two bracketing trial functions per region and Galerkin weighting. The Δk's are obtained by differencing two separate calculations.

The Δk for sodium voiding is in error by -.53%, treating the value from a 26 group calculation as exact. This is one-third the error which was obtained with a four group calculation.

Table 5-4. Sodium Void and Doppler Changes in K_{eff}.

	Sodium Void		Doppler	
	Δk	% Error	Δk	% Error
26 group	0.017845	---	-0.008036	---
2-mode-Gal.	0.017750	-0.53	-0.008106	0.88
4 groups	0.017550	-1.65	-0.00784	-2.49

The result for the change in k_{eff} in going from 300°C to 900°C are similar. Here the modal calculation produces an error of .88% while the four group calculation is in error by 2.49%, again about a factor of three.

It appears that these calculations, which depend appreciably on spectral shape, are more accurately made using synthesis methods.

5.3 Interface Conditions

5.3.1 Discussion

Before proceeding to look at different weight functions and their relative merits, it is useful to consider the interface crossing conditions for spatially discontinuous modes. First consider the modal expansion

$$\phi(r,E) = \sum_{i=1}^{N} a_i(r) f_i(E) \qquad (5\text{-}1)$$

For a given number of modes, this expansion should be more nearly an equality for spatially discontinuous modes than for continuous modes, which must be chosen to represent all regions. In the region near an interface, discontinuous modes should more accurately meet the equality than the same number of groups, whose shapes must represent region averages.

Substituting the modal expansions into the equation for continuity of energy dependent flux, one has

$$\sum_{i=1}^{N} a_i(r^-) f_i^-(E) \approx \sum_{i=1}^{N} a_i(r^+) f_i^+(E) \qquad (5\text{-}2)$$

The approximation here is different from that above, with the degree of approximation depending upon how the f_i^+ relate to the f_i^-. If the f_i are spatially continuous ($f_i^- = f_i^+$), then one has an equality when $a_i^- = a_i^+$ for all i. If the f_i^- and f_i^+ span the same energy space, an equality is also possible. As one proceeds from this to the case where the f_i^- span the spectral variation in one material region and the f_i^+ span the spectral variation in a very different material region, statement (5-2) becomes less and less an equality.

Continuing a step further, one multiplies (5-2) by a weight function $g_j(E)$ and integrates over E and requires equality.

$$\sum_{i=1}^{N} a_i(r^-) \int dE\, g_j(E) f_i^-(E) = \sum_{i=1}^{N} a_i(r^+) \int dE\, g_j(E) f_i^+(E) \qquad (5\text{-}3)$$

This provides equality in a weighted sense.

Looking at these statements, there is a conflict. One can make (5-2) more nearly an equality, and be less dependent upon the choice of weighting functions, by providing some overlap of trial function sets at the interfaces. However, providing this overlap into another region implies a poorer fit within the region for a given number of modes, or the use of more modes to maintain a given degree of fit.

The arguments for the current continuity conditions are similar. The exact condition,

$$D(r^-,E)\nabla\phi(r^-,E) = D(r^+,E)\nabla\phi(r^+,E) \qquad (5\text{-}4)$$

on substitution of the modal expansion becomes

$$\sum_{i=1}^{N} D(r^-,E) f_i^-(E) \nabla a_i(r^-) \approx \sum_{i=1}^{N} D(r^+,E) f_i^+(E) \nabla a_i(r^+) \qquad (5\text{-}5)$$

With spatially continuous modes, the flux conditions of (5-2) are satisfied with $a_i^- = a_i^+$ for all i. The current relations (5-5) cannot be met by $\nabla a_i(r^-) = \nabla a_i(r^+)$ because of the differing diffusion coefficients. However, if the diffusion coefficients on opposite sides of the interface are similar, this condition can nearly be met with continuous modes.

Again, as with the flux continuity relation, if the energy functions on the left span the same space as the energy functions on the right, relation (5-5) can be an equality. In this case the energy functions are D times f_i.

The remainder of the section on interface conditions is devoted toward investigation of two ideas. The first of these is the value of some spectral overlap of trial function sets in achieving acceptable results. That is, should the set chosen to represent a trial function region include modes representative of adjacent regions as an aid to interface coupling? The second area of investigation is the choice of weight functions to optimize the interface coupling conditions.

5.3.2 Overlap of Trial Function Sets

To examine the value of some sharing of spectral shapes between trial function sets for adjacent regions it is necessary to consider at least three trial functions per set, one from the region of interest and one to provide overlap with the set on each side.

Table 5-5 provides some evidence for the usefulness of the approach. For the G.E. radial problem, a slight overlap at the interfaces (case 11) to 1,38,41;40,45,51;50,55,60 halves the error in k_{eff} to .26% from case 10. Expanding this overlap to 1,35,45;34,45,55;45,52,60 reduces the error to -.014% (case 12). Similarly, for the EBR axial problem, we have obtained -.096% error for case 7. Overlapping at the interface to go to sets 1,8,10;9,13,23 from 1,6,9;10,13,23 reduces the error in k_{eff} to -.0031.

Table 5-5. Various Degrees of Trial Function Set Overlap with Galerkin Wts.

Case	Reactor		Error in K_{eff}
10	GE-R	1,33,40;41,45,50;51,54,60	.54
11	GE-R	1,38,41;40,44,51;50,54,60	.26
12	GE-R	1,35,45;35,45,55;45,52,60	-.014
7	EBR-A	1,6,9;10,14,23	-.096
13	EBR-A	1,8,10;9,13,23	-.0031

A similar demonstration can be presented for the EBR radial case. It appears that for this problem the spectral variation at interfaces from sodium voided core to sodium nickel reflector and then to sodium voided blanket is so great as to require overlap.

However, before proceeding further with choices of trial functions and overlap, we will look at weighting of the interface conditions. This has proved to be an extremely fruitful area of investigation and gives insight into the cause of the problems of section 5-2.

5.3.3 Weight Functions at Trial Function Interfaces: Discussion.

With spatially continuous modes, one has the advantage of exact continuity of flux across interfaces, i.e., statement 5-2 is a point by point equality in energy. Thus, flux in a group sense (integrated) and total flux are conserved. Similarly, for the multigroup formulation, the integral of

flux over each energy group is conserved. Thus, for both these cases, the total flux (integrated over all energies) is conserved across interfaces.

This is not true, in general, for the use of spatially discontinuous modes. Here flux is conserved only in certain weighted senses.

Examining the current interface conditions of equations (2-28) and (2-37) we see that integrals of current over energy are preserved across interfaces for the multigroup formulation, but are preserved only in a weighted sense for modal formulations.

Fortunately, one of the strengths of the modal method is its generality. One can obtain continuity of integrated flux and current with spatially discontinuous trial functions by using group weighting at interfaces. This is done by dividing the energy range into as many segments as one has modes and requiring the integrals over each energy segment (group) to be continuous.

$$\sum_{i=1}^{N} a_i(r^-) \int_{\Delta E_j} f_i^-(E)\,dE = \sum_{i=1}^{N} a_i(r^+) \int_{\Delta E_j} f_i^+(E)\,dE, \qquad (5\text{-}6)$$

$$j=1,2,\ldots,N$$

$$\sum_{i=1}^{N} \nabla a_i(r^-) \int_{\Delta E_j} D^-(E) f_i^-(E)\,dE = \sum_{i=1}^{N} \nabla a_i(r^+) \int_{\Delta E_j} D^+(E) \qquad (5\text{-}7)$$

$$f_i^+(E)\,dE, \quad j = 1,2\ldots,N$$

These are just the modal flux continuity equations (5-3) and the equivalent statement for the current (2-28), using weight functions which are one over group j and zero outside.

Group weighting at interfaces can be used with other weighting within the regions. Consider the Galerkin weighted EBR axial calculation which is included as case 7 in Tables 5-1 and 5-2. The error in k_{eff} for this 3 mode calculation is -.096% vs. .31% for 3 groups. Replacing the Galerkin weighting at the interfaces with group weighting, the error in k_{eff} becomes -0.25%, still a credible error, being under the three group error, but poorer than the excellent result using Galerkin weighting throughout. An example for two modes is included in Table 5-3.

It is also possible to combine conservation of total flux and current across an interface without going to a full group weighting at the interfaces. Extending the range of integration in equations (5-6) and (5-7) to include all energies assures continuity of total flux and current. These equations are insufficient by themselves, since there must be N relations each for the flux and current interface conditions. However, a combination of this weighting with other weightings has been found extremely valuable when using more than two modes in an expansion. This will be discussed in the next section.

5.3.4 Forcing the Conservation of Flux and Current Across Interfaces

The use of unity as one of two weight functions at an interface has not proved successful, as was demonstrated in Table 5-3. This is not an isolated case, the use of unity as one of two weight functions at an interface appears to be generally unacceptable.

It has been proposed by Becker (2) for space-energy synthesis and Wachspress (57) for space-space problems that for a system which has regions I, J, K, L, etc. in succession, it seems reasonable to use a mode representing region J from the center of region I to the center of region K. Similarly, the mode representing region K would be used between the centers of regions J and L, etc. Suggested interface conditions for the center of region J are either (1) combining coefficients for modes representing regions I and K equal zero or (2) they equal each other.

In the early work on this thesis, this method was examined for a two mode problem with disastrous results. This crude an approximation apparently isn't successful. Perhaps it will be more successful when using more trial functions. Note, however, that method (2) in the previous paragraph is similar to using unity as one of two weight functions at an interface with bracketing trial functions. This follows since the two functions chosen from near the interface are similar, if not idential, so that conservation

of total flux forces the other member in each set to be equated.

Getting back to the mainstream of this section, the use of unity as one of three weight functions at an interface has proven very useful and indeed almost necessary if there is little spectral overlap between the trial function sets being coupled.

In section 5.3.4, problems developed when the number of modes per region was increased from two to three for the G.E. and EBR radial problems. This section sheds some light on these problems.

Table 5-6 is a summary of some results, mostly using the G.E. radial model. Cases 3 and 10 are the two and three mode Galerkin weighted results given in Table 5-1. Case 14 uses the same modes as case 10 and the same weight functions in the material regions. The only difference is at the interfaces, where the third mode at each interface has been replaced by unity, forcing the conservation of flux and current. The results are greatly improved, with the error in k_{eff} reduced from 0.54% to .018% by this change.

Attributing the difficulty in case 10 to the use of too many weight functions chosen from a narrow spectral range, another calculation was made. Case 15 again uses the same trial functions but the weight functions are fluxes chosen to give a broader variation of spectral shapes than those used in case 10. This improves k_{eff} to a .050% error and

also improves the regional and pointwise reaction rates considerably, but not to the extent which was obtained in case 14 where conservation of flux and current was forced.

As an indication of the uncertainty in using Galerkin weighting at interfaces, the fluxes have been reconstructed and integrated over energy on opposing sides of each interface for case 15. There is a flux inequality at the core-blanket interface of 0.18% while at the blanket-reflector interface this discontinuity in total flux is 10%.

Other non-group forms of weighting are not immune to this problem. Cases 16 and 17 are an example of an absorption reaction rate weighted problem. Considerable overlap already aids the flux conservation, since the modes used are points 10,35,45 in the core and 35,45,55 in the reflector and blanket. Again the addition of unity aids considerably, reducing the error in k_{eff} by a factor of four.

One can argue that if a set of modes and trial functions produces a poor result, almost any change in the set will improve it. An equally valid question is, given a set of trial and weight functions which produces accurate results, will adding unity as a weight function at interfaces destroy these results?

A problem for which accurate results have already been obtained is the EBR axial problem using three trial functions. Cases 13 and 18 examine this problem with and without unity as the third weight function at the interface.

Table 5-6. Use of Unity as the Third Weight Function at Interfaces.

Case	Weighting	Error in K_{eff}(%)	Absorption Error (%)			Fission Error (%)	
			Core	Blanket	Reflector	Core	Blanket
3	gal. (2 mode)	-.035	-.31	10	1.3	-.35	15.5
10	gal.	.54	-	-	-	-	-
14	gal. + 1	.018	-.017	1.2	-1.8	-.035	1.5
15	gal. (broad*)	.050	.18	5.9	5.5	-.23	10.2
16	$\Sigma_a \phi$	.026	.29	4.2	.2	-0.93	5.2
17	$\Sigma_a \phi$+1	.006	.069	1.0	.15	-.012	.76
		EBR Axial					
13	gal.	-.0031	-.16		-.56		
18	gal. + 1	.044	.19		-.086		

* WF = 1,35,45;35,45,55;45,52,60

Modes are slightly overlapped, using 1,8,10;9,13,23. The results are excellent for both cases. One should note that the error of .044% in k_{eff} is as good as one should reasonably expect with cross-sectional data and size involved, and comparisons of errors of the order of a factor of ten smaller than this are meaningless. To put things in perspective, the .044% is under the 5 group error of .070%. Regional reaction rates are likewise excellent in both cases, as are reaction rates as a function of position.

Another set of results which can be used as an illustration is included in section 5.4.3. These cases use 10,35,45 in the core and 35,45,55 as trial functions in the blanket and reflector, and thus already have considerable overlap to aid interface conditions. All cases give reasonable results. Addition of unity at an interface gives a somewhat poorer weighting as was noted earlier in this section.

Over all, it appears that using unity as one of three or more weight functions can be extremely useful where the coupling between regional modes is weak and does not have any major adverse effect where coupling is good.

5.4 Regional Weighting

5.4.1 Introduction

Up to this point our demonstrations have been primarily made with Galerkin weighting. We have also demonstrated the vital importance of the interface conditions when using

spatially discontinuous modes and have shown some methods to strengthen these conditions.

This section examines the choice of weight functions within the regions. All of the calculations are for the G.E. reactor model. The choices examined will be Galerkin, adjoint, reaction rate, and group weighting. Since the results are dependent upon the choices of weighting at the interfaces and the degree of trial function set overlap, each of these weightings will be examined with a variety of trial function sets and interface weightings.

Section 5.4.2 examines the various weightings using three modes per region, section 5.4.3 using spatially continuous trial functions, and section 5.4.4 using two bracketing trial functions per region.

5.4.2 Three Modes Per Region

The results with three modes per region are summarized in Table 5-7, with modes listed in Table 5-8. The table generally is set up so that the overlap decreases from trial function set A to set D. Trial function set A has the most set overlap, using fluxes 1,35,45 in the core and 35,45,55 in the blanket and reflector. Trial function set B is the same in the core and blanket as set A, but uses 45,52,60 as a set which chould better represent the reflector spectra while retaining considerable overlap.

Table 5-7. Results with Three Modes per Region.

Case	Trial Func. Set	Weightings	Radial K_{eff} Error (%)	Regional Errors-Radial Absorption (%) Core	Blanket	Reflector	Fission (%) Core	Blanket	Axial K_{eff} Error (%)
19	A	Gal	-.013	-.017	2.5	1.0	-.087	3.4	-.13
20	A	Gal+1	-.035	-.087	4.1	2.0	-.12	5.5	+.015
16	A	$\Sigma_a\phi$	+.026	+.29	4.2	2.0	-.093	+5.2	
17	A	$\Sigma_a\phi$+1	+.006	-.069	1.0	.15	-.012	+.76	
21	A	Adj	+.018	-.056	-.78	-4.5	0.001	.016	-.070
12	B	Gal	-.014	+.011	+1.7	-11	+.041	+1.9	
22	B	Gal+1	+.016	+.013	+1.3	-35	-.009	+.55	
23	B	Adj	+.019	-.044	-.005	-3.8	.0085	+.33	-.072
11	C	Gal	+.23	1.1	31	50	-1.2	+53	
24	C	Gal+1	+.0042	.040	1.2	.45	.03	1.3	
25	C	Cont. Gal	.041	.029	1.0	-5.3	-.015	+.63	
10	D	Gal	.54						
14	D	Gal+1	+.018	-.017	1.2	-1.8	-.035	+1.5	
15	D	Wide Gal	+.050	.18	5.9	5.5	-.23	+10.2	
26	D	$\Sigma_a\phi$	+.074	-3.2	+10	+5	-.38	+17	
27	D	Grp	.005	.035	-1.2	+15	+.038	-1.3	-.021

Table 5-8. Modal Sets for Table 5-7.

Set	Modes
A	1,35;45; 35,45,55; 35,45,55 In some cases, point 10 replaces point 1 in the first set.
B	1,35,45; 35,45,55; 45,52,60
C	1,38,41; 40,44,51; 50,54,60
C	1,33,40; 41,45,50; 51,54,60

Sets A and B will be discussed together. The comments in this section will be numbered as an aid to clarity.

1. The sets 1,35,45;35,45,55 work well over the core and blanket. We note that all the values of k_{eff} are equal or less than the three group error, for all of the weightings.

2. The use of Gal+1 weighting appears to have little effect with this considerable overlap, Gal+1 being slightly worse. In Figures 5-2 and 5-3 the absorption reaction rate errors are plotted for set A. We note that Gal and Gal+1 error curves are similar in the region of the second interface, where fluxes are automatically conserved because the trial functions are continuous.

3. In the case of absorption reaction rate weighting ($\Sigma_a\phi$ = weight function, where Σ_a is the absorption cross section from the same region as ϕ), unity as a weight function at the interfaces improves the results considerably, most spectacularly the reaction rates as a function of position (Figure 5-3), with a generally excellent fit throughout.

4. The blanket to reflector interface presents a problem, since it is here that the largest spectral variation occurs. Galerkin and Galerkin+1 weighting do not appear to handle this well. Adjoint and $\Sigma_a\phi$ and $\Sigma_a\phi$+1 handle this quite well.

This appears to be primarily a weighting problem, since the change in modes doesn't cause any appreciable change.

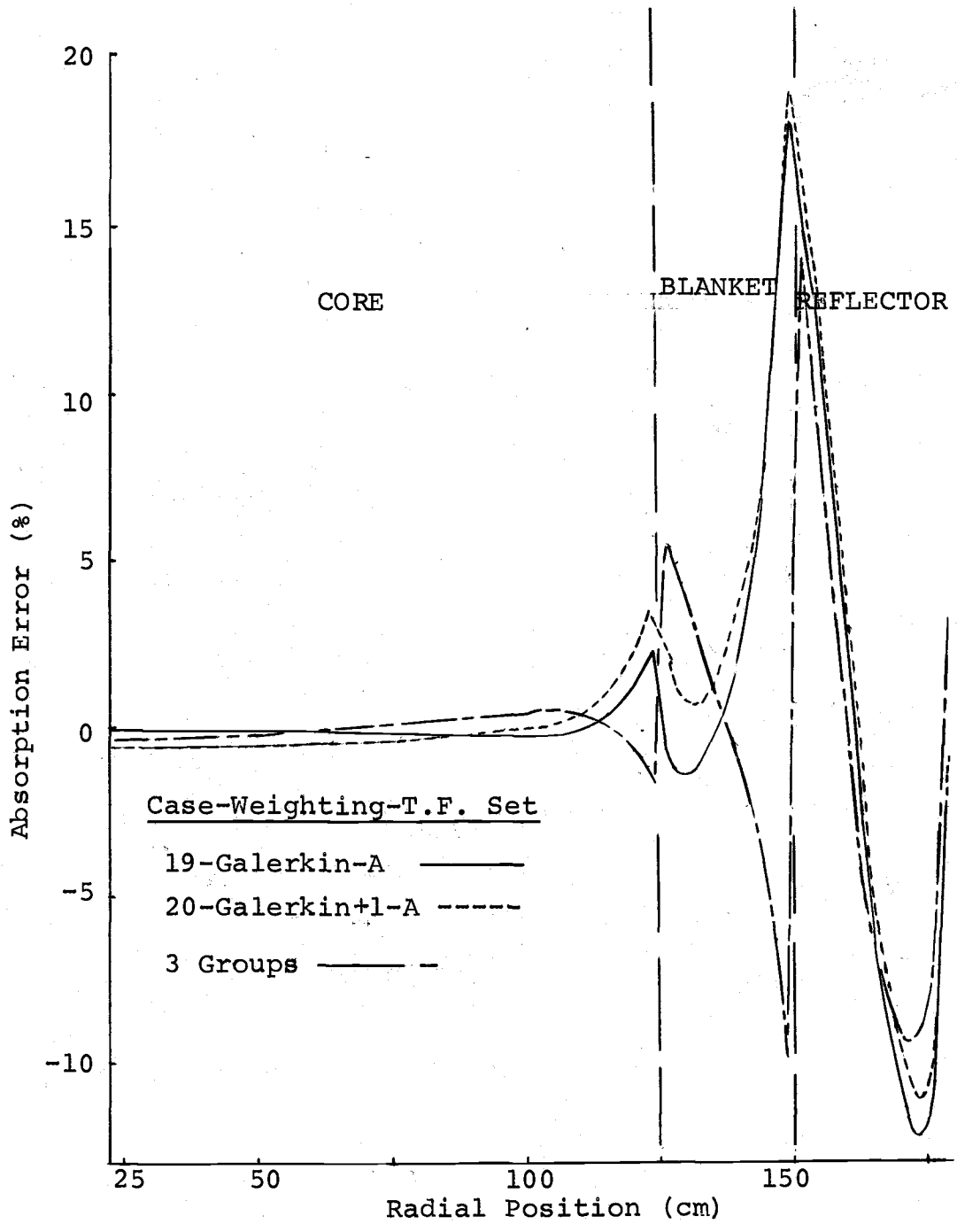

Figure 5-2. Absorption Error with Trial Function Set A.

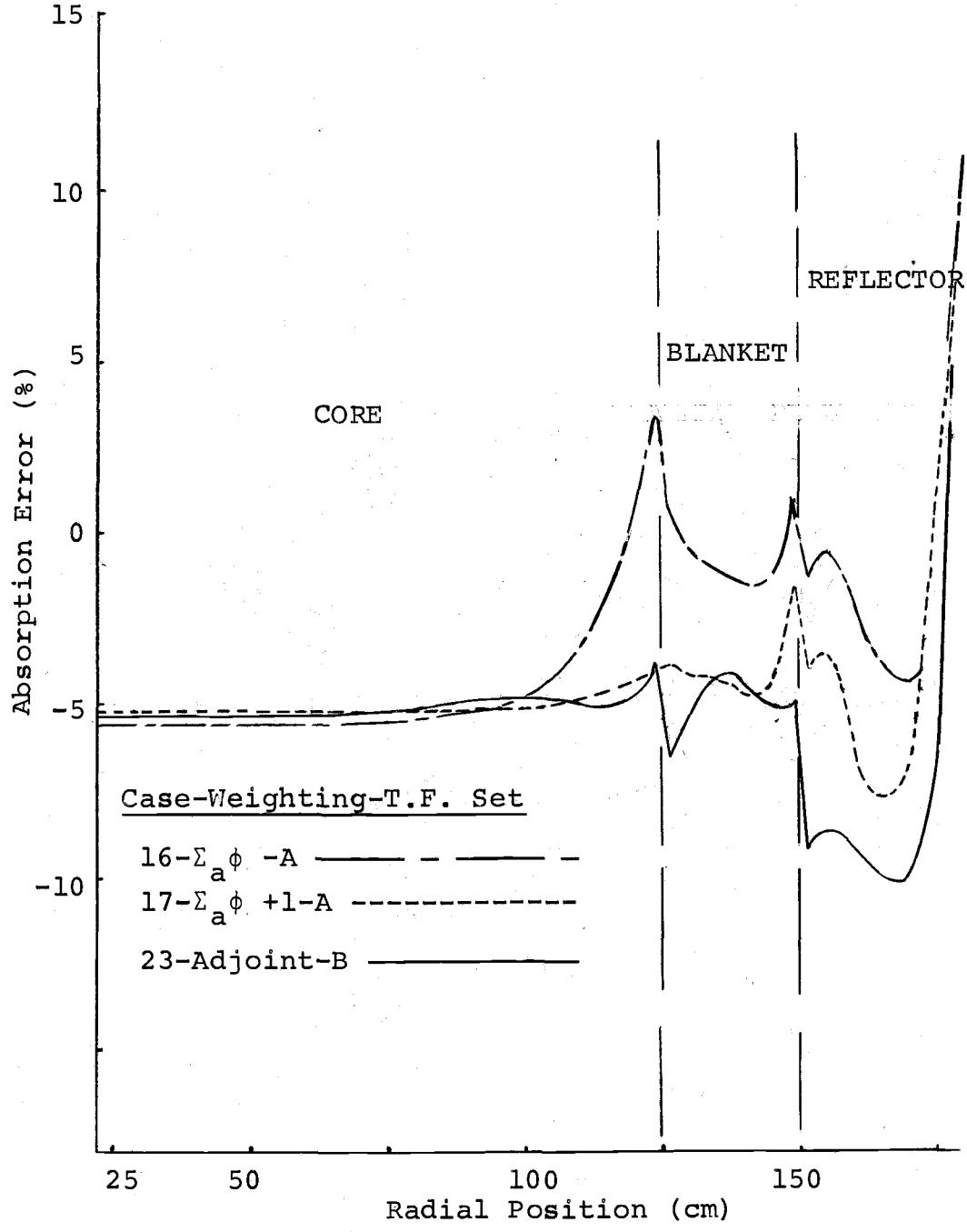

Figure 5-3. Reaction Rate and Adjoint Weighting, T.F. Sets A & B.

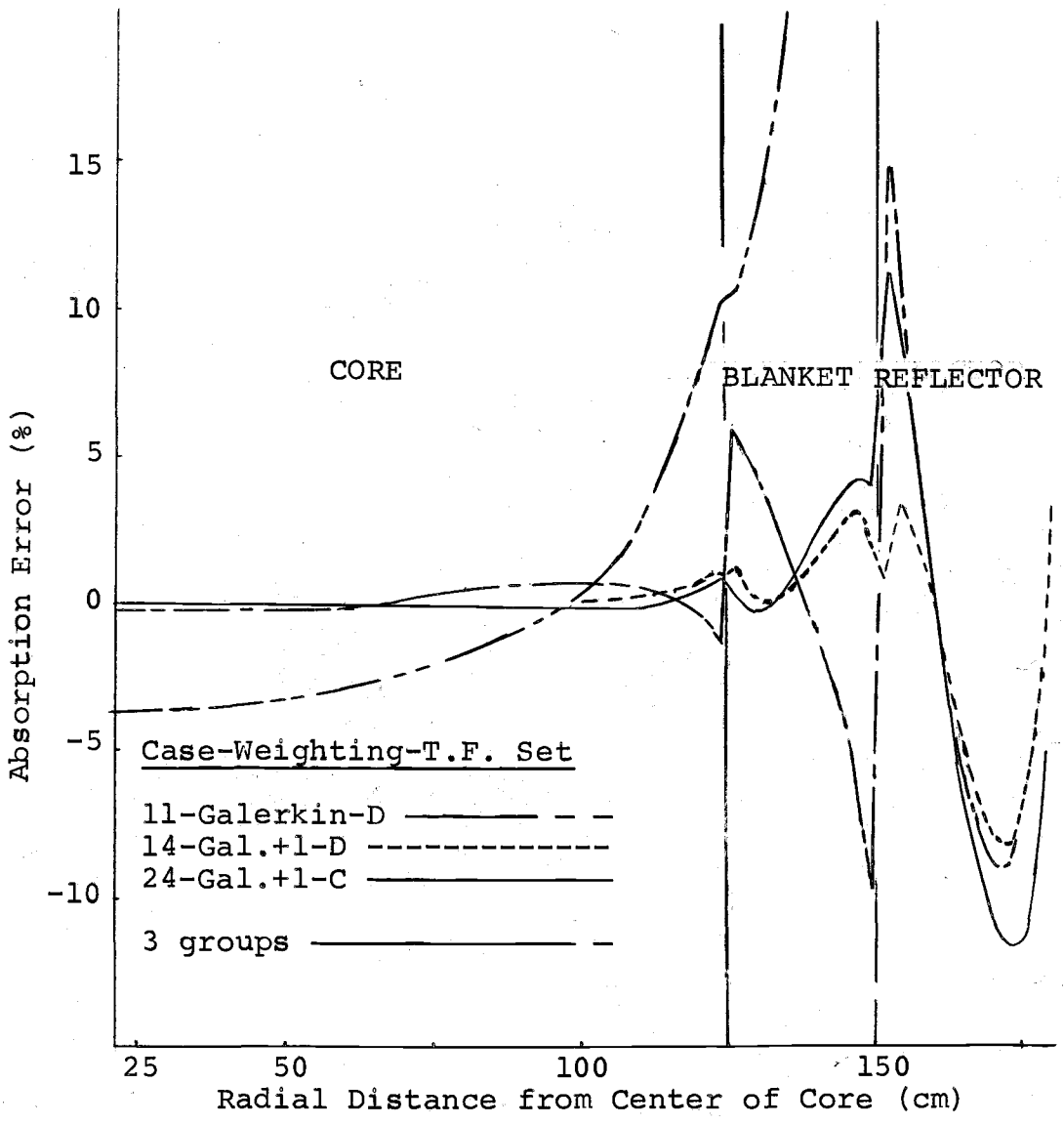

Figure 5-4. Absorption Error with Trial Function Sets C and D.

We proceed to sets C and D, which we will discuss together. C overlaps by a point at each interface while D does not.

5. As one decreases the trial function overlap, forcing the conservation of flux and current across and interface is a necessity. For trial function sets C and D the results are spectacularly improved by use of unity as one of the weight functions at interfaces. As stated in the section on interface weighting, it appears this is primarily a problem. caused by a narrow spectral range of weight functions at the interface, since use of continuous weight functions 1,44,54 for case 25 and a broader variety of weight functions 1,35, 45;35,45,55;45,52,60 for case 15, both have an appreciable positive effect, although not as good as that produced by using unity at the interface.

6. Figure 5-4 illustrates that Galerkin weighting can be very good using trial function sets chosen entirely from within the region and conservation of integrals of flux and current at interfaces.

5.4.3 Spatially Continuous Trial Functions

The use of spatially continuous trial functions can be considered the ultimate in trial function overlap. Again we use the G.E. radial model as the sample problem. The first three cases use fluxes from points 1,45, and 55, or the centers of the material regions, as trial functions.

For comparison, a three group calculation is included. This calculation uses region average fluxes for collapsing

cross sections (or, in terms of the modal method, the modes chosen are segments of the region average fluxes).

The results of these calculations are summarized in Table 5-9. Galerkin and adjoint weighting appear comparable in calculating k_{eff} and regional integrals of reaction rates and also comparable to the multigroup method. For these quantities, the group weighted modal method appears distinctly better, reducing errors in k_{eff} by about a factor of 10.

Figure 5-5 is a graph of the error in absorption rate as a function of position. Here the Galerkin weighting and the multigroup method show error curves with similar shapes and maxima. The modal method with adjoint and with group weighting is distinctly more accurate, with maxima in the error curves reduced by a factor of 4 or 5 times.

Also included in Table 5-9 is a calculation using region average fluxes as modes for a group weighted synthesis calculation. It is interesting to compare this to the standard 3-group calculation since identical information is used in both calculations, namely the region average flux shapes. The only difference is that for the multigroup calculation, one uses energy segments of these as modes while for the synthesis calculation the continuous (in energy) shapes are superimposed. The results for the synthesis approximation are clearly superior. A plot of reaction rate errors for the synthesis calculation (case 31) is not included since it is essentially identical to that for the group weighted case 30 (Figure 5-5).

Table 5-9. Results with Continuous Trial Functions.

Case	Trial Func. Set	Weightings	Radial K_{eff} Error (%)	Regional Errors-Radial					Axial K_{eff} Error (%)
				Absorption (%)			Fission (%)		
				Core	Blanket	Reflector	Core	Blanket	
28	E	Gal.	-.087	.080	.22	-1.8	-.005	.43	
29	E	ADJ	.038	-.073	.32	-4.3	-.13	.59	+.31
30	E	GRP	-.004	-.005	-.05	-1.9	-.002	+.19	
	3-Group*		-.035	-.0021	+.4	+ .14	-.012	+.52	.439
31	RA	GRP	+.0011	.0088	-.11	-1.5	-.0024	-.097	

Trial Function Sets:

E 1,45,55

RA Region Average Fluxes

* Three group calculation uses region average fluxes for cross section collapsing.

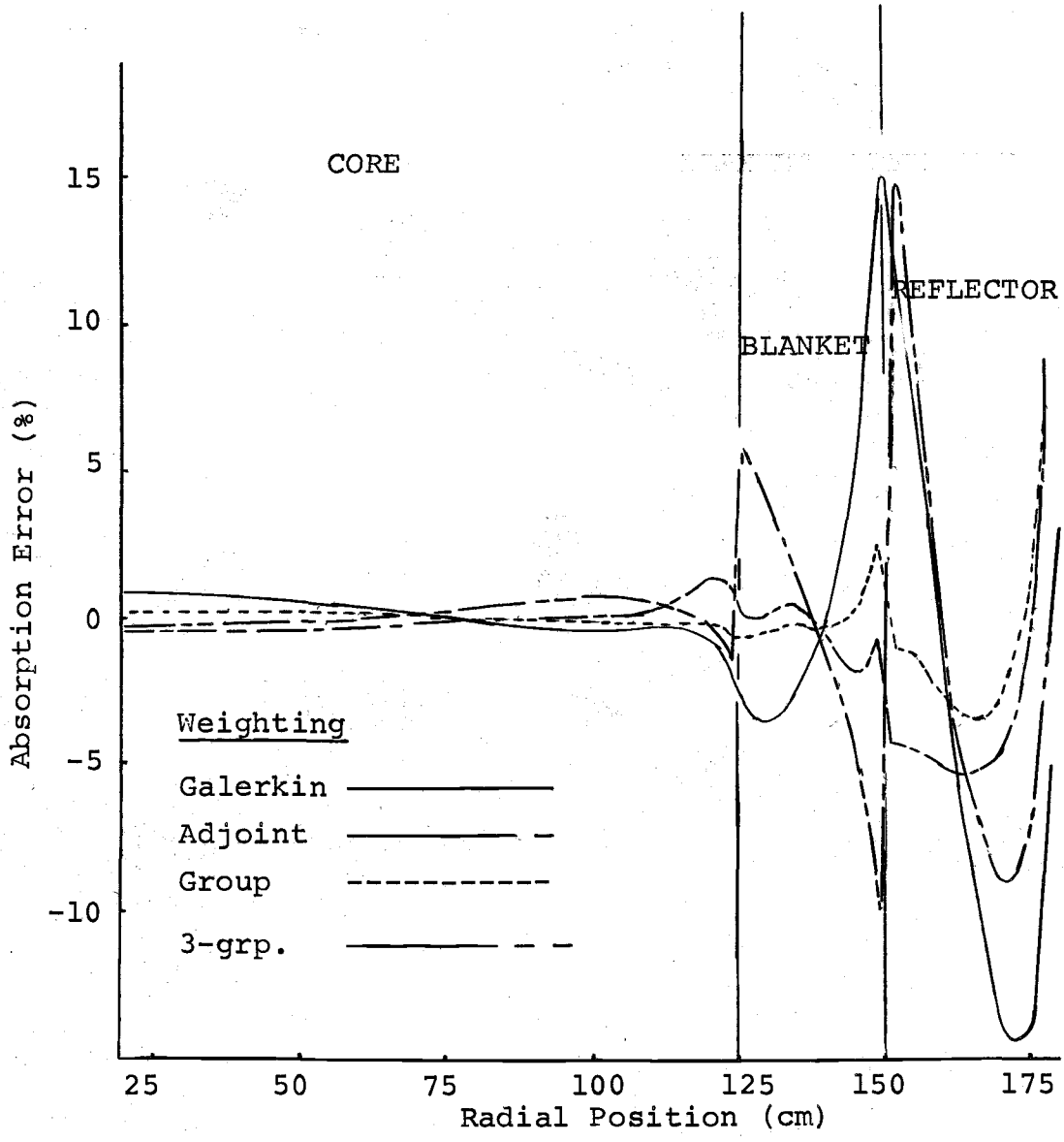

Figure 5-5. Absorption Errors with Continuous Trial Functions.

5.4.4 Two Trial Functions

In section 5.2, calculations were made using two bracketing modes per region and Galerkin weighting. This will now be examined for a broader choice of weighting. Again, the G.E. radial model will be used. The results of these calculations are included in Table 5-10 and Figure 5-6.

For this choice of trial functions, the results are comparable for Galerkin and adjoint weighting, with k_{eff} errors comparable to that for the three group calculation. Using absorption reaction rate weighting improves these results appreciably, reducing the regional absorption errors, in the blanket and point by point, by a factor of about two. Group weighting provides even better regional numbers, although its fit in the reflector is not as good.

Three different choices for dividing the fine groups among two broad groups have been made, with a split using 1-8, 9-26 giving the most accurate k_{eff}. Since the flux drops off rapidly beyond group 12 and since the splits at high energy give better results, the implication is that one should weight over the high energy end of the spectrum and essentially ignore the low energy end.

Without a one dimensional calculation, the production of flux shapes to represent the interface presents some special techniques which are somewhat more difficult than

Table 5-10. G.E. Radial Geometry - Two Modes with Various Weighting

Weight Function	k_{eff}	% of Error in k_{eff}	Absorption Error (%) Core	Blanket	Reflector
(Bracketing Modes - 1,40;41,50;51,60)					
Galerkin	1.0803118	-.035	-.32	10.%	1.3%
Adjoint	1.0801451	-.050	-.23	+ 9.3	-4.2
$\Sigma_a\phi$	1.0805638	-.011	-.20	+ 4.5	-2.0
Group (1-8 9-26)	1.0806066	-.0073	-.15	+ 2.1	-1.5
Group (1-6 7-26)	1.0805383	-.014			
Group (1-11 12-26)	1.0814613	+.070			
Split Blanket - 1,45;45,55					
Group (1-8 9-26)	1.0806217	-.0059	-.12	- 2.0	-6.6

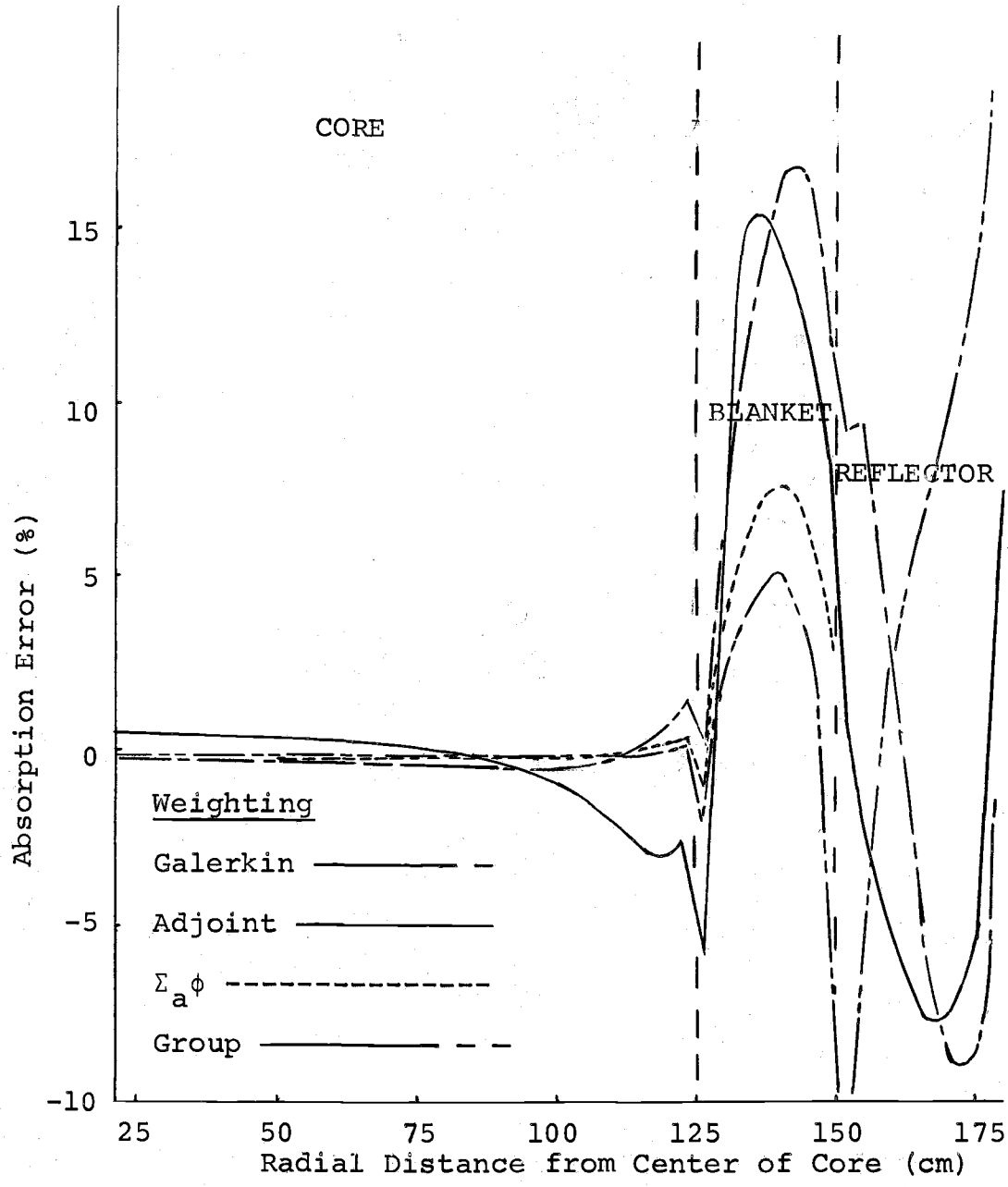

Figure 5-6. Absorption Error with Two Bracketing Modes.

producing fluxes characteristic of regions. Thus, unless a two dimensional calculation is to be made, in which case a one dimensional calculation to generate modes is justified, an expansion in terms of modes representative of regions is preferable.

The last calculation of Table 5-10, a group weighted G.E. radial problem, uses modes chosen from the centers of the regions. This yields two trial function regions with the trial function interface at the center of the blanket. Trial functions for the first region are 1,45 and for the second region 45,55. Errors in k_{eff} and in absorption of the core and blanket are all slightly less than for modes which bracket material regions, but the absorption error in the reflector is somewhat greater.

VI. TWO DIMENSIONAL METHODS AND RESULTS

6.1 Introduction

Multidimensional calculations are the probable ultimate use of modal methods due to the substantial potential cost savings involved. Extension of the modal method as developed for a single spatial dimension to multi-dimensional problems is conceptionally simple. It merely consists of replacing the spatial variable r by a vector position $\vec{r}$ to denote a point in multi-dimensional space. Again the starting point in the development is the energy dependent diffusion equation.

$$- D(E)\nabla^2\phi(\vec{r},E) + \Sigma_t(E)\phi(\vec{r},E) = \frac{1}{\lambda}\chi(E)\int\nu\Sigma_f(E')\phi(\vec{r},E')dE' + \int\Sigma_s(E'\to E)\phi(\vec{r},E')dE' \tag{6-1}$$

6.2 Developing the Method

The development of the differential equations which are the modal approximation to equation (6-1) is identical to that for the one dimensional case. Namely, one substitutes the expansion in trial functions $\phi(\vec{r},E) \approx \sum_{i=1}^{N} a_i(\vec{r})f_i(E)$ into equation (6-1), multiplies by a weight function $g_j(E)$, integrates over E, and requires an equality. Using N such weight functions, the resulting equations can be combined into a matrix equation

$$\bar{\bar{D}}\nabla^2\overline{a_i(\vec{r})} + \bar{\bar{\Sigma}}_t\overline{a_i(\vec{r})} = \frac{1}{\lambda}\overline{\overline{\chi\nu\Sigma_f}\,a_i(\vec{r})} + \bar{\bar{\Sigma}}_s\overline{a_i(\vec{r})} \qquad (6\text{-}2)$$

where the matrices are identical with those of Chapter II, for example

$$D_{ji} = \int g_j(E)\,D(E)\,f_i(E)\,dE \qquad (6\text{-}3)$$

The vector $a(\vec{r})$ is a column vector of the combining coefficients at point $\vec{r}$ in space.

In common with the developments of Chapter II, equation (6-2) has been multiplied by the inverse of the D matrix. This places the identity matrix in its position, which is advantageous since it simplifies the coupling between adjacent space points and thereby reduces the computational effort.

The interface conditions are symbolically those of the one dimensional development. The energy dependent flux in the flux and current continuity equations is replaced by the modal expansions. Then equality is required in a weighted residuals sense, i.e., one multiplies through by a weight function $g_j(E)$ and integrates over E and requires equality. This gives

$$\sum_{i=1}^{N} \int g_j(E)\,f_i^-(E)\,dE\; a_i(r^-) = \sum_{i=1}^{N} \int g_j(E)\,f_i^+(E)\,dE\; a_i(r^+) \qquad (6\text{-}4)$$

and

$$\sum_{i=1}^{N} \int g_j(E) D^-(E) f_i^-(E) dE \ \nabla a_i(r^-) = \sum_{i=1}^{N} \int g_j(E) D^+(E) f_i^+(E) dE \ \nabla a_i(r^+) \tag{6-5}$$

Again, by using N such weight functions, these can be written in matrix form. The equations are applicable in axial and radial directions and the matrices so formed can be combined into a single matrix. We will use such forms in the further development, i.e.,

$$\overline{a^{\pm}} = \overline{\overline{M}} \ \overline{a^{\mp}} \tag{6-6}$$

and

$$\overline{\nabla a^{\pm}} = \overline{\overline{N}} \ \overline{\nabla a^{\mp}}, \tag{6-7}$$

where ∇a refers to a derivative with respect to a single space variable.

Examining the equations, both at the interfaces and in homogeneous regions, one notes that the matrix elements calculated are identical with those used in the one dimensional formulation. Thus, the codes produced there to generate input cross sections are generally applicable here.

6.3 The Difference Equation for Two-Dimensional Geometry

It was considered desirable to develop a two dimensional code which will handle cartesian (x-y) as well as cylindrical (r-z) geometry. Assuming no dependence on the third coordinate (z or θ) for each of these geometries, the

Laplacian term of equation (6-2), $\nabla^2 a_i(r)$, can be written

$$\frac{\partial^2 a_i(x,y)}{\partial x^2} + \frac{\partial^2 a_i(x,y)}{\partial y^2} \tag{6-8}$$

and

$$\frac{1}{r}\frac{\partial}{\partial r}\left[r\frac{\partial a_i(r,z)}{\partial r}\right] + \frac{\partial^2 a_i(r,z)}{\partial z^2} \tag{6-9}$$

The two forms above can be combined into a single form

$$\frac{1}{r^p}\frac{\partial}{\partial r}\left[r^p \frac{\partial}{\partial r} a_i(r,z)\right] + \frac{\partial^2}{\partial z^2} a_i(r,z) \tag{6-10}$$

where p=0 for slab geometry and p=1 for cylindrical geometry. In the first case r and z now signify cartesian coordinates.

For the remainder of the development, a special form of the synthesis diffusion equation (6-2) will be used. Namely, multiplying equation (6-2) by the inverse D matrix and combining the Σ_s and Σ_t matrices yields

$$\bar{\bar{I}}\,\nabla^2\overline{a(r,z)} + \bar{\bar{\Sigma}}_{st}\,\overline{a(r,z)} = \frac{1}{\lambda}\,\overline{\overline{\chi\nu\Sigma_f}}\,\overline{a(r,z)} \tag{6-11}$$

Using the Laplacian of (6-10), this form of the diffusion equation reads:

$$\begin{aligned}\bar{\bar{I}}\left\{\frac{1}{r^p}\frac{\partial}{\partial r}\left[r^p\frac{\partial}{\partial r}\overline{a(r,z)}\right] + \frac{\partial^2}{\partial z^2}a(r,z)\right\} + \\ \overline{\overline{\Sigma_{st}}}\,\overline{a(r,z)} = \frac{1}{\lambda}\,\overline{\overline{\chi\nu\Sigma_f}}\,\overline{a(r,z)}\end{aligned} \tag{6-12}$$

where this matrix form represents N equations for an N-modal expansion. The symbols here represent the digested form of the second sentence of this paragraph. A single equation

from this matrix form, let us say the ith, is

$$\frac{1}{r^p}\frac{\partial}{\partial r}\left[r^p \frac{\partial}{\partial r} a_i(r,z)\right] + \frac{\partial^2}{\partial z^2} a_i(r,z) + \sum_{\ell=1}^{N} (\Sigma_{st})_{i\ell}$$

$$a_\ell(r,z) = \frac{1}{\lambda} \sum_{\ell=1}^{N} (\chi\nu\Sigma_f)_{i\ell}\, a_\ell(r,z) \qquad (6\text{-}13)$$

Next we lay out a mesh spacing in our generalized orthogonal r-z geometry with r having points j=1 to J and z having points k=1 to K. Points are included on interfaces and at exterior boundaries. First let us consider a point interior to a region, namely point j,k with coordinates r_j, z_k.

We multiply equation (6-13) by r^p and integrate over the region enclosed by the dashed rectangle in Figure (6-1), namely, from $r_j - \frac{\Delta r_{j-1}}{2}$ to $r_j + \frac{\Delta r_j}{2}$ and from $z_k - \frac{\Delta z_{k-1}}{2}$ to $z_k + \frac{\Delta z_k}{2}$. Thus, term by term we have

$$\int\int \frac{\partial}{\partial r} r^p \frac{\partial}{\partial r} a_i(r,z)\, dr dz = r^p \frac{\partial}{\partial r} a_k^i(r) \Bigg|_{r_j - \frac{\Delta r_{j-1}}{2}}^{r_j + \frac{\Delta r_j}{2}} \cdot$$

$$\frac{\Delta z_k + \Delta z_{k-1}}{2} = \left(r_j + \frac{\Delta r_j}{2}\right)^p \left(\frac{a^i_{j+1,k} - a^i_{j,k}}{\Delta r_j}\right)$$

$$\left(\frac{\Delta z_k + \Delta z_{k-1}}{2}\right) - \left(r_j - \frac{\Delta r_{j-1}}{2}\right)^p \left(\frac{a^i_{j,k} - a^i_{j-1,k}}{\Delta r_{j-1}}\right) \qquad (6\text{-}14)$$

$$\left(\frac{\Delta z_k + \Delta z_{k-1}}{2}\right)$$

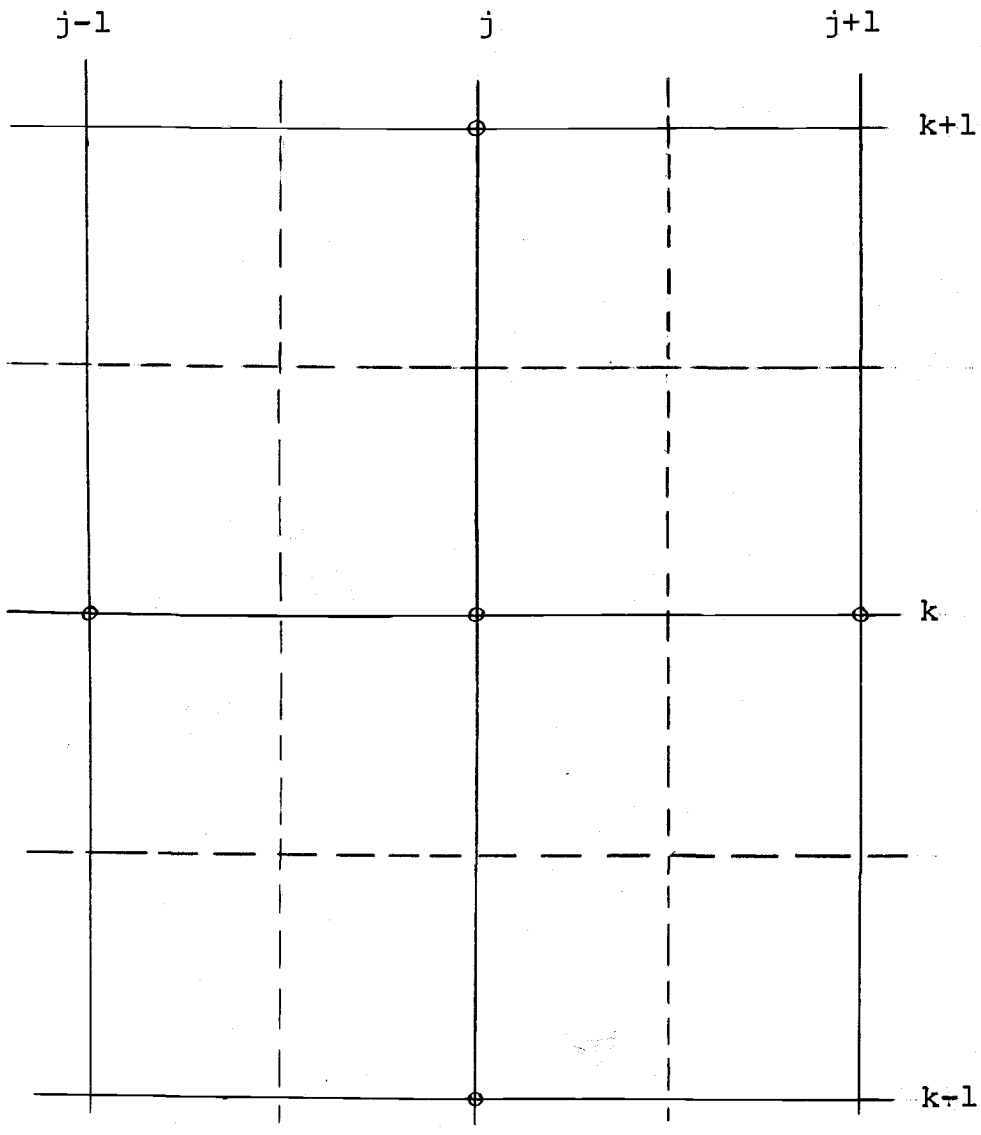

Figure 6.1. Mesh Notation.

$$\iint r^p \frac{\partial^2}{\partial z^2} a_i(r,z)\,dr\,dz = \frac{r^{p+1}}{p+1}\Bigg|_{r_j - \frac{\Delta r_{j-1}}{2}}^{r_j + \frac{\Delta r_j}{2}} \frac{\partial a_j^i(z)}{\partial z}\Bigg|_{z_k - \frac{\Delta z_{k-1}}{2}}^{z_k + \frac{\Delta z_k}{2}}$$

$$= \left[\frac{(r_j + \frac{\Delta r_j}{2})^{p+1}}{p+1} - \frac{(r_j - \frac{\Delta r_{j-1}}{2})^{p+1}}{p+1}\right] \tag{6-15}$$

$$\left[\frac{a^i_{j,k+1} - a^i_{j,k}}{\Delta z_k} - \frac{a^i_{j,k} - a^i_{j,k-1}}{\Delta z_{k-1}}\right]$$

$$\iint \sum_{\ell=1}^{N} (\Sigma_{st})_{i\ell}\, a_\ell(r,z)\, r^p\, dr\,dz = \sum_{\ell=1}^{N} (\Sigma_{st})_{i\ell} a_k^\ell(r)$$

$$\frac{r^{p+1}}{p+1}\Bigg|_{r_j - \frac{\Delta r_{j-1}}{2}}^{r_j + \frac{\Delta r_j}{2}} \frac{\Delta z_k + \Delta z_{k-1}}{2} = \tag{6-16}$$

$$\sum_{\ell=1}^{N} (\Sigma_{st})_{i\ell}\, a^\ell_{j,k} \left[\frac{(r_j + \frac{\Delta r_j}{2})^{p+1}}{p+1} - \frac{(r_j - \frac{\Delta r_{j-1}}{2})^{p+1}}{p+1}\right] \cdot$$

$$\left[\frac{\Delta z_k + \Delta z_{k-1}}{2}\right]$$

The development for the right hand side is identical with that for (6-14), giving

$$\frac{1}{\lambda} \sum_{\ell=1}^{N} \iint (\chi\nu\Sigma_f)_{i\ell}\, a^\ell(r,z)\, dr\,dz = \frac{1}{\lambda} \sum_{\ell=1}^{N} (\chi\nu\Sigma_f)_{i\ell}\, a^\ell_{j,k} \tag{6-17}$$

$$\left[\frac{(r_j + \frac{\Delta r_j}{2})^{p+1}}{p+1} - \frac{(r_j - \frac{\Delta r_{j-1}}{2})^{p+1}}{p+1}\right] \cdot \left[\frac{\Delta z_k + \Delta z_{k-1}}{2}\right]$$

To simplify this, we will use the following notation:

$$VZ_k = \frac{\Delta z_k + \Delta z_{k-1}}{2} \tag{6-18}$$

$$VR_j = \frac{(r_j + \frac{\Delta r_j}{2})^{p+1}}{p+1} - \frac{(r_j - \frac{\Delta r_{j-1}}{2})^{p+1}}{p+1} \tag{6-19}$$

$$V_{j,k} = VR_j \cdot VZ_k \tag{6-20}$$

The reason for using the symbol V is that this represents volume, of one radian third dimension for cylindrical geometry and unit length third dimension for slab geometry.

Combining the terms with these substitutions, one has

$$\begin{aligned} &\frac{(r_j + \frac{\Delta r_j}{2})^p}{\Delta r_j} VZ_k\, a^i_{j+1,k} + \frac{(r_j - \frac{\Delta r_{j-1}}{2})^p}{\Delta r_{j-1}} VZ_k\, a^i_{j-1,k} + \\ &\frac{1}{\Delta z_k} VR_j\, a^i_{j,k+1} + \frac{1}{\Delta z_{k-1}} VR_j\, a^i_{j,k-1} - \{b_{j,k} + \\ &c_{j,k} + d_{j,k} + e_{k,j} - (\Sigma_{st})_{ii} V_{j,k}\}\, a^i_{j,k} + \\ &\sum_{\ell \neq i} (\Sigma_{st})_{i\ell} V_{j,k}\, a^\ell_{j,k} = \frac{1}{\lambda} \sum_{\ell=1}^{N} (\chi\nu\Sigma_f)_{i\ell} V_{j,k}\, a^\ell_{j,k} \end{aligned} \tag{6-21}$$

where $b_{j,k}$ is the coefficient to $a^i_{j+1,k}$ in the first term of the equation and $c_{j,k}$, $d_{j,k}$ and $e_{j,k}$ are the coefficients in the second, third and fourth terms respectively.

This is a standard form for this difference equation except for two changes. First, one typically has a diagonal but not an identity D matrix and second, the scatter matrix

appears separated on the right hand side for typical multi-group codes. Because this is a two dimensional code, our choice of approximation leads to a 5-point difference equation, i.e., there are 5 space points represented in the above equation. (Note that in the above $b_{j,k} = c_{j+1,k}$ and $d_{j,k} = e_{j,k+1}$).

6.4 The Two Dimensional Code

6.4.1 The Equation Form

The choice of how to construct a two-dimensional code was an outgrowth of the success of the simultaneous solution methods used in the one dimensional code. A decision was made to solve simultaneously for all combining coefficients at all radial space points along a line of constant axial dimension Z and axial index k. This was done by shifting the terms involving $a^i_{j,k+1}$ and $a^i_{j,k-1}$ in equation (6-21) to the right hand side of the equation where they essentially become part of the source. The resulting left hand side involves three space points on a line of constant Z and is identical in form to the one dimensional equation of Chapter II.

6.4.2 Some Restrictions on Mesh Spacing for Computational Simplicity

Consider the G.E. quarter geometry as an example. All of the regional interfaces are completed (dashed lines) to

divide the regions into rectangles. In the following discussion, axial (radial) region one will refer to the lowest (left most) group of three rectangles, etc.

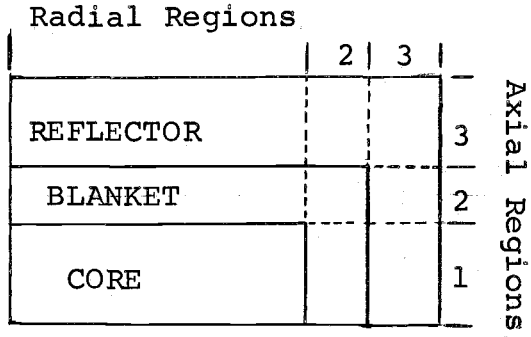

Figure 6-2. Regional Notation

A restriction will be made that all mesh lines are continuous across interfaces. It is also required that all axial mesh intervals within an axial region be equal. Radial mesh spacing within a radial region has also been kept constant, but this is not necessary for the code.

To provide a set of equations whose solution is similar to that described in Chapter III, the third and fourth terms of equation 6-19 are moved to the right hand side. Then, combining all of these equations along a radial mesh line (line of constant z with axial index k), this can be written as a single matrix equation.

$$\bar{\bar{Q}}\ \bar{a}_k = \overline{\text{Source}_k} \qquad (6\text{-}22)$$

This is a multidiagonal matrix equation with the same form as equations (3-4) and (3-5) except for the axial derivative terms.

In the Q matrix, only the cross-sections and the Δz appearing in $V_{j,k}$, VZ_k and Δz_k vary with axial position and

these change only at regional interfaces. Thus, the same Q matrix can be used, with the appropriate source, for every interior mesh line (line of constant z) of an axial region. For example, for the G.E. model, it is only necessary to produce and "invert" (Crout method) three Q matrices, one for each axial region.

In section 6.4.5, it will be demonstrated that it is also possible to use the same Q matrix for an exterior mesh line of the region.

6.4.3 General Iterative Scheme

The general scheme is to assume a flux distribution for all points and calculate a fission source. Then, beginning with the axial line at z=0, equation (6-22) is solved for the a_k vector for each successive line of increasing z (and index k). Leaving the detail of crossing interfaces until later, this cycling to solve for successive a_k is repeated to improve the axial flux shape.

This sweep through lines of increasing k to calculate new fluxes (actually combining coefficients) is called an inner iteration. Normal procedure is to sweep through a preset number of times or until the fluxes change by less than some preset fractional amount, whichever comes first.

At this point a new fission source is calculated. The ratio of this new total fission source to that for the previous iteration (the original total source) is just the

definition of the effective multiplication constant and indeed approaches that number as the flux approaches the proper shape. This is the eigenvalue λ. The calculating of the new fission source and λ is an outer iteration.

Unless the flux is to increase by λ at each outer iteration, it must be renormalized. There are a number of ways of doing this, basically all normalize the total fission source to its original magnitude. In the present code, the values of the χ_i, or the fission yields for each "group", are changed by dividing by λ after each outer iteration to normalize the fission source. After sufficient iterations, λ approaches to within some preset tolerance from unity and the eigenvalue is said to have converged. The ratio of the original χ_i to the χ_i at convergence is the effective multiplication constant. For example, if χ_i has been reduced to 0.8 of its original value, using the original (true) value will cause a neutron multiplication of 1.0/0.8=1.25 per generation.

This is the source-flux iteration of the code. A flux shape is assumed and a fission source calculated. Then inner iterations are made to improve the axial flux shape, an outer iteration calculates a new fission source and tests for convergence, etc. When the flux and eigenvalue have converged to acceptable levels, the calculation is complete.

In the discussion above the treatment at interfaces between axial regions has been neglected. This detail will be considered in the next two sections before examining the results of the calculations.

6.4.4 The Interface Between Axial Regions/Integrals Over a Half Interval

Equation (6-21) has been developed for points interior to a region. To treat the interfaces between axial regions, it will be necessary to develop equations for exterior points of a region. Figure 6-3 is included as an aid to this development. Axial region 1 has a reflected lower boundary at z=0 (and k=1) and includes two space intervals. The solid lines in the diagram separate space intervals, with the space points at the intersections of intervals. Axial indices 3 and 4 refer to expansion at the regional interface in terms of the trial function sets for region 1 and region 2, respectively. Thus, $a^i_{j,3}$ is the combining coefficient for the ith mode of the region 1 set and $a^i_{j,4}$ the coefficient for the ith mode of the region 2 set, etc.

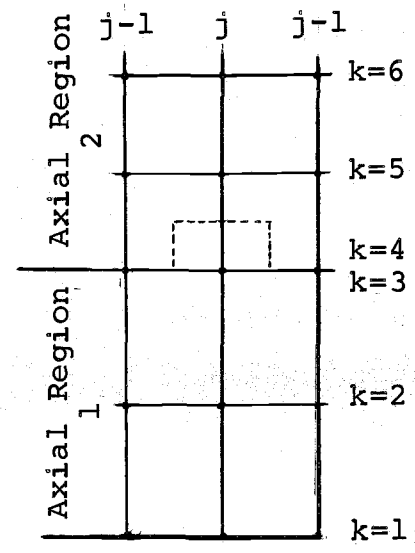

Figure 6-3. Finite Difference Mesh

Consider the integration of equation 6-13 over the region from $r_j - \Delta r_{j-1}/2$ to $r_j + \Delta r_j/2$ and from z_4 to $z_4 +$

$\Delta z_4/2$. This is a half interval in region 2. This integration produces an equation similar to equation (6-21), namely

$$\begin{aligned} & b_{j,4}\, a^i_{j+1,4} + c_{j,4}\, a^i_{j-1,4} + d_{j,4}\, a^i_{j,5} + \\ & VR_j\, \nabla_z a^i_{j,+} - [b_{j,4} + c_{j,4} + d_{j,4} - \\ & (\Sigma_{st})_{ii}\, V_{j,4}]\, a^i_{j,4} + \sum_{n\neq i} (\Sigma_{st})_{in}\, V_{j,4} \\ & a^n_{j,4} = \frac{1}{\lambda} \sum_{n=1}^{N} (\chi\nu\Sigma_f)_{in}\, V_{j,4}\, a^n_{j,4} \end{aligned} \tag{6-23}$$

The notable differences between this equation and equation (6-21) are:

1. $VZ_4 = \Delta z/2$ where Δz is the mesh interval for region 2.
2. $V_{j,4}$ thus is also a half interval.
3. $\nabla_z\, a^i_{j,+} = \frac{d}{dz}\, a^i_j$ is the axial gradient at the interface where the a^i_j are combining coefficients for the modes of region 2. The + sign is used to denote the region above the interface (- sign below) to avoid confusion with the point indices.
4. Since the gradient appears directly, the term $e_{j,4}$ does not appear.

A similar equation can be developed by integration over the top half interval in region 1, namely, from $z_3 - \Delta z_2/2$ to z_3 and from $r_j - \Delta r_{j-1}/2$ to $r_j + \Delta r_j/2$. This equation is

$$b_{j,3}\, a^i_{j+1,3} + c_{j,3}\, a^i_{j-1,3} + VR_j\, \nabla_z a^i_{j,-} +$$

$$e_{j,3}\, a^i_{j,2} - [b_{j,3} + c_{j,3} + e_{j,3} -$$

$$(\Sigma_{st})_{ii}\, V_{j,3}]a^i_{j,3} + \sum_{n\neq i}(\Sigma_{st})_{in}\, V_{j,3}\, a^n_{j,3} = \quad (6\text{-}24)$$

$$\frac{1}{\lambda} \sum_{n=1}^{N} (\chi\nu\Sigma_f)_{in}\, V_{j,3}\, a^n_{j,3}$$

The list of differences between this and equation (6-21) is similar to that above including the half intervals in volume, absence of the d terms, and their replacement with the gradient in terms of the modal expansion of region 1.

6.4.5 The Interface Between Axial Regions/General Scheme

The general iteration of section 6.4.3 treats lines of increasing z (and index k) successively. In this process the half interval equations (6-23) and (6-24) are used. The solution of these equations by using the Q matrices of equation (6-22) will first be established before discussing the actual scheme.

Consider equation (6-23). Transferring the third and fourth terms to the right hand side of the equation, the set of equations can be combined into a single multidiagonal matrix equation of the same form as equation (6-22).

$$\bar{\bar{Q}}'\, \bar{a}_4 = \overline{Source_4} \qquad (6\text{-}25)$$

Examining the elements of (6-23) which are included in Q', they are each half as large as those for a point interior to the region, except for $d_{j,4}$. However, $d_{j,k} = e_{j,k}$ for such an interior point and $e_{j,k}$ is missing from Q' thus halving this contribution also. Thus, the elements of the matrix Q' are each half of those of the Q matrix for the same region. This is fortunate, since it allows the use of the inverted Q matrix for the half interval solution. Specifically, the equation

$$2\bar{\bar{Q}}' \; \bar{a}_4 = \bar{\bar{Q}} \; \bar{a}_4 = 2 \; \overline{\text{Source}}_4 \qquad (6\text{-}26)$$

is solved. That is, the source for line 4 of Figure 6-3 is multiplied by two and the second equation of (6-26) solved for $\overline{a_4}$.

It is now possible to discuss the overall iteration scheme. A flux guess is made for all points in the system and a fission source calculated. Then an equation of the form (6-26) is solved for the set of coefficients for line 1, that is, for $\overline{a_1}$. Line 1 has a reflected boundary and thus $\nabla_z a^i_{j,+} = 0$ is used in the source term. Next the general regional matrix equation (6-22) is solved for the coefficients of line 2 ($\overline{a_2}$), with the improved $\overline{a_1}$ appearing in the source term for that calculation. This is repeated until only the equation for the last half interval of region 1 remains below the first interface.

At this point a decision must be made. Equations (6-23) and (6-24) can both be solved by using the Q matrices for their respective regions in an equation of the form of equation (6-26). However, since information about the axial flux gradient is also needed, one of the equations must be solved for the gradients. The choice used in the code, which is arbitrary and open to further investigation, is to solve the equations for the half interval below the interface for the fluxes. This assumes an initial guess of $\nabla_z a^i_{j,-}$. Then the fluxes (combining coefficients) in terms of the modal set above the interface are calculated using

$$\overline{a_{j,k+1}} = \overline{\overline{ZM}}\ \overline{a_{j,k}} \qquad (6\text{-}27)$$

where ZM is the M matrix of equation (6-6) applied in the z direction.

Next, equation (6-23) for the first half interval in region 2 is solved for $\nabla_z a^i_{j,+}$. These are calculated individually. From these the gradient in terms of the modal set below the interface are calculated using

$$\overline{\nabla_z a_{j,-}} = \overline{\overline{ZN}}\ \overline{\nabla_z a_{j,+}} \qquad (6\text{-}28)$$

The $\nabla_z a_{j,-}$ are used in the source term of the top line of region 1 for the next inner iteration. Note that ZN is the inverse of that used in the one dimensional code. That

is, it calculates gradients for the region nearer the core from gradients from the region further away.

The matrix solution method [equation (6-22] is now used for successive lines of increasing z and index k for axial region 2 until the next interface is reached, etc.

Only the exterior axial boundary remains. Consider that the fluxes go to zero at mesh line k=K. Equation (6-21) is applicable for the integration of the k=K-1 line. A value of zero is inserted for $a^i_{j,k+1} = a^i_{j,K}$ in that equation. General use of the Q matrix solution is applicable.

6.5 Results of Two Dimensional Calculations

The number of calculations in two space dimensions is necessarily limited due to the substantially increased calculational times when compared to one dimensional calculations. A summary of these calculations is included in Table 6-1.

The first calculation uses bracketing fluxes chosen from the radial case as trial functions. Fluxes from points 1 and 40 are used in the core, 41 and 50 in the blanket and 51 and 60 in the reflector. The weighting is Galerkin. The error in k_{eff} of -1.6% is large.

Considering that the above choice might not be broad enough to bracket the blanket and reflector, a broader choice was made there. Case II uses this choice with essentially identical results. Cases III-V use the same choice

Table 6-1. Two Dimensional Results

Case	WF	Reactor	Error in k_{eff}(%)	Core TF
I	Gal.	GE	-1.6	1R,40R
II	Gal.	GE	-1.5	1R,40R
III	Gal.	GE	-1.92	20R,15A
IV	Gal.	GE	-1.1	1A,20A
V	Gal.	GE	-1.04	1A,27A
VI	Gal.	EBR	3.1	1A,12A
VII	Gal.	EBR	-1.9	1A, 9A
VIII	Gal.	EBR	- .64	1A,10A
IX	Gal.	GE	-1.2	10R,35R,45R
X	Gal.+1	GE	- .73	10R,35R,45R
XI	group	GE	.5	1R,40R
XII	group	GE	.21	1,45,55

of trial functions in the blanket and reflector as for case II. Case III tests a mixture of radial and axial functions while cases IV and V test use of axial fluxes. The latter have somewhat smaller errors. The choice in going into the blanket appreciably for case V is to use a softer spectrum, perhaps more representative of the far corner of the core, which will better bracket the overall core. The change is slight.

Cases VI-VIII are a similar test for the EBR model, with a variety of trial functions for the core and bracketing trial functions for the other regions. Here the various choices bracket the correct k_{eff}, but the dependence on trial function does not provide a useful reliability. It is noted that this bracketing of the correct k_{eff} is possible here because the fluxes rapidly become softer with depth in the reflector. Changes in the G.E. blanket are much less.

Case IX is a calculation for the G.E. model using spatially discontinuous modes with considerable overlap between trial function sets. Trial functions in the core are 10R, 35R, 45R with the set in the blanket and reflector being 35R, 45R, 55R. This is set A of Chapter V. The two dimensional calculation yields an error of -1.2%. This compares with errors for the one dimensional calculations of -.013% and -.13% for the radial and axial cases respectively.

The above cases are a rather extensive group of negative results. They were obtained with a new code. Consequently, considerable effort was expended in testing the new code. For example, a cartesian (x,y) geometry problem was run with coordinates reversed to verify that the iterative (axial) solution was identical with the simultaneous radial solution.

Satisfied that the code was operating properly, the formulation itself came under scrutiny. In particular, the only other two dimensional work which had been done was that by Lorenzini and Robinson (33, 34). This method has since been evaluated by Greenspan (13). Their method, while limited to spatially continuous trial functions, yields generally better results than those above. Their interface conditions require the conservation of integrals of flux and current at interfaces. This motivated the investigation of forcing this conservation with spatially discontinuous trial functions.

Case X examines the same three mode expansion as case IX except for the use of Galerkin+1 weighting at the regional interfaces. That is, one of the weight functions at each interface is replaced by unity, conserving integrals of flux and current. This reduces the error in k_{eff} to 0.73%.

The remainder of the two dimensional results are for cases where integrals of flux and current across interfaces

are conserved. Rerunning the bracketing fluxes of Case I with group weighting (case XI) yields an error in k_{eff} of 0.5%. A three mode group weighted run with three continuous trial functions (case XII) reduces the error in k_{eff} to 0.21%.

It is reasonable that the two dimensional calculation is more sensitive to interface conditions than the one dimensional calculation. In the two dimensional calculations all of the leakage is calculated within the code, while for the one dimensional calculation that part of the leakage perpendicular to the direction of interest is treated by an artificial absorption term. If the perpendicular buckling is accurately known, this will automatically add accuracy to the latter calculation.

6.5.1 Analysis of the Two Dimensional Results

To further examine the two dimensional results a number of methods are used.

First, an attempt is made to answer the question, "Is the spectral shape at a given point as good as it can be with the given set of trial functions?" To examine this, the 26 group fluxes are synthesized using the usual expansion equation. This has been done for a number of points for Case X and is included in Tables 6-2, 6-3, and 6-4. Also included in the same tables are least square fits to the true fluxes (26 group, two dimensional) for comparison.

Table 6-2. Fit of Synthesized Flux at Core Center. Case X.

Group	Syn. Flux from 2-D Modal Calc.	Flux from 26-Group 2-D Calc.	Error (%)	Least Square Error (%)
1	5.1942E 13	5.1796E 13	.282	-0.002
2	2.6791E 14	2.6705E 14	.322	.017
3	6.5642E 14	6.5439E 14	.311	.017
4	9.1963E 14	9.1632E 14	.361	.097
5	1.1867E 15	1.1831E 15	.311	.100
6	2.2202E 15	2.2245E 15	-0.191	-0.244
7	2.7398E 15	2.7457E 15	-0.216	-0.207
8	2.7467E 15	2.7426E 15	.149	.098
9	2.2973E 15	2.2839E 15	.586	.386
10	1.7150E 15	1.7059E 15	.536	.091
11	1.0851E 15	1.0746E 15	.981	.228
12	4.6465E 14	4.6889E 14	-0.904	-1.759
13	1.6699E 14	1.6989E 14	-1.708	-2.586
14	2.3019E 14	2.3700E 14	-2.874	-4.049
15	7.3832E 13	8.2325E 13	-10.316	-11.526
16	1.3813E 13	2.1776E 13	-36.567	-36.945
17	4.4577E 11	4.3274E 12	-89.699	-87.847
18	-1.2521E 12	5.5612E 11	-325.142	-311.005
19	-5.6675E 11	8.3838E 10	-776.004	-739.655
20	-1.3217E 11	6.0152E 09	-2297.348	-2176.982
21	-1.7150E 10	4.8715E 08	-3620.542	-3428.864
22	-6.4457F 10	9.1700E 07	*	*
23	-2.3287E 10	3.5760E 06	*	*
24	-9.7519E 09	8.6971E 04	*	*
25	-2.7402E 08	4.7701E 02	*	*
26	-1.0711E 07	3.4939E 00	*	*

* Computer overflow.

Table 6-3. Fit of Synthesized Flux at Core-Blanket Interface. Case X.

Group	Syn. Flux from 2-D Modal Calc.	Flux from 26-Group 2-D Calc.	Error (%)	Least Square Error (%)
1	8.0261E 12	8.5941E 12	-6.609	-0.880
2	4.1041E 13	4.4097E 13	-6.931	-0.973
3	1.0084E 14	1.0802E 14	-6.649	-0.754
4	1.4118E 14	1.5107E 14	-6.543	-0.623
5	1.8373E 14	1.9488E 14	-5.724	.003
6	3.6913E 14	3.8254E 14	-3.505	.319
7	4.8834E 14	4.9917E 14	-2.170	-0.170
8	5.2141E 14	5.2463E 14	-0.613	-0.196
9	4.6646E 14	4.6166E 14	1.039	-0.179
10	3.8304E 14	3.7120E 14	3.192	-0.240
11	2.5779E 14	2.4612E 14	4.738	-0.074
12	1.2401E 14	1.1507E 14	7.764	.448
13	4.6395E 13	4.2574D 13	8.975	.813
14	7.0465E 13	6.3635E 13	10.732	.693
15	3.0104E 13	2.5335E 13	18.824	3.461
16	1.2393E 13	8.8748E 12	39.640	12.714
17	4.1536E 12	2.4291E 12	70.993	29.839
18	1.4532E 12	5.4453E 11	166.869	90.351
19	4.8526E 11	1.4668E 11	230.828	131.156
20	9.8356E 10	1.7639E 10	457.611	284.949
21	1.2455E 10	2.0411E 09	510.192	320.287
22	4.4884E 10	4.0952E 09	996.016	651.830
23	1.6133E 10	5.5493E 08	2807.217	1893.226
24	6.7515E 09	1.1551E 08	5744.994	3907.143
25	1.8970E 08	9.0315E 05	20904.384	14299.891
26	7.4151E 06	3.0486E 04	24223.185	16575.137

Table 6-4. Fit of Synthesized Flux in Blanket. Case X.

Group	Syn. Flux from 2-D Modal Cald.	Flux From 26-Group 2-D Calc.	Error (%)	Least Square Error (%)
1	2.2209E 12	2.2743E 12	-2.349	2.209
2	1.0980E 13	1.1235E 13	-2.271	2.554
3	2.7297E 13	2.9825E 13	-2.249	2.455
4	3.8293E 13	3.9143E 13	-2.171	2.487
5	5.1868E 13	5.2835E 13	-1.830	1.975
6	1.3065E 14	1.3382E 14	-2.371	.072
7	2.0278E 14	2.0749E 14	-2.267	-0.364
8	2.4360E 14	2.4575E 14	-0.876	-0.449
9	2.3943E 14	2.4019E 14	-0.317	.046
10	2.2061E 14	2.1908E 14	.695	.197
11	1.5749E 14	1.5485E 14	1.708	.614
12	8.4371E 13	8.2704E 13	2.015	.401
13	3.2675E 13	3.1919E 13	2.369	.274
14	5.3221E 13	5.1374E 13	3.596	.181
15	2.6897E 13	2.5554E 13	5.255	-0.686
16	1.4094E 13	1.3064E 13	7.881	-2.089
17	5.8154E 12	5.0173E 12	15.907	-6.095
18	2.5978E 12	1.9694E 12	31.911	-14.023
19	1.1546E 12	6.7475E 11	71.114	-34.708
20	4.8480E 11	1.3864E 11	248.964	-134.525
21	2.4873E 11	1.7596E 10	1313.493	-739.896
22	2.0692E 11	6.3029E 10	228.303	-120.397
23	9.4379E 10	2.2653E 10	316.625	-170.345
24	3.7452E 10	9.4641E 09	295.726	-158.165
25	8.4142E 09	2.6611E 08	3061.946	-1729.393
26	6.7411E 08	1.0443E 07	6354.968	-3600.367

The two fits are generally very comparable, except that the modal fit is somewhat poorer at the core-blanket interface. This indicates that the two dimensional code determines the spectral shape about as well as can be done within the limits of the trial functions available.

Next, for cases X, XI, and XII an examination is made of the accuracy of fit along a radial traverse. The synthesized fluxes along the traverse are used to calculate reaction rates as a function of position and these are compared to the 26 group two dimensional calculation for the same traverse. Normalization is to the same source. These comparisons are made with the aid of a Lagrangian interpolation scheme since the mesh spacings are different.

The results of this comparison are summarized in the regional reaction rate errors of Table 6-5 and the absorption errors as a function of position in Figure 6-4. The fit is generally highly acceptable except for the reflector for case X. This is noted by comparing case X with case 20 of Table 5-7 and on the graph of Figure 5-2. Similarly, Case XI can be compared to the group weighted two mode calculation of Table 5-10 and Figure 5-6 and Case XII corresponds to case 30 of Table 5-9 and Figure 5-5. Since the error curves for the two dimensional calculation are nearly identical to that for the one dimensional case, it appears that the numerical treatment for the two dimensional code is performing well. The fit in the core is not as good as

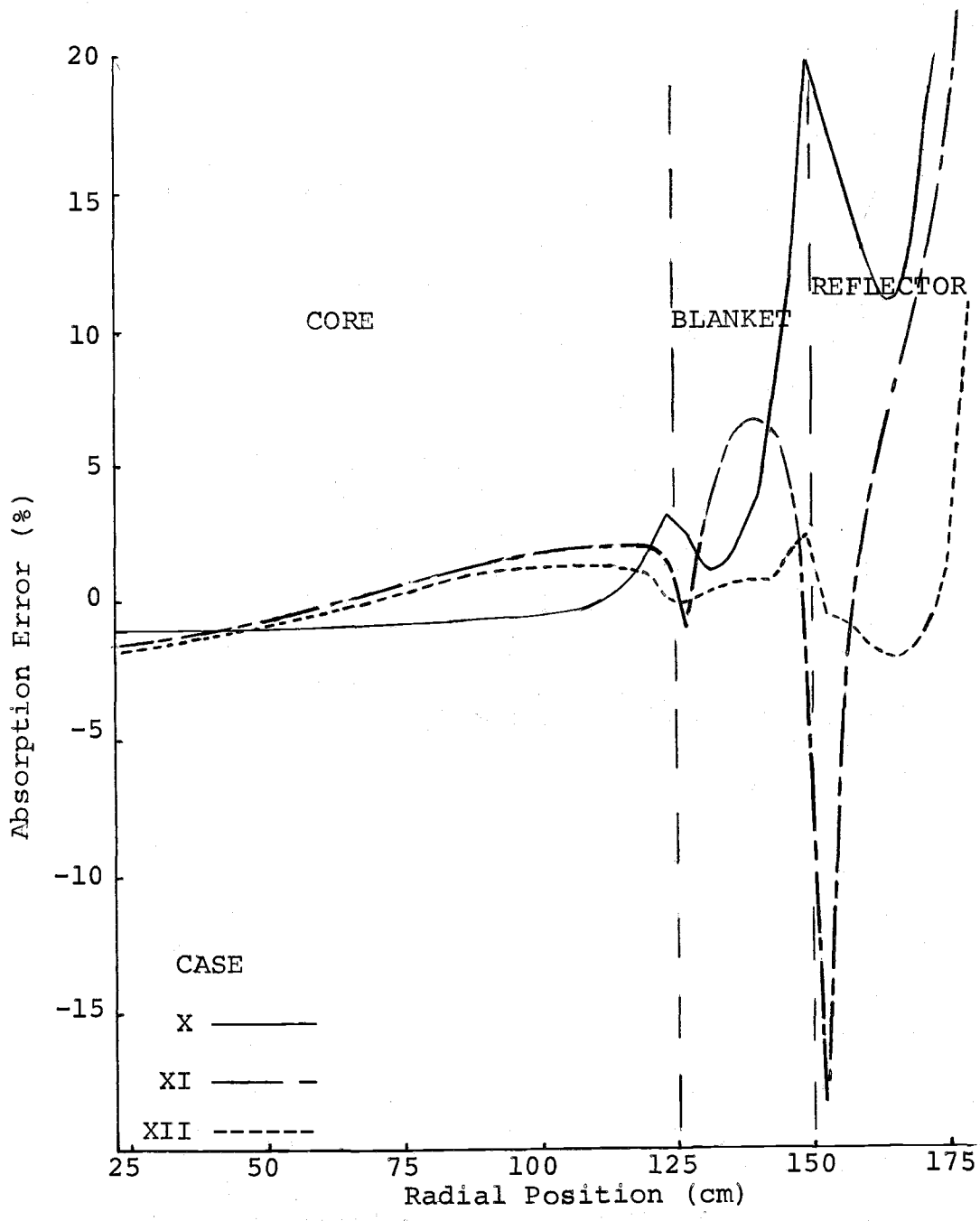

Figure 6-4. Absorption Error as a Function of Radial Position.

the one dimensional fit. This is thought to be caused by the flux not being fully converged.

Table 6-5. Regional Reaction Rate Errors for Two Dimensional Calculations

Case	T.F. Set	Wts.	Absorption Error (%) Core	Blanket	Reflector	Fission Error (%) Core	Blanket
X	A	Gal.+1	-.60	6.6	17.5	-.23	9.7
XI	F	Group	.25	3.8	-1.2	-.20	9.8
XII	E	Group	-.13	1.7	-1.5	-.085	4.0

T.F. Sets: A 10,35,45; 35,45,55; 35,45,55

F 1,40; 41,50; 51,60

E 1,45,55; 1,45,55; 1,45,55

6.2 Assessment of the Code, Suggestions

The two dimensional code in its present form has demonstrated reasonable convergence properties and speed. It has converged for the continuous trial function case and for a number of cases using discontinuous trial functions. We have experienced convergence failure for three cases using discontinuous trial functions: with considerable set overlap using adjoint and reaction rate weighting, and with slight set overlap using Galerkin+1 weighting. All were three mode calculations.

The author feels that the direction taken in producing the present code is correct. Other attempts in two dimensions have been with continuous trial functions and have

been done in standard multigroup codes. Here the problem which is of concern is the large upscatter terms inherent in overlapping groups. This has been approached by iteration on groups. In explanation, for a multigroup calculation with no upscatter, given a fission source, one can calculate the flux in the highest energy group and from this the down scatter to lower energy groups. This is repeated for the next highest energy group, etc., and when completed, one has exact answers for the fluxes caused by the assumed fission source. With upscatter terms, this is not the case since the source for the first group depends upon scatter from lower groups. To iterate on the groups means to recalculate the source for group one (and other groups) after calculations are made for succeeding groups.

The simultaneous solution method of this thesis provides an exact answer for a given fission source, independent of direction of scatter.

We feel that the primary difficulty with the present code is associated with the interface crossing method in the axial iterative procedure. The reason for so adjudging is experience. We have found that an underrelaxation of the derivative term $\nabla_z a(r,z)$ is a necessity in operating the code. Briefly, over-relaxation is a technique usually used to speed convergence of an iteration procedure (10). One writes

$$b_{or}^{p+1} = b^p + \alpha\ (b^{p+1} - b^p),$$

where p refers to the pth iteration and p + 1 to the p + 1th iteration. The over-relaxed value is on the left. If α, or the over-relaxation, is one, the new value is just that obtained by a standard iterative procedure. If it is greater than one, the difference between old and new values is increased.

The two dimensional code has typically been run with an α of .5 for the $\nabla_z a(r,z)$ at the interface between axial regions to control oscillatory behavior. The general fluxes and fission sources have been moderately over-relaxed (1.0-1.2).

A suggested method to solve this problem is to adopt an alternating direction scheme. That is, equation (6-21) can be adopted for Q matrix solution along both radial and axial lines. Specifically, for the axial lines, the a and b terms of (6-21) (the radial derivative terms) are moved to the right hand side of the equation. Then, dividing the resulting equation by VR_j, the resulting equation is soluble by a single Q matrix for each radial region. With this alternating direction scheme, the complicated iterative crossing between axial regions is not used and the Q matrix solution can be used throughout.

BIBLIOGRAPHY

1. Ball, T. W. Synthesis of lifetime power distribution in r-z geometry. Bettis Technical Review, no. WAPD-BT-8, p. 39-45. 1958.

2. Becker, Martin. Overlapping group methods with discontinuous trial functions. Nuclear Science and Engineering 34:339-341. 1968.

3. Becker, Martin. Asymmetric discontinuities in synthesis techniques for initial-value problems. Nuclear Science and Engineering 34:343-344. 1968.

4. Becker, Martin. A principle of information flow for the treatment of discontinuities in synthesis techniques. Nuclear Science and Engineering 47:365-370. 1972.

5. Bell, G. I. and S. Glasstone. Nuclear reactor theory. New York, Van Nostrand Reinhold, 1970. 619 p.

6. Bondarenko, I. I. (ed.). Group constants for nuclear reactor calculations. New York, Consultants Bureau, 1964. 151 p.

7. Buslik, A. J. The description of the thermal neutron spatially dependent spectrum by means of variational principles. Bettis Technical Review, no. WAPD-BT-25, p. 1-24. 1962.

8. Buslik, A. J. Interface conditions for few group neutron diffusion equations with flux-adjoint weighted constants. Nuclear Science and Engineering 32:233-240. 1968.

9. Calame, G. P. and F. D. Federighi. A variational procedure for determining spatially dependent thermal spectra. Nuclear Science and Engineering 10:190-201. 1961.

10. Clark, M. and K. F. Hansen. Numerical methods of reactor analysis. New York, Academic, 1964. 340 p.

11. Cockayne, J. E. and K. O. Ott. Successive space-energy synthesis for neutron fluxes in fast reactors. Nuclear Science and Engineering 43:159-172. 1971.

12. Federighi F. D. and P. A. Ombrellaro. Spatially dependent spectra at energies above thermal. Transactions of the American Nuclear Society 5:40. 1962.

13. Greenspan, H. Studies in spectral neutron flux synthesis. Nuclear Science and Engineering 50:75-78. 1973.

14. Halgas, R. S. and M. Bender. Half height cadmium slab. Bettis Technical Review, no. WAPD-BT-8, p. 15-22. 1957.

15. Hardie, R. W. and W. W. Little, Jr. IDX, a one-dimensional diffusion code for generating effective nuclear cross sections. Richland, Washington. Battelle Memorial Institute, 1969. 23 p. (U.S. Atomic Energy Commission. BNL-954).

16. Henry, A. F. Few group approximations based on a variational principle. Nuclear Science and Engineering 27: 493-510. 1967.

17. Herriot, J. G. Methods of mathematical analysis and computation. New York, Wiley, 1963. 198 p.

18. Hetrick, D. L. Dynamics of nuclear reactors. Chicago, University of Chicago Press, 1971. 542 p.

19. Horst, R. B. Synthesis methods in r-z geometry. Bettis Technical Review, no. WAPD-BT-8, p. 26-38. 1958.

20. Kantorovich, L. V. and V. I. Kryloff. Approximate methods of higher analysis, tr. by Curtis D. Benster. 3rd ed. Groningen, Noordhoff, 1958. 681 p.

21. Kaplan, S. On the best method for choosing the weighting functions in the method of weighted residuals. Transactions of the American Nuclear Society 6:3-4. 1963.

22. Kaplan, S. Some new methods of flux synthesis. Nuclear Science and Engineering 13:22-31. 1962.

23. Kaplan, S. Synthesis methods in reactor analysis. In: Advances in nuclear science and technology, ed. by P. Greebler and E. J. Hensly. Vol. 3. New York, Academic, 1966. p. 233-266.

24. Kiguchi, T., S. An and A. Oyama. Energy modal synthesis in fast reactor analysis. Nuclear Science and Engineering 43:328-340. 1971.

25. Lamarsh, J. R. Introduction to nuclear reactor theory. Reading, Addison-Wesley, 1966. 585 p.

26. Lambropoulos, P. and V. Luco. Functionals for discontinuous trial functions flux synthesis. Journal of Nuclear Energy A/B 24:551-564. 1970.

27. Lancefield, M. J. Space-energy flux synthesis in transport theory. Nuclear Science and Engineering 37:423-442. 1969.

28. Little, W. W., Jr. and R. W. Hardie. Methods for collapsing fast-reactor neutron cross sections. Nuclear Science and Engineering 29:402-407. 1967.

29. Little, W. W., Jr. and R. W. Hardie. FCC-IV, a revised version of the FCC fundamental mode fast reactor code. 1967. 23 p. (U.S. Atomic Energy Commission. BNWL-450.)

30. Little, W. W., Jr. and R. W. Hardie. 2DB user's manual -- revision 1. 1969. 21 p. (U.S. Atomic Energy Commission. BNWL-831.)

31. Little, W. W., Jr. et al. Numerical comparison of data processing codes for fast reactors. Transactions of the American Nuclear Society 12:144. 1969.

32. Lorentz, W. N. Synthesis of three-dimensional power shapes-application of flux-weighted synthesis technique. Bettis Technical Review, no. WAPD-BT-8, p. 46-52. 1958.

33. Lorenzini, P. G. Energy models for computing fast reactor parameters. Ph.D. thesis. Corvallis, Oregon State University, 1970. 161 numb. leaves.

34. Lorenzini, P. G. and A.H. Robinson. Solutions of the diffusion equation by the spectral synthesis method. Nuclear Science and Engineering 44:27-36. 1971.

35. McLean, J. G. and W. B. Davis. Guide to National Petroleum Council report on United States energy outlook. Washington, D. C., National Petroleum Council, 1971. 40 p.

36. McNelly, M. J. Liquid metal fast breeder reactor study. 2 vols. 1964. (U.S. Atomic Energy Commission. GEAP-4418.)

37. Meghreblian, R. V. and D. K. Holmes. Reactor analysis. New York, McGraw-Hill, 1960. 808 p.

38. Meyer, J. E. Synthesis of three dimensional power distributions for a non-uniformly depleted core. Bettis Technical Review, no. WAPD-BT-4, p. 29-41. 1957.

39. Murley, T. E. and I. Kaplan. A modal representation of fast reactor spectra. Transactions of the American Nuclear Society 8:1. 1965.

40. Natelson, M. and E. J. Gelbard. A two overlapping-group transport computational method for thermal neutron problems. Nuclear Science and Engineering 49:202-212. 1972.

41. National Petroleum Council's Committee on U.S. Energy Outlook. U.S. energy outlook, an initial appraisal, vols. 1 and 2. Washington, D.C., National Petroleum Council, 1971. 75 and 195 p.

42. Neuhold, R. J. Multiple weighting functions in fast reactor space-energy synthesis. Nuclear Science and Engineering 43:74-86. 1971.

43. Neuhold, R. J. and K. O. Ott. Improvements in fast reactor space-energy synthesis. Nuclear Science and Engineering 39:14-24. 1970.

44. Ombrellaro, P. A. Synthesis of fast reactor space-energy neutron fluxes. Nuclear Science and Engineering 44:204-220. 1971.

45. Ombrellaro, P. A. A variational procedure for calculating high energy, few group, spatially dependent spectra. Transactions of the American Nuclear Society 7:10-11. 1964.

46. Ombrellero, P. A. and F. O. Federighi. A variational procedure for calculating fast group constants. Nuclear Science and Engineering 16:343-356. 1963.

47. Sawyer, C. D. and P. R. Hill. Acceleration of fixed source and upscatter problems. Transactions of the American Nuclear Society 12:144-145. 1969.

48. Selengut, D. S. Variational analysis of multi-dimensional systems. In: Nuclear physics research quarterly report, October, November, December, 1958, Richland, Washington, Hanford Laboratories, 1959. p. 89-124. (U.S. Atomic Energy Commission. HW-59126).

49. Shiff, R. R. Synthesis of three dimensional power distributions for a non-uniformly depleted core. Bettis Technical Review, no. WAPD-BT-4, p. 23-28. 1957.

50. Stacey, Weston, M., Jr. Variational flux synthesis methods for multigroup neutron diffusion theory. Nuclear Science and Engineering 47:449-469. 1972.

51. Stacey, Weston M., Jr. Modal approximations; theory and an application to reactor physics. Cambridge, Riverside, 1967. 122 p.

52. Storrer, F. and J. M. Chaumont. The application of space-energy synthesis to the interpretation of fast multizone critical experiments. In: Proceedings of the International Conference of Fast Critical Experiments and Their Analysis, Argonne National Laboratory, Illinois, 1966. p. 439-477. (U.S. Atomic Energy Commission. ANL-7320.) (Microfilm)

53. Tobias, M. L. and T. B. Fowler. The application of the equipoise iterative method to diffusion and transport theory. In: Proceedings of the Conference on the Application of Computing Methods to Reactor Problems, Argonne National Laboratory, Illinois, 1965. p. 191-205. (U.S. Atomic Energy Commission. ANL-7050.)

54. Toivanen, T. On the variational and Bubnov-Galerkin synthesis of epithermal, spatially dependent neutron energy spectra. Journal of Nuclear Energy A/B 22:283-297. 1968.

55. Vaughn, E. U., P. F. Rose, and D. F. Hausknecht. Spectrum synthesis with spatially discontinuous basis spectra. Transactions of the American Nuclear Society 11: 528-529. 1968.

56. Wachspress, E. L., R. D. Burgess and S. Baron. Multichannel flux synthesis. Nuclear Science and Engineering 12:381-389. 1962.

57. Wachspress, E. L. On the use of different radial trial functions in different axial zones of a neutron flux synthesis computation. Nuclear Science and Engineering 34:342-343. 1968.

58. Wachspress, E. L. and M. Becker. Variational synthesis with discontinuous trial functions. In: Proceedings of the Conference on the Application of Computing Methods to Reactor Problems, Argonne National Laboratory, Illinois, 1965. p. 191-205. (U.S. Atomic Energy Commission. ANL-7050.)

59. Yasinsky, J. B. The solution of the space-time neutron group diffusion equations by a time discontinuous … method. Nuclear Science and Engineering 29:381-391. 1967.

APPENDIX

APPENDIX: THE ONE DIMENSIONAL DIFFUSION THEORY CODE WDIF1.

WDIF1 is a code of the type outlined in Chapter III. The form given is fairly specialized, namely; it uses the identity matrix in the D matrix position and is restricted to two or three modes. This can easily be modified. Over relaxation should also be added. After the first Crouting, a subroutine specialized to the number of modes treats successive new right hand sides. This was done for speed, since the code is an important building block in the two dimensional code. The code is extremely stable, it has always converged.

The input is as follows:

Input from the teletype (this could be put on cards) are extrapolation distance, convergence limit on the eigenvalue and perpendicular buckling TTYIN is applicable to the OSU computer.

Input from unit 37

Card 1 50 characters of identifying information

Card 2 NG = # of groups (modes), NR = number of regions, p = geometry factor, p = 0, slab; p = 1, cylinder; p = 2 sphere (3I5 FORMAT)

Card 4 NP(1) = No. of intervals in region 1; W(1) = width of region 1 (cm) (I5, E10.5)

Card 5 (CHI(1,IG),IG = 1,NG) Fission Fractions for modes (5E14.7)

Card 6 (SIGFN(IG),IG=1,NG) $\nu\Sigma_f$ for each group (mode)
(5 E14.7)

Card 7 (SST(1,JG),JG=1,NG) $\Sigma_{st}(1, JG)$ (5 E14.7)

Card 8 (SST(2,JG),JG=1,NG) $\Sigma_{st}(2,JG)$ (5 E14.7)

.

.

Card N (SST(NG,JG),JG = 1,NG) (5 E14.7)

Cards 4 to N repeated for successive regions.

Input from unit 19: Interface matrices M and N (all 5 E14.7)

Card 1 (XM(1,JG),JG = 1,NG) first line of M matrix at first interface

:

Card NG (XM(NG,JG),JG = 1,NG) last line of M matrix at first interface

Card NG+1 (XN(1,JG),JG = 1,NG) first line of N matrix at first interface

:

Card 2NG (XN(NG,JG),JG=1,NG) last line of N matrix

Cards for successive interfaces

```
00001:       PRØGRAM WDIF1
00002:       INTEGER P,PP1
00003:       CØMMØN A(200,7),SS(200),NØ(4,6),BØX(6,20),NR,MØD,IMAX
00004:       DIMENSIØN H(6),W(6),SST(4,4),CHI(6,4),XM(4,4),XN(4,4),
00005:      1 SIGFN(4),F(200),FISS(200),R(100),NP(6)
00006:       EFFK=EFFKØLD=1.0
00007:       REWIND 37
00008:       REWIND 19
00009:       READ(37,907)
00010:907    FØRMAT(1X,50H
     )
00011:       PRINT 907
00012:       EXTRAP=TTYIN(4HEXTR,4HAP= )
00013:       EP=TTYIN(4HEP= )
00014:       BUCK=TTYIN(4HBUCK,4H =  )
00015:       READ(37,98)NG,NR,P
00016:       MØD=NG
00017:       PP1=P+1
00018:102    FØRMAT(6E12.5)
00019:98     FØRMAT(3I5)
00020:       PRINT 99,NG,NR,P
00021:99     FØRMAT('ODIFFUSIØN THEØRY PRØBLEM'/' # ØF GRØUPS=',I5,
00022:      1 '  # ØF REGIØNS=',I5/' GEØMETRY FACTØR= ',I5)
00023:904    FØRMAT(5E14.7)
00024:C****** CALCULATE SØME CØNSTANTS ******************
00025:       MID=MØD+1
00026:       MØM1=MØD-1
00027:       MP1=MID+1
00028:       JMAX=2*MØD+1
00029:       MP2=MID+2 $ MP3=MID+3 $ MM1=MID-1 $ MM2=MID-2
00030:       MM3=MID-3 $ JMM1=JMAX-1 $ JMM2=JMAX-2
00031:       DØ 91 IR=1,NR
00032:       READ(37,901)NP(IR),W(IR)
00033:901    FØRMAT(I5,E10.5)
00034:       H(IR)=W(IR)/NP(IR)
00035:       WRITE(61,902)IR,NP(IR),W(IR)
00036:902    FØRMAT('OREGIØN',I3,' HAS',I3,'  INTERVALS & WIDTH',E10.2)
00037:       READ(37,904)(CHI(IR,IG),IG=1,NG)
00038:       PRINT 909,(CHI(IR,IG),IG=1,NG)
00039:909    FØRMAT(' FISSIØN FRACTIØN:'/6E11.3)
00040:       READ(37,904)(SIGFN(IG),IG=1,NG)
00041:       PRINT 905,(SIGFN(IG),IG=1,NG)
00042:905    FØRMAT('OSIGFN'/6E11.3)
00043:       PRINT 908
00044:908    FØRMAT('OSIGST MATRIX')
00045:       DØ 90 IG=1,NG
00046:       READ(37,904)(SST(IG,JG),JG=1,NG)
00047:       WRITE(61,101)(SST(IG,JG),JG=1,NG)
00048:101    FØRMAT(1H ,5E12.5)
00049:       SST(IG,IG)=SST(IG,IG)+BUCK
00050:90     CØNTINUE
00051:       IF(IR.EQ.1)GØ TØ 92
00052:       DØ 93 IG=1,NG
00053:93     READ(19,904)(XN(IG,JG),JG=1,NG)
00054:92     IF(IR.EQ.NR)GØ TØ 94
00055:       DØ 94 IG=1,NG
00056:       READ(19,904)(XM(IG,JG),JG=1,NG)
00057:94     CØNTINUE
00058:CCC**** SETTING UP MATRIX *************************
00059:C ******* LEFT BØUNDRY CØNDITIØNS *****************
00060:       IF(IR.NE.1)GØ TØ 444
```

```
00061:       J1=MID $ J2=2*MØD
00062:       LJ=1 $  R(1)=0.  $ V=VP=(.5*H(1))**PP1/PP1
00063:       RX=-(.5*H(1))**P/H(1)
00064:       DØ 4 IG=1,MØD
00065:       I=IG
00066:       IPMØ=I+MØD
00067:       A(I,JMAX)=A(IPMØ,1)=RX
00068:       A(I,MID)=-RX
00069:       FISS(I)=SIGFN(IG)*V
00070:       F(I)=1.0
00071:       DØ 5 J=J1,J2
00072:       JG=J-J1+1
00073:5      A(I,J)=A(I,J)+SST(IG,JG)*V
00074:       J1=J1-1  $  J2=J2-1
00075:4      CØNTINUE
00076:       N2=1
00077:       GØ TØ 445
00078:444    CØNTINUE
00079:CC **** LEFT EDGE ØF REGIØN********************
00080:       II=N2=N2+MØD
00081:       J1=MID  $  J2=2*MØD
00082:       LJ=LJ+1  $  R(LJ)=R(LJ-1)
00083:       V=VP  $  VP=(R(LJ)+.5*H(IR))**PP1/PP1  $  V=VP-V
00084:       RX=-(R(LJ)+.5*H(IR))**P/H(IR)
00085:       RP=R(LJ)**P
00086:       DØ 9 IG=1,MØD
00087:       I=II+IG-1
00088:       IPMØ=I+MØD
00089:       A(I,JMAX)=A(IPMØ,1)=RX
00090:       A(I,MID)=-A(I,JMAX)
00091:       FISS(I)=SIGFN(IG)*V
00092:       F(I)=1.0
00093:       DØ 8 J=J1,J2
00094:       JG=J-J1+1
00095:       KJG=J-MØD $ IF(KJG.LT.1)GØ TØ 8
00096:       A(I,KJG)=A(I,KJG)+RP*XN(IG,JG)
00097:8      A(I,J)=A(I,J)+SST(IG,JG)*V
00098:       J1=J1-1  $  J2=J2-1
00099:9      CØNTINUE
00100:       IRM1=IR-1
00101:       BØX(IRM1,11)=RP*XN(2,1)
00102:       IF(MØD.EQ.2)GØ TØ 443
00103:       BØX(IRM1,12)=RP*XN(3,1)
00104:       BØX(IRM1,13)=RP*XN(3,2)
00105:       IF(MØD.EQ.3)GØ TØ 443
00106:       BØX(IRM1,14)=RP*XN(4,1)
00107:       BØX(IRM1,15)=RP*XN(4,2)
00108:       BØX(IRM1,16)=RP*XN(4,3)
00109:       IF(MØD.EQ.4)GØ TØ 443
00110:443    CØNTINUE
00111:445    CØNTINUE
00112:C* * * MAIN BØDY ØF MATRIX * * * * * * * * *
00113:       N1=N2+MØD  $  N2=N1+(NP(IR)-2)*MØD
00114:       DØ 7 II=N1,N2,MØD
00115:       J1=MID $ J2=2*MØD
00116:       LJ=LJ+1  $  R(LJ)=R(LJ-1)+H(IR)
00117:       V=VP  $  VP=(R(LJ)+.5*H(IR))**PP1/PP1 $ V=VP-V
00118:       RX=-(R(LJ)+.5*H(IR))**P/H(IR)
00119:       DØ 10 IG=1,MØD
00120:       I=II-1+IG
```

```
00121:       IPMØ=I+MØD
00122:       A(I,JMAX)=A(IPMØ,1)=RX
00123:       A(I,MID)=-A(I,1)-A(I,JMAX)
00124:       FISS(I)=SIGFN(IG)*V
00125:       F(I)=1.0
00126:       DØ 11 J=J1,J2
00127:       JG=J-J1+1
00128:11     A(I,J)=A(I,J)+SST(IG,JG)*V
00129:       J1=J1-1  $  J2=J2-1
00130:10     CØNTINUE
00131:7      CØNTINUE
00132:       IF(IR.EQ.NR)GØ TØ 6
00133:       J1=MID  $  J2=2*MØD
00134:       II=N2=N2+MØD
00135:       LJ=LJ+1  $  R(LJ)=R(LJ-1)+H(IR)
00136:       V=VP $ VP=R(LJ)**PP1/PP1 $ V=VP-V
00137:       RX=-R(LJ)**P
00138:       DØ 12 IG=1,MØD
00139:       I=II+IG-1
00140:       A(I,JMAX)=RX
00141:       A(I,MID)=-A(I,1)
00142:       FISS(I)=SIGFN(IG)*V
00143:       F(I)=1.0
00144:       DØ 13 J=J1,J2
00145:       JG=J-J1+1
00146:13     A(I,J)=A(I,J)+SST(IG,JG)*V
00147:       J1=J1-1  $  J2=J2-1
00148:12     CØNTINUE
00149:       II=N2=N2+MØD
00150:       J1=MID  $  J2=2*MØD
00151:       LJ=LJ+1  $  R(LJ)=R(LJ-1)
00152:       V=0.0
00153:       DØ 16 IG=1,MØD
00154:       I=II+IG-1
00155:       A(I,JMAX)=-1.0
00156:       FISS(I)=0.0
00157:       DØ 17 J=J1,J2
00158:       JG=J-J1+1
00159:       IPMØ=J-MØD $ IF(IPMØ.LT.1)GØ TØ 17
00160:       A(I,IPMØ)=XM(IG,JG)
00161:17     CØNTINUE
00162:       J1=J1-1  $  J2=J2-1
00163:16     CØNTINUE
00164:       BØX(IR,1)=XM(2,1)  $  IF(MØD.EQ.2)GØ TØ 19
00165:       BØX(IR,2)=XM(3,1) $ BØX(IR,3)=XM(3,2)
00166:       IF(MØD.EQ.3)GØ TØ 19
00167:       BØX(IR,4)=XM(4,1) $ BØX(IR,5)=XM(4,2) $ BØX(IR,6)=XM(4,3)
00168:       IF(MØD.EQ.4)GØ TØ 19
00169:19     CØNTINUE
00170:91     CØNTINUE
00171:6      CØNTINUE
00172:C *****  RIGHT BØUNDRY  **********************************
00173:       J1=MID  $  J2=2*MØD
00174:       LJ=LJ+1  $  R(LJ)=R(LJ-1)+H(NR)
00175:       V=VP  $  VP=(R(LJ)+.5*EXTRAP)**PP1/PP1  $  V=VP-V
00176:       RX=-(R(LJ)+.5*EXTRAP)**P/EXTRAP
00177:       II=N2
00178:       DØ 24 IG=1,MØD
00179:       I=II+MØM1+IG
00180:       A(I,MID)=-A(I,1)-RX
```

```
00181:       FISS(I)=SIGFN(IG)*V
00182:       DØ 25 J=J1,J2
00183:       JG=J-J1+1
00184:25     A(I,J)=A(I,J)+SST(IG,JG)*V
00185:       J1=J1-1  $  J2=J2-1
00186:24     CØNTINUE
00187:       IMAX=NP(1)+1
00188:       DØ 3 IR=2,NR
00189:3      IMAX=IMAX+NP(IR)+2
00190:       IMAX=IMAX*MØD
00191:C * * * CRØUTING MATRIX * * * * * * * * * * * * * * * * *
00192:       DØ 71 J=MP1,JMAX
00193: 71    A(1,J)=A(1,J)/A(1,MID)
00194:       A(2,MID)=A(2,MID)-A(1,MP1)*A(2,MM1)
00195:       DØ 72 J=MP1,JMM1
00196: 72    A(2,J)=(A(2,J)-A(1,J+1)*A(2,MM1))/A(2,MID)
00197:       A(2,JMAX)=A(2,JMAX)/A(2,MID)
00198:       IF(MØD.EQ.2)GØ TØ 76
00199:       A(3,MM1)=A(3,MM1)-A(3,MM2)*A(1,MP1)
00200:       A(3,MID)=A(3,MID)-A(3,MM2)*A(1,MP2)-A(3,MM1)*A(2,MP1)
00201:       DØ 73 J=MP1,JMM2
00202: 73    A(3,J)=(A(3,J)-A(1,J+2)*A(3,MM2)-A(2,J+1)*A(3,MM1))/A(3,MI
D)
00203:       A(3,JMM1)=(A(3,JMM1)-A(2,JMAX)*A(3,MM1))/A(3,MID)
00204:       A(3,JMAX)=A(3,JMAX)/A(3,MID)
00205:       IF(MØD.EQ.3)GØ TØ 76
00206:       A(4,MM2)=A(4,MM2)-A(4,MM3)*A(1,MP1)
00207:       A(4,MM1)=A(4,MM1)-A(4,MM2)*A(2,MP1)-A(4,MM3)*A(1,MP2)
00208:       A(4,MID)=A(4,MID)-A(4,MM3)*A(1,MP3)-A(4,MM2)*A(2,MP2)
00209:       A(4,MID)=A(4,MID)-A(4,MM1)*A(3,MP1)
00210:       JMM3=JMAX-3
00211:       DØ 74 J=MP1,JMM3
00212:       A(4,J)=A(4,J)-A(4,MM3)*A(1,J+3)-A(4,MM2)*A(2,J+2)
00213: 74    A(4,J)=(A(4,J)-A(4,MM1)*A(3,J+1))/A(4,MID)
00214:       A(4,JMM2)=A(4,JMM2)-A(2,JMAX)*A(4,MM2)-A(3,JMM1)*A(4,MM1)
00215:       A(4,JMM2)=A(4,JMM2)/A(4,MID)
00216:       A(4,JMM1)=(A(4,JMM1)-A(3,JMAX)*A(4,MM1))/A(4,MID)
00217:       A(4,JMAX)=A(4,JMAX)/A(4,MID)
00218:       IF(MØD.EQ.4)GØ TØ 76
00219: 76    CØNTINUE
00220:       N2=MØD
00221:C ****** REGIØNAL CRØUTING ****************
00222:       DØ 300 IR=1,NR
00223:       N1=N2+1 $ N2=N1+NP(IR)*MØD
00224:       IF(IR.EQ.NR)N2=N2-1
00225:       NØ(3,IR)=N1
00226:       NØ(4,IR)=N2
00227:       DØ 30 I=N1,N2
00228:       DØ 31 JJ=1,MM1
00229:       IK=I-MID+JJ $ J1=JJ+1 $ J2=J1+MØD-1
00230:       DØ 32 J=J1,J2
00231:       JK=J-J1+MP1
00232:32     A(I,J)=A(I,J)-A(I,JJ)*A(IK,JK)
00233:31     CØNTINUE
00234:       DØ 35 J=MP1,JMAX
00235:35     A(I,J)=A(I,J)/A(I,MID)
00236:30     CØNTINUE
00237:       IF(IR.EQ.NR)GØ TØ 300
00238:C *****CRØUTING AT INTERFACE ************************
00239:       N1=N2+1 $ N2=N1+2*MØD-2 $ NX=(N1+N2)/2
00240:       I1=1 $ I2=2 $ I3=3 $ I4=4 $ I5=5 $ I6=6
```

```
00241:       DØ 170 I=N1,N2
00242:       IF(I.LE.NX)GØ TØ 169
00243:       I1=11 $ I2=12 $ I3=13 $ I4=14 $ I5=15 $ I6=16
00244:169    IF(I.EQ.NX)GØ TØ 180
00245:       IF(I.EQ.N1)GØ TØ 171
00246:       IF(I.EQ.N1+1)GØ TØ 172
00247:       IF(I.EQ.NX+1)GØ TØ 171
00248:       IF(I.EQ.N1+2)GØ TØ 173
00249:       IF(I.EQ.NX+2)GØ TØ 172
00250:       IF(I.EQ.NX+3)GØ TØ 173
00251:C     **  SINGLE BØX  **
00252:171    IK=I-MØD-1
00253:       DØ 181 J=1,MM1
00254:       JK=MID+J
00255:181    A(I,J)=A(I,J)-BØX(IR,I1)*A(IK,JK)
00256:       GØ TØ 180
00257:C     ** DØUBLE BØX  **
00258:172    IK=I-MØD-2 $ KK=I-MØD-1
00259:       BØX(IR,I3)=BØX(IR,I3)-BØX(IR,I2)*A(IK,MID+1)
00260:       DØ 182 J=1,MM2
00261:       JK=MID+J+1
00262:182    A(I,J)=A(I,J)-BØX(IR,I2)*A(IK,JK)
00263:       DØ 183 J=1,MM1
00264:       JK=MID+J
00265:183    A(I,J)=A(I,J)-BØX(IR,I3)*A(KK,JK)
00266:       GØ TØ 180
00267:C  **  TRIPLE BØX  **
00268:173    IK=I-MØD-3 $ KK=I-MØD-2 $ LJ=I-MØD-1
00269:       BØX(IR,I5)=BØX(IR,I5)-BØX(IR,I4)*A(IK,MID+1)
00270:       BØX(IR,I6)=BØX(IR,I6)-BØX(IR,I4)*A(IK,MID+2)
00271:       DØ 185 J=1,MM3
00272:       JK=J+MID+2
00273:185    A(I,J)=A(I,J)-BØX(IR,I4)*A(IK,JK)
00274:       BØX(IR,I6)=BØX(IR,I6)-BØX(IR,I5)*A(KK,MID+1)
00275:       DØ 186 J=1,MM2
00276:       JK=MID+J+1
00277:186    A(I,J)=A(I,J)-BØX(IR,I5)*A(KK,JK)
00278:       DØ 187 J=1,MM1
00279:       JK=MID+J
00280:187    A(I,J)=A(I,J)-BØX(IR,I6)*A(LJ,JK)
00281:       GØ TØ 180
00282:180    CØNTINUE
00283:       JJ=0 $ J1=1 $ J2=MID-1
00284:188    JJ=JJ+1 $ J1=J1+1 $ J2=J2+1
00285:       DØ 191 J=J1,J2
00286:       JK=MID+J-JJ $ IK=I-MØD+JJ-1
00287:191    A(I,J)=A(I,J)-A(I,JJ)*A(IK,JK)
00288:       IF(IK.LT.I-1)GØ TØ 188
00289:       DØ 192 J=MP1,JMAX
00290:192    A(I,J)=A(I,J)/A(I,MID)
00291:170    CØNTINUE
00292: 300   CØNTINUE
00293:C ******CALCULATE SØME NUMBERS **********************
00294:       NØ(1,1)=1  $  NØ(2,1)=(NP(1)+1)*MØD+1
00295:       DØ 214 IR=2,NR
00296:       NØ(1,IR)=NØ(2,IR-1)+MØD
00297: 214   NØ(2,IR)=NØ(1,IR)+(NP(IR)+1)*MØD
00298:       NØ(2,NR)=NØ(2,NR)-MØD
00299:C ******CALC. INITIAL FISSIØN SØURCE  *****************
00300:       FISHØ=0.0
```

]

```
00301:       DØ 303 I=1,IMAX
00302:       F(I)=1.0
00303:303    FISHØ=FISHØ+FISS(I)
00304:       WRITE(61,141)
00305:141    FØRMAT('0ITER      K-EFF           CHANGE')
00306:CC ******** MAIN ITERATIØN LØØP  **********************
00307:       DØ 60 ITER = 1,100
00308:C ******* SET UP SØURCE *******************************
00309:       DØ 62 IR=1,NR
00310:       N1=NØ(1,IR)
00311:       N2=NØ(2,IR)
00312:       DØ 63 I4=N1,N2,MØD
00313:       JK=I4-1
00314:       S4=0.0
00315:       DØ 64 IG=1,NG
00316:       I=JK+IG
00317:64     S4=F(I)*FISS(I)/EFFK+S4
00318:       DØ 65 JG=1,NG
00319:       I=I4-1+JG
00320:65     SS(I)=S4*CHI(IR,JG)
00321:63     CØNTINUE
00322:62     CØNTINUE
00323:C * * * * SØLVING FØR NEW FLUX * * : * * * * * : * * * * :
00324:       GØ TØ(66,66,67,68,69),MØD
00325: 66    CALL SØLV2
00326:       GØ TØ 77
00327: 67    CALL SØLV3
00328:       GØ TØ 77
00329: 68    CØNTINUE
00330: 69    CØNTINUE
00331: 77    CØNTINUE
00332:C * * * * NEW FLUXES ARE IN SS * * * * * * * * * *
00333:C ********CALCULATIØN ØF K-EFFECTIVE ********************
00334:       FISH=0.0
00335:       DØ 82 I=1,IMAX
00336:       F(I)=SS(I)
00337:82     FISH=FISH+FISS(I)*F(I)
00338:       EFFK=EFFKØLD*FISH/FISHØ
00339:       DELK=EFFK-EFFKØLD
00340:       WRITE(61,148)ITER,EFFK,DELK
00341:148    FØRMAT(I5,2E15.7)
00342:       IF(ABS(DELK).LT.EP)GØ TØ 85
00343:       FISHØ=FISH
00344:       EFFKØLD=EFFK
00345:60     CØNTINUE
00346:C                END ØF LØØP
00347: 85    CALL EQUIP(9,5HFILE )
00348:       PRINT 107
00349:107    FØRMAT('OPØINT  RADIUS     FLUXES FØR MØDE 1,2,---')
00350:       DØ 86 I4=1,IMAX,MØD
00351:       IJ=I4/MØD+1
00352:       IM=I4+MØD-1
00353:       WRITE(9,102)R(IJ),(F(I),I=I4,IM)
00354:86     WRITE(61,108)IJ,R(IJ),(F(I),I=I4,IM)
00355:108    FØRMAT(I3,F7.2,1X,5E12.5)
00356:       END
00357:
00358:       SUBRØUTINE SØLV2
00359:       CØMMØN A(200,7),SS(200),NØ(4,6),BØX(6,20),NR,MØD,IMAX
00360:       SS(1)=SS(1)/A(1,3)
```

```
00361:       SS(2)=(SS(2)-SS(1)*A(2,2))/A(2,3)
00362:       DØ 93 IR=1,NR
00363:       N1=NØ(3,IR) $ N2=NØ(4,IR)
00364:       DØ 94 I=N1,N2
00365:       SS(I)=(SS(I)-A(I,2)*SS(I-1)-A(I,1)*SS(I-2))/A(I,3)
00366: 94    CØNTINUE
00367:       IF(IR.EQ.NR)GØ TØ 93
00368:       I=N2+1
00369:       SS(I)=SS(I)-BØX(IR,1)*SS(I-3)-A(I,1)*SS(I-2)-A(I,2)*SS(I-1
)
00370:       SS(I)=SS(I)/A(I,3)
00371:       I=N2+2
00372:       SS(I)=(SS(I)-A(I,1)*SS(I-2)-A(I,2)*SS(I-1))/A(I,3)
00373:       I=N2+3
00374:       SS(I)=SS(I)-BØX(IR,11)*SS(I-3)-A(I,1)*SS(I-2)
00375:       SS(I)=(SS(I)-A(I,2)*SS(I-1))/A(I,3)
00376: 93    CØNTINUE
00377:C ********BACKWARD SUBSTITUTIØN ********************
00378:       IMP=IMAX+1
00379:       DØ 50 II=1,IMAX
00380:       I=IMP-II
00381: 50    SS(I)=SS(I)-A(I,4)*SS(I+1)-A(I,5)*SS(I+2)
00382:       RETURN
00383:       END
00384:       SUBRØUTINE SØLV3
00385:       CØMMØN A(200,7),SS(200),NØ(4,6),BØX(6,20),NR,MØD,IMAX
00386:       SS(1)=SS(1)/A(1,4)
00387:       SS(2)=(SS(2)-SS(1)*A(2,3))/A(2,4)
00388:       SS(3)=(SS(3)-SS(2)*A(3,3)-SS(1)*A(3,2))/A(3,4)
00389:       DØ 93 IR=1,NR
00390:       N1=NØ(3,IR) $ N2=NØ(4,IR)
00391:       DØ 94 I=N1,N2
00392:       SS(I)=(SS(I)-A(I,3)*SS(I-1)-A(I,2)*SS(I-2)-A(I,1)*SS(I-3))
/A(I,4)
00393: 94    CØNTINUE
00394:       IF(IR.EQ.NR)GØ TØ 93
00395:       I=N2+1
00396:       SS(I)=SS(I)-BØX(IR,1)*SS(I-4)-A(I,1)*SS(I-3)-A(I,2)*SS(I-2
)
00397:       SS(I)=(SS(I)-A(I,3)*SS(I-1))/A(I,4)
00398:       I=N2+2
00399:       SS(I)=(SS(I)-BØX(IR,2)*SS(I-5)-BØX(IR,3)*SS(I-4)
00400:      1-A(I,1)*SS(I-3)-A(I,2)*SS(I-2)-A(I,3)*SS(I-1))/A(I,4)
00401:       I=N2+3
00402:       SS(I)=(SS(I)-A(I,1)*SS(I-3)-A(I,2)*SS(I-2)-A(I,3)*SS(I-1))
/A(I,4)
00403:       I=N2+4
00404:       SS(I)=SS(I)-BØX(IR,11)*SS(I-4)-A(I,1)*SS(I-3)
00405:       SS(I)=(SS(I)-A(I,2)*SS(I-2)-A(I,3)*SS(I-1))/A(I,4)
00406:       I=N2+5
00407:       SS(I)=(SS(I)-BØX(IR,12)*SS(I-5)-BØX(IR,13)*SS(I-4)-A(I,1)
00408:      1*SS(I-3)-A(I,2)*SS(I-2)-A(I,3)*SS(I-1))/A(I,4)
00409: 93    CØNTINUE
00410:C ********BACKWARD SUBSTITUTIØN ********************
00411:       IMP=IMAX+1
00412:       DØ 50 II=1,IMAX
00413:       I=IMP-II
00414: 50    SS(I)=SS(I)-A(I,5)*SS(I+1)-A(I,6)*SS(I+2)-A(I,7)*SS(I+3)
00415:       RETURN
00416:       END
```